1999

Investigations of a Phenanthroline-Based Azo Dye Ligand and of Re(I) and Ru(II) Complexes Based on This Ligand

Yan Zhang
Eastern Illinois University

THESIS REPRODUCTION CERTIFICATE

TO: Graduate Degree Candidates (who have written formal theses)

SUBJECT: Permission to Reproduce Theses

The University Library is receiving a number of request from other institutions asking permission to reproduce dissertations for inclusion in their library holdings. Although no copyright laws are involved, we feel that professional courtesy demands that permission be obtained from the author before we allow these to be copied.

PLEASE SIGN ONE OF THE FOLLOWING STATEMENTS:

Booth Library of Eastern Illinois University has my permission to lend my thesis to a reputable college or university or the purpose of copying it for inclusion in that institution's library or research holdings.

_____ 7-15-99

Author's Signature Date

I respectfully request Booth Library of Eastern Illinois University **NOT** allow my thesis to be reproduced because:

_____

_____

_____

_____

Author's Signature Date

Investigations of a Phenanthroline-Based Azo Dye Ligand and of Re(I) and Ru(II) Complexes Based on This Ligand

(TITLE)

BY

Yan Zhang

1971-

THESIS

SUBMITTED IN PARTIAL FULFILLMENT OF THE REQUIREMENTS
FOR THE DEGREE OF

Master of Science in Chemistry

IN THE GRADUATE SCHOOL, EASTERN ILLINOIS UNIVERSITY
CHARLESTON, ILLINOIS

1999
YEAR

I HEREBY RECOMMEND THIS THESIS BE ACCEPTED AS FULFILLING
THIS PART OF THE GRADUATE DEGREE CITED ABOVE

7-15-99
DATE

ADVISER

7-15-99
DATE

DEPARTMENT HEAD

Investigations of a Phenanthroline-Based Azo Dye Ligand and of Re(I) and Ru(II) Complexes Based on This Ligand

Approved by Thesis Committee:

Dr. Mark E. McGuire	7-15-99 Date
Dr. Jerry W. Ellis	7-15-1999 Date
Dr. Douglas G. Klarup	7/15/99 Date
Dr. Daniel J. Sheeran	7/15/99 Date

Abstract

Title of thesis:	Investigations of a Phenanthroline-Based Azo Dye Ligand and of Re(I) and Ru(II) Complexes Based on This Ligand
Name:	Yan Zhang
Thesis directed by:	Dr. Mark E. McGuire

A 1,10-phenanthroline based azo dye ligand, phen-azo-phenol, produced by diazotizing 5-amino-1,10-phenanthroline (5-NH_2-phen) and then coupling to phenol, and several transition metal complexes containing this ligand, have been synthesized and characterized. The phen-azo-phenol ligands attach to Re(I) and Ru(II) through the phenanthroline linkage to form stable polypyridyl complexes. These complexes show greatly enhanced absorption properties in the visible region when compared to the well-known analogous bipyridine and phenanthroline containing complexes. The visible light absorption of the free ligand and the complexes containing this ligand are greatly affected by the position of the deprotonation equilibrium of the –OH group on the phenol moiety in the phen-azo-phenol ligand. The pKa of one of the Ru(II) complexes, $[Ru^{II}(bpy)_2(phen\text{-}azo\text{-}phenol)](PF_6)_2$, has been determined to be 7.7 in aqueous solution.

Acknowledgements

I would like to express my sincere and deep appreciation to Dr. Mark E. McGuire, my research advisor, for his knowledgeable guidance, great patience, and kind encouragement and help on this research project.

I wish to thank Dr. Ellen A. Keiter for her help with the instruction of operating the QE-300 NMR spectrometer.

I would also like to thank the entire faculty and staff of Chemistry Department and the other members of our research group for all the advice and assistance I received during my two-year study at Eastern Illinois University.

Table of Contents

List of Tables

List of Figures

Introduction

Polypyridyl complexes of transition metals are widely studied and have a long history.[1-3] Serving as chelating agents, 2,2′-bipyridine (bpy) and 1,10-phenanthroline (phen), as shown in Figure 1.1, are parents of a broad family of polypyridine ligands that have been shown to be capable of complexing with a number of metal ions.

2,2'-bipyridine (bpy)

1,10-phenanthroline (phen)

Figure 1.1 Structures and abbreviations of 2,2′-bipyridine and 1,10-phenanthroline.

A large amount of effort has been devoted to polypyridyl complexes because of their rich photophysics and photochemistry and the numerous derivatives that can be easily prepared. Complexes with various polypyridyl derivatives and related ligands and changes in the metal center allow controlled variation of the ground and excited state properties and reactivities ("fine tuning"). Interest in the photochemistry of polypyridyl complexes has grown in the last decade due in part to their potential applications to solar energy conversion schemes.[3]

Coordination complexes containing polypyridyl ligands have been characterized for quite a large number of transition metals. Photophysical and photochemical studies, however, have been concentrated on complexes of specific metal ions. The most extensively studied are the d^6 systems represented by Ru(II), Os(II), Fe(II), Rh(III), Ir(III), Pt(IV), and Pd(IV). Other systems often considered are d^3, represented by Cr(III) and V(II), d^{10}, represented by Cu(I), and d^8, represented by Pd(II) and Pt(II). Polypyridyl

complexes of Re(I), Mo(0), Cr(0) and W(0) containing carbonyl ligands are also included because of their extensive display of photophysical behaviors that are similar to that of simple polypyridyl complexes. The number of complexes studied with different polypyridyl ligands is large and growing at a very rapid rate, especially for Ru(II) polypyridyls.[2] Figure 1.2 presents the structures of some of the common polypyridyl ligands along with their abbreviations.

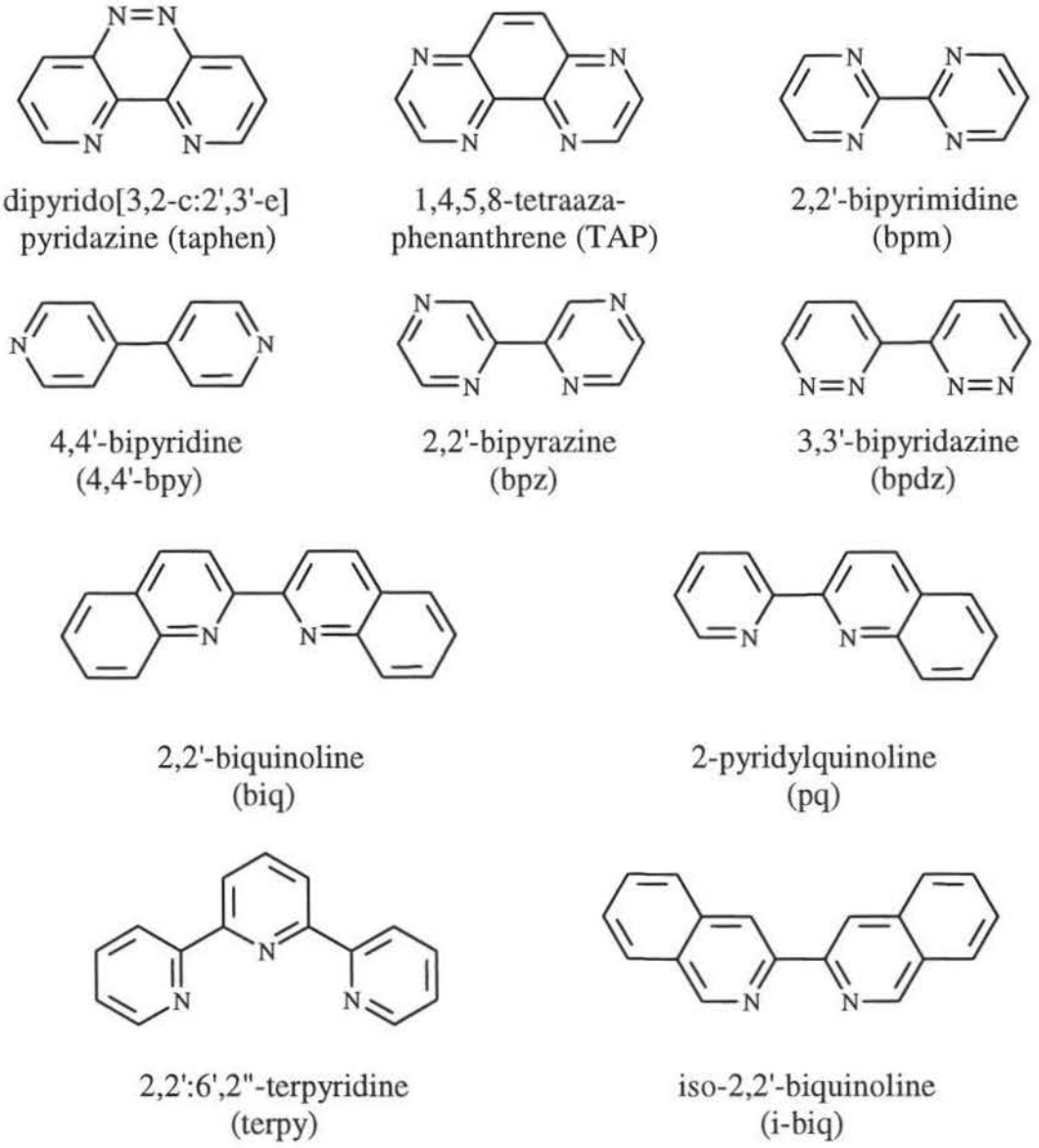

Figure 1.2 Structures of some polypyridyl ligands along with their abbreviations.

The principal interaction between a metal and a polypyridyl ligand is a σ-type involving the metal *d*-orbitals and the lone pairs of electrons on the ligand nitrogens. The filled π and vacant π^* orbitals on the polypyridine rings are also important in the bonding. Appropriate matching of energies of these orbitals with the central metal *d*-orbitals enables polypyridine ligands to act as π donors in complexes with high-oxidation-state metals (with empty π-type *d*-orbitals; d_{xy}, d_{yz}, d_{xz}) or as π acceptors in complexes with low-oxidation-state metals (with filled π-type *d*-orbitals).

Construction of a qualitative MO diagram to represent a typical polypyridyl transition metal complex is complicated by the variety of metals and ligands available. Nevertheless, a schematic MO diagram for an octahedral polypyridyl transition metal complex (taken from ref. 3) is shown in Figure 1.3. The various MO's can be conveniently classified according to their predominant atomic orbital contribution as:

I. strongly bonding, ligand-centered σ_L orbitals.

II. bonding, ligand-centered π_L orbitals.

III. essentially nonbonding $\pi_M(t_{2g})$ metal-centered *d* orbitals.

IV. anti-bonding $\sigma_M^*(e_g)$ metal-centered *d* orbitals.

V. anti-bonding, ligand-centered π_L^* orbitals.

In the ground electronic configuration of an octahedral complex of a d^n metal ion, orbitals of types I and II are completely filled, while *n* electrons occupy orbitals of types III and IV.

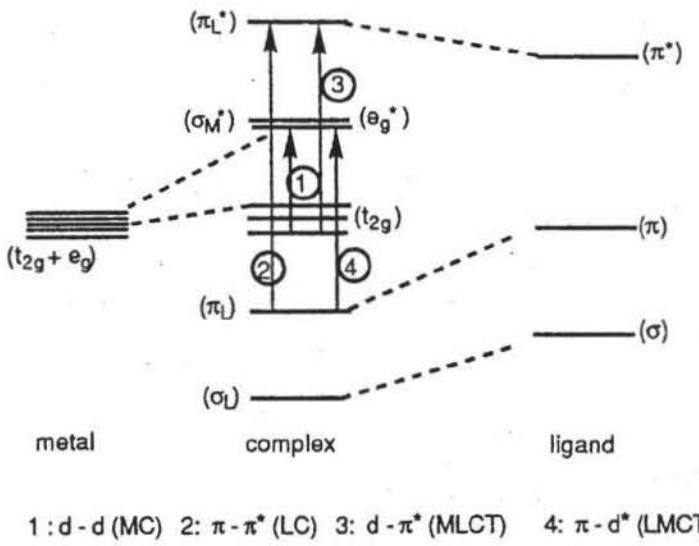

Figure 1.3 Relative positions of metal and ligand orbitals and possible electronic transitions in an octahedral ligand field of a polypyridyl transition metal complex. (taken from ref. 3)

Absorption of a photon of energy in the ultraviolet (UV) or visible (Vis) region by a metal complex M leads to its transformation to an electronically excited state M^*:

$$M + h\nu \rightarrow M^*$$

Figure 1.3 presents possible electronic transitions in the octahedral complex:

(1) metal centered (MC) or ligand field (LF), labeled as ①; essentially metal-localized *d-d* transitions.

(2) intraligand (IL) or ligand-centered (LC), labeled as ②; arise from π-π^* transitions involving ligand-localized orbitals. These transitions could be denoted as $\pi_L \rightarrow \pi_L^*$.

(3) charge transfer (CT). The charge transfer process can be further subdivided into metal to ligand charge transfer (MLCT; $d \rightarrow \pi_L^*$, labeled as ③), or ligand to metal charge transfer (LMCT; $\pi_L \rightarrow d$, labeled as ④). Other possible charge transfer could involve charge transfer to solvent (CTTS), intervalence charge transfer (IVCT), and ion-pair charge transfer (IPCT).

A complex in excited state M^* often relaxes rapidly (in a few picoseconds or less) to the lowest energy excited state, which can be labeled as S^*. Electron or energy transfer processes typically occur from the lowest energy excited states in polypyridyl transition metal complexes.[3] For example, S^* can undergo either radiationless transition by releasing the excess electronic energy in the form of heat to the surrounding medium or radiative relaxation through emission of a photon. Another important pathway is an intermolecular one where S^* undergoes energy or electron transfer with a quencher molecule.

The nature of the lowest energy excited state S^* of a polypyridyl complex can be altered through appropriate synthetic modifications (variation of metal ion and/or ligands). This is because the extent of crystal field splitting along with the relative disposition of the metal *d* orbitals with respect to ligand π orbitals vary with the nature of the metal ion and the ligands, leading to complexes having very different types of lowest excited states and photochemical reactivities. For example, for a series of transition metal tris(bipyridine) complexes $[M^n(bpy)_3]^{n+}$, the lowest energy excited state of the complex with Fe(II) is assigned as metal-centered (MC), those of Ru(II) and Os(II) as metal-to-ligand charge transfer (MLCT), and those of Rh(III) and Ir(III) as ligand centered (LC), as shown in Figure 1.4.[3] Changing the ligands while keeping the metal ion the same can have similar consequences. For example, Balzani et al.[4,5] showed that for the series of complexes $[Ru^{II}(i\text{-}biq)_2(LL)]^{2+}$ (i-biq = isobiquinoline), the lowest energy excited state is LC when LL = i-biq, and MLCT when LL = bpy.

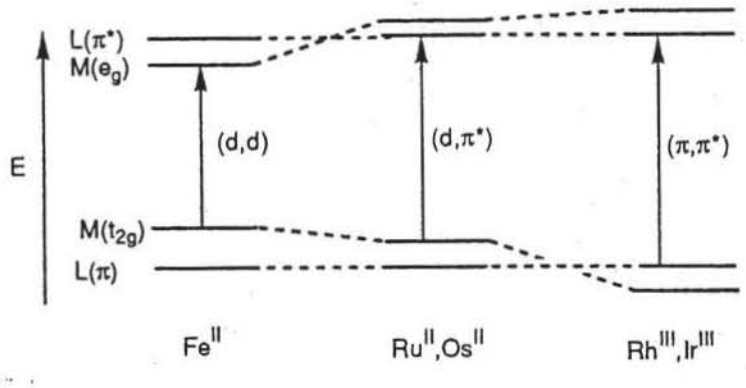

Figure 1.4 Schematic representation of various orbital dispositions in strong-field (nd^6) complexes $[M^n(bpy)_3]^{n+}$. (taken from ref. 3)

A major reason for the growth in the number of studies on transition metal polypyridyl complexes has been their application as photosensitizers in a wide variety of chemical reactions, such as solar energy conversion,[6, 7, 13-15] photo-decomposition of water into hydrogen and oxygen,[3, 8] and reduction of CO_2 to CO.[3, 9-14]

Solar energy conversion by photoelectrochemical cells has been extensively investigated.[15-17] The diagram in Figure 1.5 illustrates the principle of a dye-sensitized photovoltaic cell. Dye-sensitized cells are different from the conventional semiconductor devices in that they separate the function of light absorption from charge carrier transport. As shown in Figure 1.5, current is generated when a photon absorbed by dye molecules (process ①) gives rise to electron injection into the conduction band of the semiconductor (process ②). To complete the circuit, the dye must be regenerated by electron transfer from a redox species in solution (labeled as ⑤) which had been reduced at the counterelectrode.

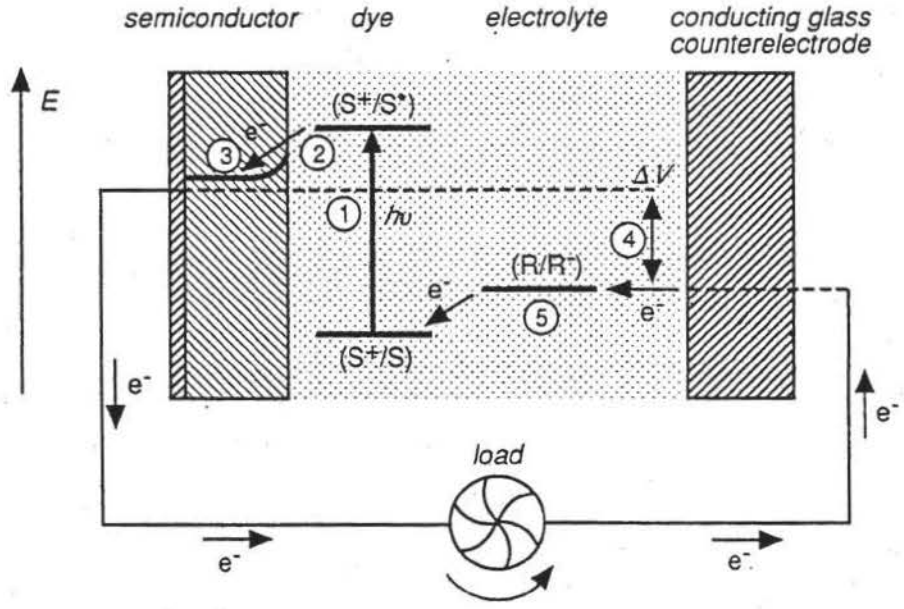

Figure 1.5 Diagram illustrating a dye-sensitized photovoltaic cell.
S: sensitizer; S^*: electronically excited sensitizer; S^+: oxidized sensitizer.
(taken from ref. 15)

Although attempts to use dye-sensitized photoelectrochemical cells in solar energy conversion have been made, the efficiency of such devices has been extremely low. This makes the large-scale use of photovoltaic devices for electricity generation prohibitively expensive. However, Grätzel et al. recently reported remarkably high photon-to-current conversion efficiencies from a photochemical cell using dye-sensitized porous nanocrystalline TiO_2 electrodes.[15] The cell, created from low to medium purity materials through low-cost processes, exhibited a commercially realistic energy conversion efficiency. The device was based on a 10-μm-thick optically transparent film of TiO_2 particles of a few nanometers in size deposited on a conductive glass sheet and coated with a monolayer of a charge-transfer dye (a trimeric ruthenium complex) which sensitized the film for light harvesting.[16] Because of the high surface area of the semiconductor film and the ideal spectral characteristics of the dye, the device harvested a high proportion of the incident solar energy (46%). The overall light-to-electric energy conversion yield was 7.1–7.9% in simulated solar light and 12% in diffuse daylight. The large current densities (greater than 12 mA cm^{-2}), exceptional stability (sustaining at least five million turnovers without decomposition), and the low cost, make practical applications seem feasible.

The trimeric complex used as the sensitizer molecule in Grätzel's cell consisted of a bis(dicarboxylbipyridyl) ruthenium(II) fragment connected to two bis(bipyridyl) ruthenium(II) moieties through cyano bridges (See Figure 1.6). Absorption of visible light by the two bis(bipyridyl) ruthenium(II) fragments is followed by energy transfer to the bis(dicarboxylbipyridyl) ruthenium(II) and then electron transfer (electron injection) to the semiconductor surface. The trimeric ruthenium complex, as a whole, absorbs both blue and green photons, thus enhancing the light harvesting capability of the semiconductor.

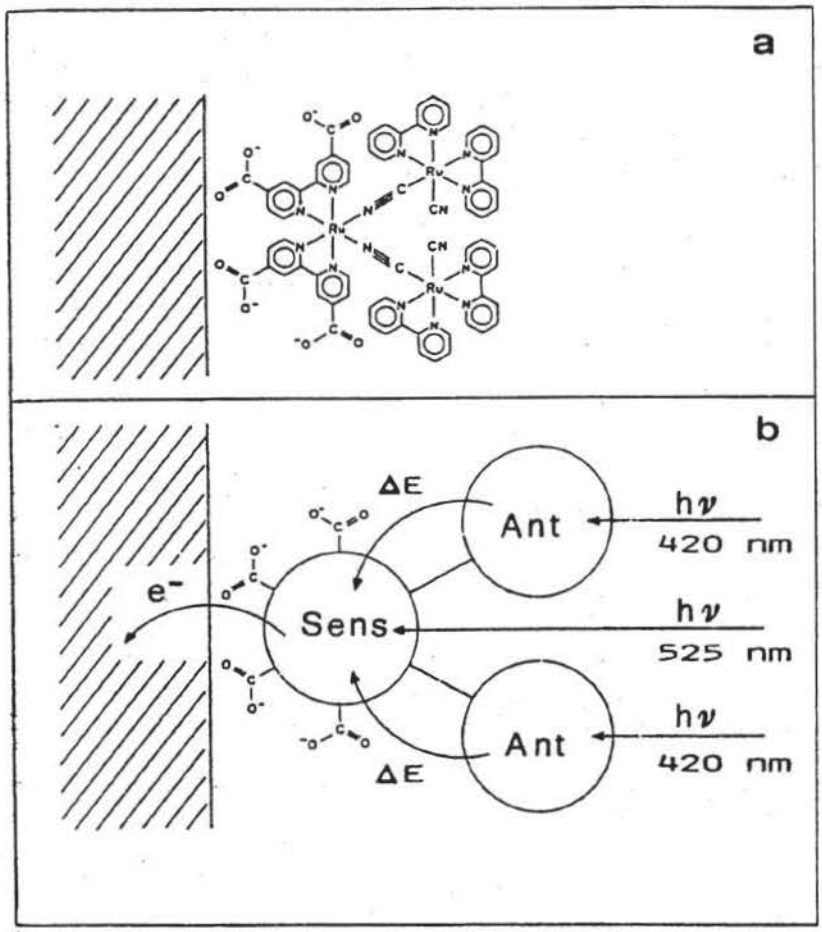

Figure 1.6 Energy and electron flow within the triruthenium complex used in Grätzel solar cell. (taken from ref. 16)

The design and synthesis of polypyridyl transition metal complexes that strongly absorb sunlight over a broad spectrum of wavelengths would increase the probability of successfully harnessing the sun's energy. Traditionally there have been three ways to approach this problem:

1. *Construction of multimetallic complexes using bridging ligands that allow for significant metal-metal interactions.* An excellent example of this is the trimeric ruthenium complex shown in Figure 1.6. This complex, designed by Amadelli et al.,[16] has visible absorption peaks at 420 ($\varepsilon = 1.91 \times 10^4$ M^{-1} cm^{-1}, approximated from Figure 1.7) and 525 nm ($\varepsilon = 1.23 \times 10^4$ M^{-1} cm^{-1}, approximated from Figure 1.7) in aqueous (pH = 3.5) solution, as shown in Figure 1.7. This can be compared with the absorption for

$Ru^{II}(bpy)_3^{2+}$, which shows a visible peak at only 452 nm ($\varepsilon = 1.44 \times 10^4\ M^{-1}\ cm^{-1}$) in aqueous solution.[3] The trimeric ruthenium complex clearly absorbs not only in the same region as $Ru^{II}(bpy)_3^{2+}$, but also out to significantly longer wavelengths.

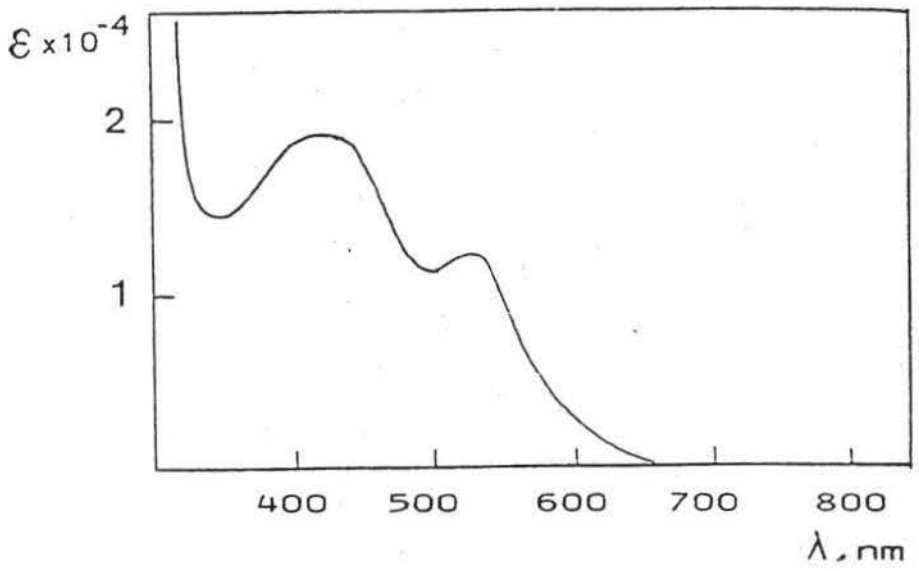

Figure 1.7 Absorption spectrum of $[\{Ru^{II}(bpy)_2(CN)_2\}_2Ru^{II}\{bpy(COO)_2\}_2]^{2-}$ in aqueous (pH = 3.5) solution. (taken from ref. 16)

Ligands such as 2,2′-bipyrimidine (bpm) and 2,3-bis(2-pyridyl)pyrazine (dpp) can serve as templates for building multimetallic complexes. Figure 1.8 shows the structure of some of the bridging polypyridyl ligands commonly used for the synthesis of multimetallic complexes.

Multimetallic systems often show CT transitions well into the visible region.[18, 19] Another example involves polypyridyl complexes with ammine ligands. The electronic spectroscopy of the monometallic complex $[(NH_3)_4Ru^{II}(bpm)]^{2+}$ shows an intense MLCT band in the visible region centered at 402 nm while the bimetallic complex $[\{(NH_3)_4Ru^{II}\}_2(bpm)]^{4+}$ has intense MLCT absorption bands at 424 and 697 nm.[20] The bimetallic absorption maxima for $[\{(NH_3)_4Ru^{II}\}_2(bpm)]^{4+}$ are both at lower energy than the $[(NH_3)_4Ru^{II}(bpm)]^{2+}$ monometallic absorption maximum. The reason for this shift is that the coupling of two Ru^{II} d_π orbitals with the ligand π^* LUMO orbital creates a set of bonding (ψ_b), nonbonding (ψ_n) and antibonding (ψ_a) orbitals, as shown in Figure 1.9 (b).

The presence of the nonbonding (ψ_n) HOMO in the bimetallic complex gives rise to a lower energy transition than in the corresponding monometallic complex (Figure 1.9 (a)).

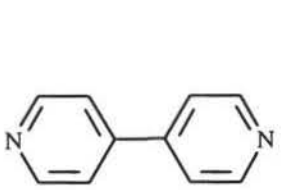

4,4'-bipyridine
(4,4'-bpy)

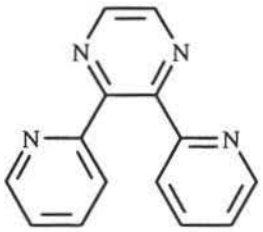

2,3-bis(2-pyridyl)-
pyrazine (dpp)

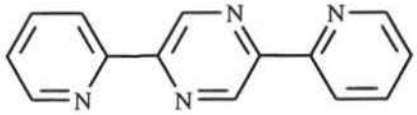

2,5-bis(2-pyridyl)-
pyrazine (2,5-dop)

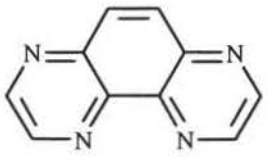

tetraazaphenanthrene
(TAP)

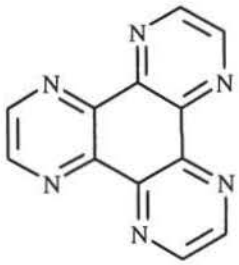

hexaazatriphenylene
(HAT)

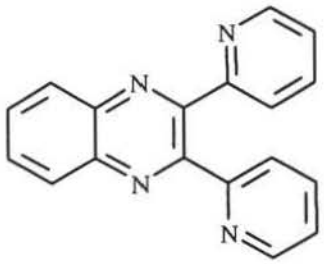

2,3-bis(2-pyridyl)-
quinoxaline (dpq)

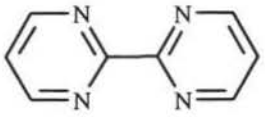

2,2'-bipyrimidine
(bpm)

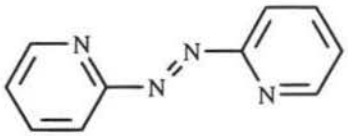

azo-2,2'-pyridine
(Azpy)

3,6-bis(2-pyridyl)-
tetrazine (bptz)

Figure 1.8 Multidentate polypyridyl ligands commonly used in the synthesis of polynuclear polypyridyl complexes.

A similar trend for a series of Ru^{II} polypyridyl complexes was demonstrated by Rillema et al.[21] For series of monometallic, bimetallic, trimetallic, and tetrametallic complexes containing ruthenium(II) metal centers bridged by 2,2′-bipyrimidine (bpm), there was increasing absorption out in the red portion of the spectrum, as shown in Figure 1.10.

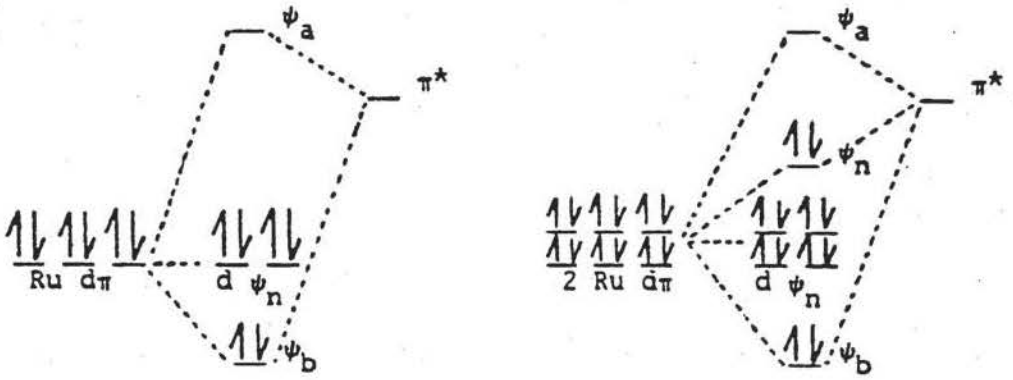

(a) (b)

Figure 1.9 Molecular orbital diagram for monometallic (a) and bimetallic (b) Ru^{II} complexes. (taken from ref. 20)

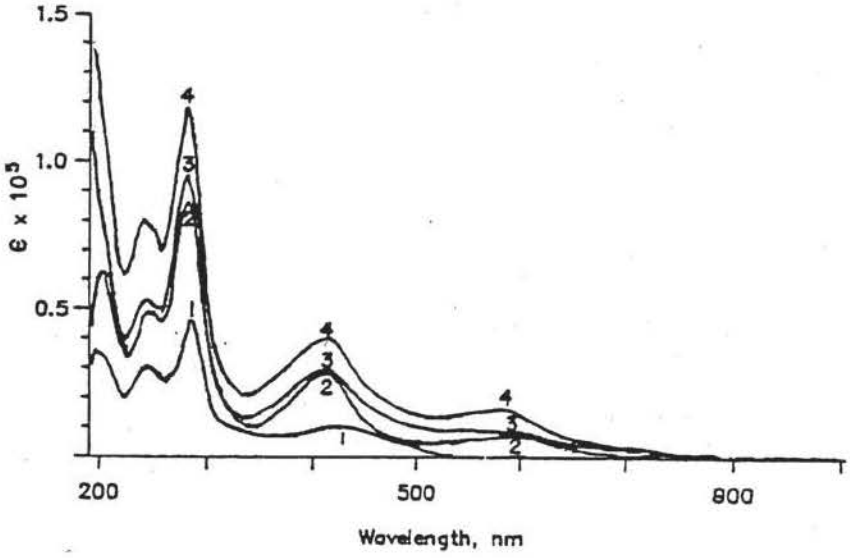

Figure 1.10 UV-Vis spectral comparison of Ru^{II}-bpm complexes (in CH_3CN), (1) $[Ru^{II}(bpy)_2bpm]^{2+}$; (2) $[(Ru^{II}(bpy)_2)_2bpm]^{4+}$; (3) $[(bpy)Ru^{II}(bpmRu^{II}(bpy)_2)_2]^{6+}$; (4) $[Ru^{II}(bpmRu^{II}(bpy)_2)_3]^{8+}$. (taken from ref. 21)

2. *Attachment of several different ligands on the same metal center.* The energy of the MLCT absorptions characteristic of polypyridyl complexes can be altered by varying the types of ligands used and/or by using different derivatives of the same ligand. This is because the energy of a MLCT transition for these complexes can usually be approximated as the absolute energy difference between the oxidation potential of the

metal center and the reduction potential of the ligand. For example, tris(heteroleptic) complexes which contain three different bidentate ligands (e.g. $[Ru^{II}(Me_2bpy)\{(EtCO_2)_2bpy\}(BL)]^{2+}$, where Me_2bpy is 4,4′-dimethyl-2,2′-bipyridine, $(EtCO_2)_2bpy$ is 4,4′-bis(carboxyethyl)-2,2′-bipyridine, and BL is 2,3-bis(2-pyridyl)pyrazine(dpp), 2,3-bis(2-pyridyl)quinoxaline(dpq), or 2,3-bis(2-pyridyl)-1,4-diazaanthracene(dpa)) have recently been synthesized by Meyer et al.[22] These complexes, called "black MLCT absorbers", show enhanced MLCT absorptions throughout the near-UV and visible spectral regions (200–700 nm) which are sufficiently long-lived to undergo efficient electron and energy transfer. Figure 1.11 shows the UV-Vis spectra for the series of $[Ru^{II}(Me_2bpy)\{(EtCO_2)_2bpy\}(BL)]^{2+}$ complexes.

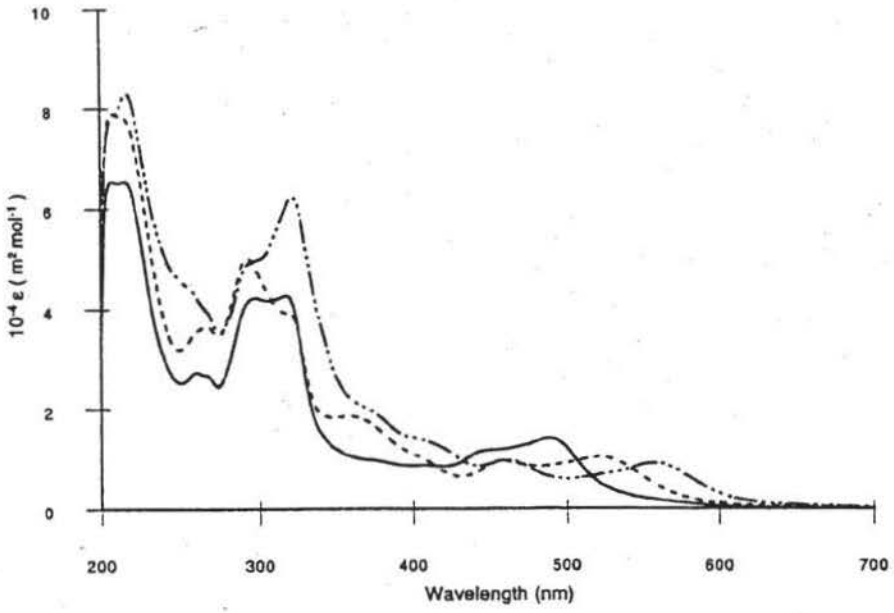

Figure 1.11 UV-Vis absorption spectra of $[Ru^{II}(Me_2bpy)\{(EtCO_2)_2bpy\}(BL)]^{2+}$ (in CH_3CN), BL = dpa (– ··· –), dpq (– – –), dpp (——). (taken from ref. 22)

3. *Utilization of ligands that strongly absorb in the visible region.* The ligand-centered (LC) absorptions for polypyridyl complexes typically occur at wavelengths less than 300 nm. Absorption of UV photons (which represents only about 2% of the distribution of solar energy reaching earth) results in excited states that rapidly decay to the lowest energy excited state of the complex. For better utilization of the visible range

(which represents about 40% of the solar energy distribution), chemical solar energy conversion schemes depend on the synthesis of particular compounds that strongly absorb visible light. If some LC absorptions occurred in the visible region, the total absorptivity of the complex in the visible would increase (LC absorptions on top of the normal MLCT absorptions). This would, in principle, increase the utilization of visible photons in populating the lowest energy excited state of the complex.

The work described in this thesis focuses on this approach. This project involves the synthesis of a series of transition metal complexes using a synthetically modified phenanthroline. The modified phenanthroline absorbs visible light, thus enhancing the absorption properties of metal complexes containing these ligands.

The new phenanthroline ligand incorporates an azo dye into its structure and the $\lambda_{max} \cong 380$ nm, with significant absorption at wavelengths greater than 500 nm. Coordination of transition metals through the N-atoms (1,10 positions) of the phenanthroline portion of the ligand would provide complexes that are expected to retain the stability and redox properties of traditional polypyridyl complexes while possessing enhanced abilities to absorb visible light due to the presence of the dye. Figure 1.12 shows the structures and abbreviations of the original and modified phenanthroline ligands.

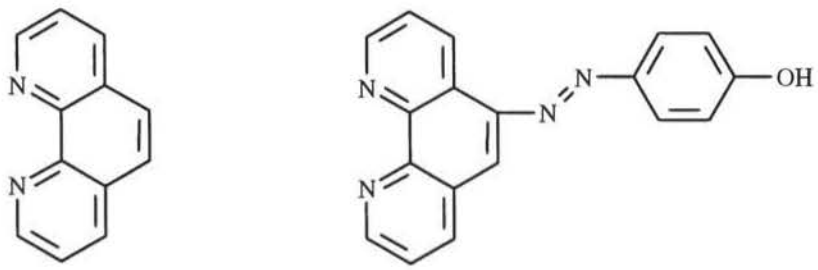

phen
(colorless)

(a)

phen-azo-phenol
(orange)

(b)

Figure 1.12 Original and modified phenanthroline ligands.

Azo dyes are compounds containing azo groups ($-N=N-$) which are linked to sp^2–hybridized carbon atoms. Azo dyes represent the largest group of colorants used as dyes and pigments.[23] They are usually synthesized by diazotization of aromatic amines in acidic solution followed by azo coupling at higher pH with coupling components. The use of various aromatic and heterocyclic amines and variation in the coupling components provide a rich array of azo dyes and absorption properties. In this work, 5-amino-1,10-phenanthroline (5-NH_2-phen), prepared from 5-nitro-1,10-phenanthroline (5-NO_2-phen), was diazotized and coupled to phenol to produce the ligand 5-(4-hydroxyphenylazo)-1,10-phenanthroline (Figure 1.12 (b), "phen-azo-phenol").

Replacement of one or more bipyridines and/or phenanthrolines with the highly colored phen-azo-phenol dye ligand in polypyridyl transition metal complexes might provide for more efficient use of visible light for population of low-lying excited states. The idea is to absorb visible photons at a highly absorbing but unreactive phen-azo dye ligand ("antenna fragment"), and then transfer the energy to the lowest energy excited state of the complex.

The synthesis, purification, and characterization of the phen-azo-phenol are described along with three metal complexes using this ligand: (1) tricarbonylchloro{5-(4-hydroxyphenylazo)-1,10-phenanthroline}rhenium(I), $Re^{I}(CO)_3Cl$(phen-azo-phenol); (2) bis(2,2′-bipyridine){5-(4-hydroxyphenylazo)-1,10-phenanthroline}ruthenium(II) hexafluorophosphate, $[Ru^{II}(bpy)_2$(phen-azo-phenol)$](PF_6)_2$; and (3) tris{5-(4-hydroxyphenylazo)-1,10-phenanthroline}ruthenium(II) hexafluorophosphate, $[Ru^{II}$(phen-azo-phenol$)_3](PF_6)_2$. The preparation of the ligand and the Re^{I} complex had been reported in an earlier thesis.[24] However, more extensive purification procedures are presented here for the ligand and Re^{I} complex. Moreover, the previous work did not present electrochemical data for these compounds.

The ligand and the three metal complexes were characterized using NMR, IR, and UV-Vis spectroscopy, as well as by cyclic voltammetry (CV) and elemental analysis. It should be noted that the ultimate question to be answered is whether or not the new ligand provides for more efficient population of the lowest energy excited states in these complexes than when phenanthroline or bipyridine alone are used as ligands. For example,

using the appropriate spectroscopic techniques, the overall efficiency of excited state population (the number of excited states formed per molecule/the number of photons available) for the new complexes could be compared with the literature data on standard compounds. Table 1.1 shows the comparisons that could be made:

Complexes using phen-azo-phenol	Standard compounds
$Re^{I}(CO)_3Cl$(phen-azo-phenol)	$Re^{I}(CO)_3Cl$(phen)
$[Ru^{II}(bpy)_2$(phen-azo-phenol)$]^{2+}$	$[Ru^{II}(bpy)_2$(phen)$]^{2+}$
$[Ru^{II}$(phen-azo-phenol)$_3]^{2+}$	$[Ru^{II}(phen)_3]^{2+}$

Table 1.1 Comparisons between synthesized complexes and standard compounds

Although some useful comparisons of properties can be made with equipment available (NMR, IR, UV-Vis, CV), substantial excited state characterization will have to wait for collaboration with research groups (such as those of Dr. Karen Brewer at Virginia Polytechnic Institute) having the appropriate expertise.

Experimental

Materials:

All materials and reagents were used as received unless otherwise indicated. The following were purchased from Aldrich Chemical Company, Inc.: 1,10-phenanthroline monohydrate (phen, 99%), palladium (10 wt. %) on activated carbon (Pd/C), hydrazine monohydrate ($N_2H_4 \cdot H_2O$, 98%), phenol (99+ %), aluminum oxide (activated, neutral, Brockmann I, standard grade, ~150 mesh), pentacarbonyl chlororhenium(I) ($Re^{I}(CO)_5Cl$, 98%), 2,2′-bipyridine (bpy, 99+ %), anhydrous N,N′-dimethylformamide (DMF, 99+ %), ammonium hexafluorophosphate (NH_4PF_6, 99.99%), dimethylsulfoxide (DMSO, 99.9%, A.C.S. spectrophotometric grade), ethylene glycol (99+ %, spectrophotometric grade), and potassium bromide (KBr, 99+ %, FT-IR grade). Anhydrous diethyl ether (certified A.C.S.), silica gel (60–200 mesh), chloroform, and lithium chloride (LiCl, dried in the vacuum oven at 100 °C for 5 h before using) were purchased from Fisher Scientific Co. Fuming sulfuric acid (approx. 20% free SO_3), dichloromethane (CH_2Cl_2, HPLC grade), N,N′-dimethylformamide (DMF), 2,2′,4-trimethylpentane (nanograde), and anhydrous methanol were purchased from Mallinckrodt. Concentrated nitric acid (conc. HNO_3), acetone (reagent grade), and acetonitrile (CH_3CN, distilled, suitable for HPLC, spectrophotometry, and gas chromatography) were obtained from EM Science. The absolute ethanol was from Midwest Grain Products. Ruthenium(III) trichloride hydrate was formulated as either $RuCl_3 \cdot 3H_2O$ (Alfa Products, dried under vacuum for 3 h before using) or as $RuCl_3 \cdot xH_2O$ (3.8% H_2O, Aldrich Chemical Company, Inc.). Glacial acetic acid was purchased from Fisher Scientific, Mallinckrodt, and EM Science. Tetrabutylammonium hexafluorophosphate (TBAH) was obtained from Bioanalytical Systems, Inc. and dried under vacuum for 5 h before using. NMR solvents were obtained from Cambridge Isotope Laboratories. Ethanol (95%), sodium hydroxide, and sodium nitrite were from the EIU stockroom. All water used for reactions and solutions was

purified by a Millipore™ "Milli-Q" system equipped with a 0.22 μm filter fed by house deionized water.

The 5-NO_2-1,10-phenanthroline (5-NO_2-phen) was prepared by the nitration of 1,10-phenanthroline with concentrated nitric acid in the presence of fuming sulfuric acid using a procedure analogous to that reported by Amouyal et al.[25] The 5-NH_2-1,10-phenanthroline (5-NH_2-phen) was then prepared by reduction of 5-NO_2-phen with hydrazine monohydrate in absolute ethanol (10% Pd/C catalyst) using a procedure similar to that outlined by Nasielski–Hinkens et al.[26] We have obtained 5-NH_2-phenanthroline in about 90% yield (based on 5-NO_2-phen) in our lab by using this procedure.

Syntheses:

5-(4-Hydroxyphenylazo)-1,10-phenanthroline, phen-azo-phenol:

This ligand was prepared by a method similar to that reported in an earlier thesis.[24] In a typical preparation, 3.0 mL of 6 M HCl was added slowly with stirring to 5-NH_2-phen (0.1220 g, 0.625 mmol) in a 15-mL beaker immersed in an ice/water bath. The greenish-yellow 5-NH_2-phen dissolved in the HCl to form a red solution. Meanwhile, a solution of $NaNO_2$ (0.0440 g, 0.638 mmol) in 1.672 mL of H_2O was prepared in a separate 15-mL beaker and cooled to 0 °C in an ice/water bath. The $NaNO_2$ solution was added all at once to the cold 5-NH_2-phen/HCl solution and this gave a dark orange-red solution with some foam on the top. No precipitate formed in this step. Stirring was continued for 3 min in the ice/water bath.

In a 50-mL beaker, 8 mL of a 10% aqueous solution of NaOH was added to phenol (0.0588 g, 0.625 mmol) at room temperature to form a colorless solution. The solution was then diluted with 20 mL of water. The diazotized phenanthroline mixture was then transferred into the phenol solution all at once with stirring. A dark brownish red precipitate formed immediately, and the stirring was continued for 3 min. The pH of the mixture was greater than 13 at that time. The precipitate was collected in a 15-mL Buchner funnel containing a medium (M) glass frit filter. The mixture filtered very slowly and the filtrate was dark red. The dark red gelatinous solid on the frit was washed with a small amount of water and the wash was dark brownish red. The frit with precipitate was

dried under vacuum for 3 h. The dried solid was rinsed thoroughly with diethyl ether (to remove any remaining unreacted phenol) and filtered giving a colorless wash. The resulting solid was dried under vacuum for 3 h.

The crude phen-azo-phenol was purified by silica gel column chromatography (90:10 acetic acid/methanol) and then by alumina column chromatography (60:40 ethanol (95%)/chloroform). In the silica gel chromatography procedure, one batch of crude product (about 0.9–1.1 g) was dissolved in a minimum amount (~ 5 mL) of eluant (90:10 acetic acid/methanol) and filtered through a 15-mL M-frit before loading onto a column which was 10 cm long and 2.8 cm wide. The column was developed with a flow rate of about 30 drops/min. Over a 30-min time period, three different bands developed from bottom to top: light yellow, orange-red, and dark purple. The light yellow fraction appeared to be a minor component and was discarded. Based on the results of TLC and previous work, the desired compound was thought to be the orange fraction. About 200 mL of this fraction was collected from the column, and this solution was filtered through a 15-mL F-frit to remove small silica particles. The solvent was removed by rotary evaporation and the orange solid was dried under vacuum for 3 h. In the alumina chromatography procedure, the batch of product from the silica column was dissolved in a minimum amount (~ 4 mL) of DMF and filtered through a 2-mL F-frit before loading onto a column which was 10 cm long and 2.8 cm wide. The column was developed with 60:40 ethanol (95%)/chloroform with a flow rate of 30 drops/min. Over a 30-min time period, two significant bands were observed from bottom to top: orange-yellow and beige. The orange-yellow fraction was thought to be the target product based on previous work. About 150 mL of the desired yellow fraction was collected and filtered through a 15-mL F-frit to remove small alumina particles. The solvent was removed by rotary evaporation and the orange product was dried under vacuum for 3 h, and then dried in the vacuum oven at 120 °C for 8 h. Average yield of purified product: 0.0711 g, 37.9 % based on 5-NH_2-phen. Elemental analysis: Calcd for $C_{18}H_{12}N_4O{\cdot}0.2H_2O$: C, 71.14; H, 4.11; N, 18.43. Found: C, 71.26; H, 4.10; N, 18.32. The melting range of the phen-azo-phenol was 295-297 °C. ^{1}H-NMR spectrum (Figure 3.1) in d_6-DMSO (ppm vs TMS): 7.03 (d,

2H), 7.81 (dd, 1H), 7.92 (dd, 1H), 8.04 (d, 2H), 8.16 (s, 1H), 8.70 (d, 1H), 9.14 (m, 1H), 9.23 (m, 1H), 9.31 (d, 1H), 10.52 (s, 1H).

fac-Tricarbonylchloro{5-(4-hydroxyphenylazo)-1,10-phenanthroline}rhenium(I), _fac_-$Re^{I}(CO)_3Cl$(phen-azo-phenol):

This complex was synthesized using a procedure similar to that reported by Guarr et al.[27, 28] for the preparation of _fac_-[(Mebpy-Mebpy)$Re^{I}(CO)_3Cl$]. Methanol (120 mL) was added to a 250-mL 3-neck round-bottom (RB) flask equipped with a reflux column and a stirring bar. The methanol was deoxygenated with methanol-saturated N_2 for 20 min. $Re^{I}(CO)_5Cl$ (0.0454 g, 0.126 mmol) was added with stirring followed by phen-azo-phenol (0.0400 g, 0.126 mmol). The mixture was heated to reflux under N_2. Refluxing and stirring were continued for 40 h. During the procedure the color of the reaction mixture changed from orange to darker orange-red. The reaction was monitored by TLC (45:55 ethanol (95%)/hexanes). A yellow spot ($R_f \cong 0.8$) and a very light intermediate spot ($R_f \cong 0.4$) developed during the first several hours and then no detectable changes were observed. The phen-azo-phenol spot ($R_f \cong 0$) decreased in intensity over the reaction period. The reflux column was then removed while heating and stirring were continued in order to evaporate the solvent until the total volume was ~ 40 mL. During this time, orange-red precipitate began to form. Heating was stopped and the suspension was cooled to room temperature, and more precipitate formed. The precipitate was collected on a 15-mL F-frit, and the filtrate was orange. The orange-red precipitate on the frit was washed with a small amount of methanol and then three times with 2,2′,4-trimethyl pentane (to remove any remaining unreacted free ligand and $Re^{I}(CO)_5Cl$). The resulting solid was dried on the frit under vacuum for 3 h. Yield of crude product: 0.062 g, 81.2% based on $Re^{I}(CO)_5Cl$.

The crude _fac_-$Re^{I}(CO)_3Cl$(phen-azo-phenol) was purified by recrystallization from methanol. The solid was suspended in 400 mL of deoxygenated methanol in a 500-mL 3-neck RB flask equipped with a reflux column and a stirring bar. The orange suspension was refluxed under N_2 for 5 h. Most of the solid dissolved but the mixture was still cloudy. The hot suspension was filtered through a 60-mL F-frit to remove any insoluble

particles. The orange filtrate was clear, and the frit contained a small amount of orange solid. The filtrate was transferred to a 500-mL 3-neck RB flask equipped with a stirring bar and heated to boiling with stirring under N_2 in order to reduce the volume of methanol until precipitate began to form (~ 20 mL). The mixture was cooled to room temperature, sealed, and stored in the freezer for 10 h (overnight). The orange precipitate that formed was collected on a 2-mL F-frit (orange filtrate), and washed with a small amount of cold methanol. The frit with solid was dried under vacuum for 3 h, and the product was then dried in the vacuum oven at 70 °C for 5 h. Yield of purified *fac*-$Re^{I}(CO)_3Cl$(phen-azo-phenol): 0.0462 g, 60.5% based on $Re^{I}(CO)_5Cl$. Elemental analysis: Calcd for $Re^{I}(CO)_3Cl$(phen-azo-phenol): C, 41.62; H, 2.00; N, 9.25. Found: C, 43.78; H, 2.61; N, 8.74. ^{1}H-NMR spectrum (Figures 3.2a-b) in d_6-DMSO (ppm vs TMS): 7.05 (d, 2H), 8.11 (d, 2H), 8.12 (m, 1H), 8.23 (dd, 1H), 8.47 (s, 1H), 9.15 (d, 1H), 9.45 (d, 1H), 9.56 (d, 1H), 9.68 (d, 1H), 10.72 (s, 1H). IR in KBr (Figure 3.5): $\nu_{C\equiv O}$ 2026.92, 1924.33, and 1895.40 cm^{-1}.

Bis(2,2′-bipyridine){5-(4-hydroxyphenylazo)-1,10-phenanthroline}ruthenium(II) hexafluorophosphate, $[Ru^{II}(bpy)_2$(phen-azo-phenol)$](PF_6)_2$:

The starting material *cis*-bis(2,2′-bipyridine)dichlororuthenium(II) dihydrate, *cis*-$Ru^{II}(bpy)_2Cl_2\cdot 2H_2O$, was prepared and purified using procedures reported in a previous thesis.[29] $RuCl_3\cdot 3H_2O$ (1.95 g, 7.45 mmol), bpy (2.34 g, 15.0 mmol) and LiCl (2.10 g, 50.0 mmol) were heated under reflux in anhydrous DMF (15 mL) for 8 h. The dark purple reaction mixture was cooled to room temperature, poured into 75 mL of reagent grade acetone (which gave an almost black mixture), and stored in the freezer overnight. The mixture was filtered through a 15-mL M-frit which resulted in a fine, almost black crystalline solid and a purple filtrate. The crystals were washed three times with 25-mL portions of water which gave dark red-purple washes, followed by three 25-mL portions of diethyl ether which gave colorless washes. The solid was then dried under vacuum for 3 h. Yield of crude product: 1.7828 g, 46.0% based on $RuCl_3\cdot 3H_2O$.

The crude *cis*-$Ru^{II}(bpy)_2Cl_2\cdot 2H_2O$ was purified by refluxing in a 1:1 ethanol (95%)/water solution (285 mL) for 1 h. The mixture was protected from light during this

time. The insoluble impurities were removed by filtering through a 30-mL M-frit. LiCl (34.2 g, 0.807 mol) was added to the dark purple filtrate and then the ethanol was removed by rotary evaporation. The solution turned from dark purple to almost black and some black solid precipitated. The mixture was cooled in an ice bath for 30 min, and the fine, greenish-black precipitate was collected on a 30-mL M-frit (blackish-green filtrate), washed with a small amount of cold water, and then dried under vacuum for 3 h. Yield of purified product: 1.6839 g, 43.4% based on $RuCl_3 \cdot 3H_2O$. The purity was checked by ^{1}H-NMR (Figure 2.1) in d_6-DMSO (ppm vs TMS): 7.10 (t, 2H), 7.51 (d, 2H), 7.68 (t, 2H), 7.77 (t, 2H), 8.06 (t, 2H), 8.49 (d, 2H), 8.64 (d, 2H), 9.98 (d, 2H).

Bis(2,2′-bipyridine){5-(4-hydroxyphenylazo)-1,10-phenanthroline}ruthenium(II) hexafluorophosphate, $[Ru^{II}(bpy)_2(phen\text{-}azo\text{-}phenol)](PF_6)_2$, was prepared by a procedure similar to that reported by Rillema et al.[30] for the synthesis of $[(bpy)_2Ru^{II}(L_2)](PF_6)_2$, where L_2 was a polypyridyl ligand. In a typical reaction, 95% ethanol (50 mL) in a 100-mL 3-neck RB flask was deoxygenated by ethanol-saturated N_2 for 20 min. Phen-azo-phenol (0.0606 g, 0.202 mmol) and *cis*-$Ru^{II}(bpy)_2Cl_2 \cdot 2H_2O$ (0.1000 g, 0.192 mmol) were added and heated to reflux under N_2 for 3 h. The reaction mixture turned from a dark purple suspension with some orange particles to an intense red solution. The procedure was monitored by UV-Vis (in 95% ethanol) every hour. The spectra showed that the 520 nm peak of the starting material *cis*-$Ru^{II}(bpy)_2Cl_2 \cdot 2H_2O$ decreased while two peaks at about 450 and 420 nm increased over the refluxing period. While the reaction mixture was still warm, about 4 mL of a saturated aqueous solution of NH_4PF_6 was added dropwise with stirring, followed by the addition of 10 mL H_2O. The ethanol was removed by rotary evaporation resulting in a red suspension. The red precipitate was collected on a 15-mL F-frit (red filtrate) and washed with a small amount of cold water (yellow wash). The solid was dried on the frit under vacuum for 3 h. Yield of crude product: 0.2015 g, 104.6 % based on *cis*-$Ru^{II}(bpy)_2Cl_2 \cdot 2H_2O$.

The crude $[Ru^{II}(bpy)_2(phen\text{-}azo\text{-}phenol)](PF_6)_2$ was dissolved in 30 mL of 95% ethanol and filtered through a 15-mL F-frit to remove any insoluble impurities. The dark red solution was transferred to a 100-mL 3-neck RB flask and heated to boiling with N_2 introduced from a side neck while the middle neck was left open to let ethanol vapor

escape. When approximately 10 mL of solution remained, the solution was cooled to room temperature (some red precipitate formed), and then sealed and stored in the freezer for 5 h. The precipitate that formed was collected on a 15-mL F-frit (dark red filtrate) and washed with a few drops of cold ethanol (dark red wash). The frit with solid was dried under vacuum for 3 h, and the product was then dried in the vacuum oven at 70 °C for 5 h. Yield of purified product: 0.0958g, 49.7% based on *cis*-$Ru^{II}(bpy)_2Cl_2 \cdot 2H_2O$. Elemental analysis: Calcd for $[Ru^{II}(bpy)_2(phen\text{-}azo\text{-}phenol)](PF_6)_2 \cdot 1H_2O$: C, 44.67; H, 2.96; N, 10.97. Found: C, 44.73; H, 2.98; N, 10.94. ^{1}H-NMR spectrum (Figure 3.3a) in d_6-DMSO (ppm vs TMS): 7.05 (d, 2H), 7.36 (m, 2H), 7.62 (m, 4H), 7.87 (m, 3H), 7.98 (dd, 1H), 8.11 (m, 5H), 8.22 (m, 3H), 8.49 (s, 1H), 8.87 (m, 4H), 8.96 (d, 1H), 9.45 (d, 1H), 10.72 (s, 1H).

Diethyl ether (about 25 mL) was added with stirring to the filtrate from the previous step, which caused more precipitation of product and left a yellow supernatant. The flask with contents was stored in the freezer for 10 h (overnight) and more precipitate formed. The red precipitate that formed was collected on a 15-mL F-frit (red filtrate) and washed with a small amount of 1:2 ethanol/ether (yellow washes). The frit with solid was dried under vacuum for 3 h, and the product was then dried in the vacuum oven at 70 °C for 5 h. Yield of this second recrystallization: 0.0389 g, 20.2% based on *cis*-$Ru^{II}(bpy)_2Cl_2 \cdot 2H_2O$. Elemental analysis: Calcd for $[Ru^{II}(bpy)_2(phen\text{-}azo\text{-}phenol)](PF_6)_2 \cdot 0.6H_2O$: C, 44.99; H, 2.90; N, 11.04. Found: C, 44.98; H, 2.91; N, 11.08. The ^{1}H-NMR spectrum of this second crop (Figure 3.3b) was almost identical to that of the first one.

Tris{5-(4-hydroxyphenylazo)-1,10-phenanthroline}ruthenium(II) hexafluorophosphate, $[Ru^{II}(phen\text{-}azo\text{-}phenol)_3](PF_6)_2$:

The $[Ru^{II}(phen\text{-}azo\text{-}phenol)_3](PF_6)_2$ was prepared using a procedure analogous to that reported in a previous thesis[31] for the synthesis of $[Ru^{II}(Pptd)_3](PF_6)_2 \cdot 3H_2O$. $RuCl_3 \cdot xH_2O$ (3.8% H_2O, 0.0250 mg, 0.116 mmol) and phen-azo-phenol (0.1393 g, 0.464 mmol) were mixed in 15 mL of ethylene glycol in a 100-mL 3-neck RB flask equipped with a reflux column and a stirring bar. The mixture, which initially appeared as almost

black suspension with some orange particles, was refluxed under N_2 for 2 h (everything eventually dissolved to give a dark red solution). The reaction was monitored with UV-Vis (in ethylene glycol) every 0.5 h. During the procedure, the strong absorption at 390 nm decreased and the shoulder at about 460 nm increased. While the reaction mixture was still warm, a solution of NH_4PF_6 (0.189 g, 1.16 mmol) in 15 mL water was added with stirring, which gave a dark dull red suspension. After it was cooled to room temperature, the dark red precipitate was collected on a 15-mL F-frit. It filtered very slowly. Gelatinous solid was left on the frit and the filtrate was light orange. The solid was washed with three portions of water (about 5 mL each, very slowly filtered, yellow washes), and then dried under vacuum for 3 h. The dried solid was washed thoroughly with diethyl ether (very light orange wash) and dried under vacuum for 3 h, resulting in a fine, dark red powder. Yield of crude product: 0.1464 g, 97.7% based on $RuCl_3 \cdot xH_2O$.

The crude product was recrystallized from acetone/water to remove any remaining unreacted NH_4PF_6 and any Ru complexes containing less than three coordinated phen-azo-phenol ligands. It was dissolved in 20 mL of acetone and filtered through a 15-mL F-frit to remove any insoluble particles. The dark red filtrate and 20 mL of water were mixed in a 100-mL 3-neck RB flask equipped with a stirring bar. The mixture was heated with stirring to evaporate the acetone. When the acetone was evaporated, some dark red precipitate came out of solution and was collected on a 15-mL F-frit after it was cooled to room temperature (yellow filtrate). The solid was washed with a small amount of water and dried under vacuum for 3 h. Yield: 0.1139 g, 76.0% based on $RuCl_3 \cdot xH_2O$.

The ^{1}H-NMR spectrum of this product showed that a fairly large amount of free phen-azo-phenol dye was present. Based on solubility tests of both the free ligand and the metal complex (which showed that phen-azo-phenol was much more soluble in chloroform than was the complex), the product was suspended in 100 mL chloroform and sonicated for 1 h. The mixture was then filtered through a 15-mL F-frit (yellow filtrate). The solid left on the frit was washed with a small amount of chloroform, and then dried under vacuum for 3 h. Yield: 0.0924 g, 61.6% based on $RuCl_3 \cdot xH_2O$. The ^{1}H-NMR spectrum showed that the amount of free phen-azo-phenol dye had decreased significantly, but had not disappeared entirely.

The product from the previous step was then recrystallized from 95% ethanol. It was suspended in 200 mL ethanol (95%) and refluxed for 30 min. Most of the solid dissolved but the mixture was still cloudy. The hot mixture was filtered through a 60-mL F-frit to remove any insoluble particles. The dark red filtrate was transferred to a 300-mL 3-neck RB flask equipped with a stirring bar, and heated to boiling with N_2 blowing over the mixture to reduce the volume. When approximately 15 mL of solution remained, precipitate began to appear. The solution was cooled to room temperature. The dark red precipitate that formed was collected on a 15-mL F-frit (dark red filtrate), washed with several drops of ethanol, and then dried under vacuum for 3 h. Yield: 0.0078 g, 5.2% based on $RuCl_3 \cdot xH_2O$.

Chloroform (about 15 mL) and diethyl ether (about 30 mL) were added with stirring to the filtrate from the previous step, and this caused a brownish orange precipitate to form. The precipitate was collected on a 15-mL F-frit (dark orange-red filtrate) and washed with a small amount of 1:1:2 ethanol/chloroform/ether. The frit with solid was dried under vacuum for 3 h and was then dried in the vacuum oven at 70 °C for 5 h. Yield of this second recrystallization: 0.0346 g, 23.1% based on $RuCl_3 \cdot xH_2O$. Elemental analysis: Calcd for $[Ru^{II}(phen\text{-}azo\text{-}phenol)_3](PF_6)_2 \cdot 1.2H_2O$: C, 49.38; H, 2.95; N, 12.80. Found: C, 49.52; H, 3.05; N, 12.72. ^{1}H-NMR spectrum (Figure 3.4a) in d_6-DMSO (ppm vs TMS): 7.05 (d, 6H), 7.80 (m, 3H), 7.88 (m, 3H), 8.09 (d, 6H), 8.20 (m, 3H), 8.27 (m, 3H), 8.52 (s, 3H), 8.96 (d, 3H), 9.45 (d, 3H), 10.73 (s, 3H). The ^{1}H-NMR spectrum (Figure 3.4b) of the small (7.8 mg) sample previously obtained from neat ethanol looked quite similar to this sample. No detectable free phen-azo-phenol dye peaks were observed in either spectrum.

Physical Measurements:

The melting point measurements were obtained with a Laboratory Devices MelTemp melting point apparatus. The pH measurements were obtained with an Orion Research Model SA230 pH meter. ^{1}H-NMR spectra were obtained using a General Electric QE-300 FT-NMR spectrometer. UV-Vis spectra were obtained using Shimadzu

UV-3100 and UV-160 spectrophotometers. Elemental analyses were carried out by Atlantic Mircolabs, Norcoross, GA.

Electrochemical measurements were performed on a Princeton Applied Research Model 173 potentiostat/galvanostat connected to a Model 175 universal programmer and a Recorder Company Model 200 XY recorder. TBAH (tetrabutylammonium hexafluorophosphate, 0.1 M) was used as a supporting electrolyte for the measurements in either acetonitrile or dimethylsulfoxide (dried over 3 Å sieves). All samples (where cathodic scans were run) were purged with N_2 prior to measurement. A three-electrode system consisting of a platinum disk or glass carbon working electrode (Bioanalytical Systems, Inc.), a platinum-wire counter electrode (Bioanalytical Systems, Inc.), and a saturated sodium chloride calomel reference (SSCE) electrode (Bioanalytical Systems, Inc.) was used.

Results and Discussion

Synthesis and Purification of Compounds

1. Phen-azo-phenol

The synthesis and purification of the phen-azo-phenol dye were described in a previous thesis.[24] In that thesis, the crude product was purified by either column chromatography using alumina (60:40 ethanol (95%)/chloroform) with the purity checked by elemental analysis and ^{1}H-NMR, or column chromatography using silica gel (90:10 acetic acid/methanol) with the purity checked by only ^{1}H-NMR. In the present work, however, the elemental analysis for the product from the silica gel column was found to be fairly poor (Calcd for $C_{18}H_{12}N_4O$: C, 71.99; H, 4.03; N, 18.66. Found: C, 62.21; H, 3.98; N, 14.76), even though the ^{1}H-NMR spectrum did not show any impurities other than acetic acid and water. Moreover, acetic acid was found to be quite difficult to remove completely by vacuum oven drying. In the ^{1}H-NMR spectra of the products purified on silica, a small peak at 1.90 ppm was always observed which was assigned to the $-CH_3$ group from acetic acid. The above information seems to indicate that purification of phen-azo-phenol on alumina would be the preferred method. However, when sample and alumina column sizes were increased, it was found that the pink-colored impurities were harder to separate from the orange-yellow product fraction compared to the narrower columns used previously. Therefore, in this work, the crude phen-azo-phenol product was purified on silica gel (90:10 acetic acid/methanol) followed by alumina (60:40 ethanol (95%)/chloroform). The silica gel removed a large amount of dark purple impurities and this probably increased the efficiency of the subsequent alumina column. The solid remaining from the evaporation of the solvent after the silica column was not very soluble in the combination of ethanol (95%) and chloroform used for the alumina column. Therefore, the solid was dissolved in a small amount of DMF for loading on the alumina column. The alumina appeared to remove both the DMF and trace acetic acid (based on ^{1}H-NMR spectra). Other than the main yellow fraction, the alumina column showed a

small beige fraction which barely moved and remained at the top of the column. The ethanol/chloroform mix used as an eluant on alumina was easily removed from the products, leaving only the residual water. Therefore, use of two consecutive columns (instead of only alumina) resulted in improvements in the elemental analysis, the melting point, and the overall yield (based on 5-NH_2-phen) as shown in Table 3.1.

		Alumina (60:40 EtOH/$CHCl_3$) only (narrow and long column)			Silica gel (90:10 Hac/MeOH) +Alumina (60:40 EtOH/$CHCl_3$ (wide and short columns)[a]		
Elemental Analysis	$C_{18}H_{12}N_4O$	C, 71.99	H, 4.03	N, 18.66	C, 71.99	H, 4.03	N, 18.66
	$C_{18}H_{12}N_4O \cdot 0.2\ H_2O$				C, 71.14	H, 4.11	N, 18.43
	Found	C, 68.28	H, 4.28	N, 17.36	C, 71.26	H, 4.10	N, 18.32
Melting point		280–282 °C			295–297 °C		
Overall yield (based on 5-NH_2-phen)		19 %			37.9 %		

Table 3.1 Comparisons between phen-azo-phenol products from alumina and silica + alumina columns

The phen-azo-phenol dye was dried under vacuum at 120 °C for 8 h before being sent out for elemental analysis, but it still appeared to contain a small amount of water. Moreover, the amount seemed to vary slightly from batch to batch. The ^{1}H-NMR spectra of each batch of the products showed increased water peaks at 3.4 ppm compared to that of the blank DMSO background spectra.

2. *fac*-$Re^I(CO)_3Cl$(phen-azo-phenol)

The synthesis and purification of this complex were also reported in the previous thesis.[24] However, the compound was never purified completely, and so more extensive purification procedures were attempted in this work. In the preparation of this complex, $Re^I(CO)_5Cl$ and an equivalent amount of phen-azo-phenol were refluxed under N_2 and the

reaction was monitored by TLC (45:55 ethanol (95%)/hexanes). A main spot ($R_f \cong 0.8$) and a very light intermediate spot ($R_f \cong 0.4$, which was thought to be a small amount of an impurity) were observed increasingly during the first few hours, but then they remained almost unchanged. A small amount of free phen-azo-phenol dye was also observed on the TLC's. The precipitate from the reaction was washed with methanol to remove any remaining unreacted free dye, and then by 2,2′,4-trimethyl pentane to remove remaining unreacted $Re^{I}(CO)_5Cl$. Recrystallization from methanol was employed to remove the remaining impurities.

The ^{1}H-NMR (Figure 3.2b) showed that there were some weak peaks at 0.83 and 1.23 ppm which indicated that the purified product was probably contaminated by a small amount of long chain hydrocarbons which were thought to be vacuum grease. It should be noted that vacuum drying the product at elevated temperatures (70 °C) still failed to rid the sample of the upfield ^{1}H-NMR peaks. Grinding in hexane was done to remove the long chain hydrocarbons, but only a slight improvement was observed in the ^{1}H-NMR spectra. Overall, the elemental analysis for the purified product was disappointing but improved when a small amount of long chain hydrocarbons were calculated into the formulation, as shown in Table 3.2. However, the TLC of the purified product still showed a very light shadow at $R_f \cong 0.4$ which appeared to be an impurity. Therefore, if vacuum grease is not the problem, it does appear that the impurity may at least be rich in C and H.

	C	H	N
Calcd for $Re^{I}(CO)_3Cl$(phen-azo-phenol)	41.62	2.00	9.25
Calcd for $Re^{I}(CO)_3Cl$(phen-azo-phenol) $\cdot 0.2C_{10}H_{22}$	43.54	2.60	8.83
Found	43.78	2.61	8.74

Table 3.2 Elemental analyses for $Re^{I}(CO)_3Cl$(phen-azo-phenol)

3. $[Ru^{II}(bpy)_2(phen\text{-}azo\text{-}phenol)](PF_6)_2$

A slight excess (5%) of phen-azo-phenol dye over *cis*-$Ru^{II}(bpy)_2Cl_2 \cdot 2H_2O$ was used in the preparation of this complex. The large excess of NH_4PH_6 was removed by washing with water. There seemed to be a trace amount of free phen-azo-phenol dye in the crude product based on the result of TLC (90:10 acetic acid/methanol) although the ^{1}H-NMR spectrum did not show any definitive free ligand peaks. Due to the relatively high solubility of phen-azo-phenol in ethanol, recrystallization from ethanol (95%) was employed to purify this complex. Diethyl ether was added to the red filtrate from the ethanol recrystallization to produce a second crop of precipitate. Elemental analyses and ^{1}H-NMR spectra of the two batches of products were acceptable with the second crop showing a slightly better elemental analysis.

4. $[Ru^{II}(phen\text{-}azo\text{-}phenol)_3](PF_6)_2$

This complex was synthesized by using a 4-fold (33.3% excess) of phen-azo-phenol dye and a 10-fold (400% excess) of NH_4PF_6 in the preparation in order to drive the equilibrium to the desired product. A fairly large amount of the free phen-azo-phenol dye was observed in the ^{1}H-NMR spectrum of the crude product. TLC was not very suitable for determination of the purity of this compound because of the similarity of the R_f values of the free phen-azo-phenol and the Ru(II) complex coordinated with three phen-azo-phenol ligands. Recrystallization from acetone/water was applied to remove excess NH_4PF_6 and any Ru(II) complexes containing less than three coordinated phen-azo-phenol ligands. Since the free phen-azo-phenol appeared to be significantly more soluble in chloroform than the complex, the product was ultrasonically treated in chloroform to remove unreacted free dye. ^{1}H-NMR spectrum of the sonicated product showed a significant decrease of free phen-azo-phenol. Moreover, the ^{1}H-NMR spectrum of the solid resulting from evaporation of the chloroform filtrate showed almost only free dye. To complete the removal of remaining free ligand, recrystallization from ethanol was employed. Only a small amount of dark red solid was retrieved from this recrystallization. Therefore, an amount of chloroform equal to the volume of the ethanol filtrate, and about twice that amount of diethyl ether were added to the filtrate of the ethanol recrystallization

and this caused precipitation of a large amount of brownish-orange solid. Even though the two solids isolated were significantly different colors, their ^{1}H-NMR spectra were identical and showed no detectable free ligand peaks.

^{1}H-NMR spectra

1. Phen-azo-phenol

The ^{1}H-NMR spectrum of phen-azo-phenol in d_6-DMSO is shown in Figure 3.1 and the data is summarized in Table 3.3. The peak assignments have been revised compared to those reported in a previous thesis.[24] Referring to the numbered phen-azo-phenol structure in Table 3.3, H-4 and H-7 are thought to be similarly coupled to H-3 and H-8, respectively. Moreover, H-2 and H-9 are thought to be similarly coupled to H-3 and H-8. The previous thesis had assigned the peaks centered at 9.31 ppm, 9.23 ppm, and 9.14 ppm to H-2, H-9, and H-4, respectively. As shown in Figure 3.1, the peak pattern and coupling constant of the doublet at 9.31 ppm (H-4, J = 8 Hz) are close to those of the 8.70 ppm doublet (H-7, J = 8 Hz). The peak patterns and coupling constants of other two multiplets at 9.23 ppm (H-2, J = 4 Hz) and 9.14 ppm (H-9, J = 4 Hz) are quite similar. The H-2 and H-9 protons are each coupled to adjacent protons (H-3 and H-8, respectively) that have very similar chemical shifts (7.92 and 7.81 ppm, respectively). The same is true for the H-4 and H-7 positions. The fact that H-4 shows the highest downfield shift could probably be due to the effect of the π-electron circulation on the diazo group.

The two apparent doublets from the phenol moiety are assigned based on the assumed inductive effects from the electron-donating hydroxyl group and the electron-withdrawing diazo group. In addition, the 3′ and 5′ positions on the phenol moiety would be expected to be effected the most from remote metal coordination. This is in fact what was observed (see Table 3.3).

The peak at 10.52 ppm is assigned to be the proton from the –OH group in the phenol moiety. The downfield position of this peak is due to two factors. First, H-bonding with d_6-DMSO causes this resonance to appear far downfield. (The –OH proton for phenol in d_6-DMSO appears at around 9.3 ppm.) Secondly, the electron withdrawing diazo group would be expected to shift the –OH resonance even further downfield. It

should also be noted that the –OH peak has an integrated intensity of slightly less than one (~ 0.9H). This could be due to partial deprotonation of the –OH group in the phenol moiety in the solution of DMSO (see UV-Vis results described later). For this to be true, the $-O^- \leftrightarrow$ –OH exchange rate would have to exceed the ^{1}H-NMR time scale, since only one species could be detected in the spectrum.

2. *fac*-$Re^I(CO)_3Cl$(phen-azo-phenol)

The ^{1}H-NMR spectrum (in d_6-DMSO) of *fac*-$Re^I(CO)_3Cl$(phen-azo-phenol) is shown in Figure 3.2 and the data is summarized in Table 3.3. As described above, the peak assignments for the phen-azo-phenol portion have been revised compared to those reported in a previous thesis.[24] Since all the peaks from *fac*-$Re^I(CO)_3Cl$(phen-azo-phenol) should be from the coordinated phen-azo-phenol fragment, the peak patterns of the free phen-azo-phenol dye and the *fac*-$Re^I(CO)_3Cl$(phen-azo-phenol) complex are quite similar. All peaks from the dye fragment in the Re(I) complex are shifted downfield compared to those of the free phen-azo-phenol. The positive charge on the metal center and the three electron withdrawing carbonyl groups attached to the Re(I) appear to reduce the overall electron density of the phen-azo-phenol fragment. The peaks from the phen moiety of the coordinated phen-azo-phenol are much more affected (downfield shifted by 0.31 – 0.45 ppm) than are those of aromatic protons in the phenol moiety (downfield shifted by 0.02 – 0.07 ppm) because the phen moiety is directly connected to the Re(I) while the phenol moiety is relatively remote from the metal center. However, the peak from the –OH group in the phenol moiety is shifted downfield (by 0.20 ppm) much more than ring hydrogens on the phenol. As in the spectrum of the free phen-azo-phenol, the integrated intensity of the –OH proton is slightly less than one (~ 0.8H).

Table 3.3 Comparison of ^{1}H-NMR (in d_6-DMSO) peak assignments for phen-azo-phenol and *fac*-$Re^I(CO)_3Cl$(phen-azo-phenol)

a. phenanthroline moiety:

	Chemical shift (ppm)[a]							
	2	3	4	5	6	7	8	9
Phen-azo-phenol	9.23	7.92	9.31	—	8.16[b]	8.70	7.81	9.14
fac-$Re^I(CO)_3Cl$ (phen-azo-phenol)	9.56	8.23	9.68	—	8.47[b]	9.15	8.12[d]	9.45
Shift upon coordination	0.33	0.31	0.37	—	0.31	0.45	0.31	0.31

b. phenol moiety:

	Chemical shift (ppm)[a]					
	2′	3′	4′	5′	6′	7′
Phen-azo-phenol	7.03	8.04	—	8.04	7.03	10.52[c]
fac-$Re^I(CO)_3Cl$ (phen-azo-phenol)	7.05	8.11[d]	—	8.11[d]	7.05	10.72[c]
Shift upon coordination	0.02	0.07	—	0.07	0.02	0.20

[a] Unless otherwise noted, all chemical shifts reported are from centers of multiplets.

[b] singlet.

[c] broad singlet.

[d] multiplet obscured by overlapping peaks.

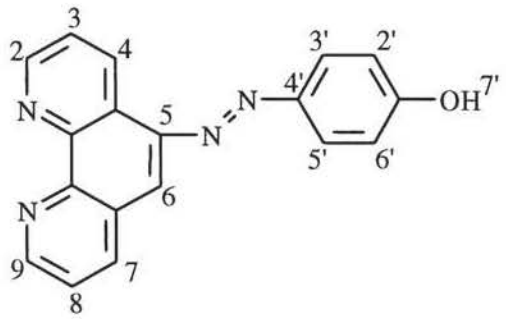

phen-azo-phenol

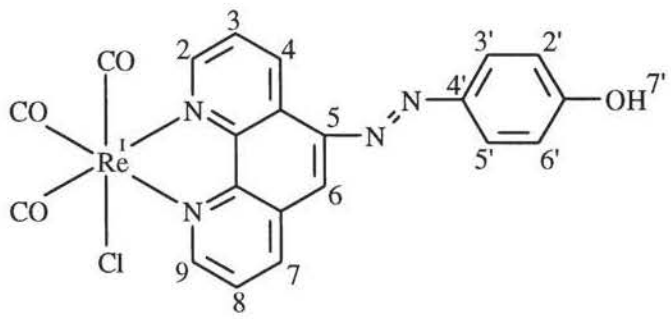

fac-$Re^I(CO)_3Cl$(phen-azo-phenol)

3. $[Ru^{II}(bpy)_2(phen\text{-}azo\text{-}phenol)](PF_6)_2$

The ^{1}H-NMR spectrum (in d_6-DMSO) of $[Ru^{II}(bpy)_2(phen\text{-}azo\text{-}phenol)](PF_6)_2$ is shown in Figure 3.3. The ^{1}H-NMR signals integrate to about 28H, which is the total number expected. Complete assignment of peaks is difficult for this complex due to the overlapping bpy signals. (Therefore, no table equivalent to Table 3.3 is given for this complex.) The singlet at 8.49 ppm can be assigned to the single H on phenanthroline ortho to the diazo linkage. This peak can be compared to the same proton on the phen-azo-phenol coordinated to Re(I) (8.47 ppm, H-6; Table 3.3). The slightly broad singlet peak at 10.72 ppm is assigned to the proton in the –OH group in the phenol moiety. This assignment is also based on a comparison to the spectrum of *fac*-$Re^I(CO)_3Cl(phen\text{-}azo\text{-}phenol)$ (Figure 3.2), in which the –OH proton resonance is at 10.72 ppm. The integrated intensity of this peak is slightly less than one (~ 0.8H).

4. $[Ru^{II}(phen\text{-}azo\text{-}phenol)_3](PF_6)_2$

The ^{1}H-NMR spectrum (in d_6-DMSO) of $[Ru^{II}(phen\text{-}azo\text{-}phenol)_3](PF_6)_2$ is shown in Figure 3.4. In the spectrum of this complex, all proton resonances are from the three phen-azo-phenol ligands coordinated to the Ru(II) center. If the peak at 8.52 ppm is assumed to integrate to 3H (three H atoms ortho to diazo groups), the signals from the whole complex integrate to around 36H, which is the total number expected. As with the previous complexes, the peak at 10.73 ppm is assigned to the –OH proton in the phenol moiety. Once again, the –OH peak has an integrated intensity slightly less than expected.

It might be expected that the ^{1}H-NMR spectrum for this homoleptic complex would be simpler than that for $[Ru^{II}(bpy)_2(phen\text{-}azo\text{-}phenol)](PF_6)_2$. This is in fact the case, although it does not seem to simplify to the spectrum seen for the single phen-azo-phenol coordinated to Re(I). Besides the peaks at 10.73 ppm and 8.52 ppm, Figure 3.4 shows multiplets at 7.05 and 8.09 ppm that can clearly be assigned to the aromatic protons on the phenol moiety. Since the phenol moieties are on the "outside" of the structure, they are free of ligand/ligand interactions and the peak assignments are clear. The phenanthroline resonances, on the other hand, appear broadened due to close and overlapping signals. Moreover, based on the comparisons of the peak patterns and the

coupling constants with those of the free ligand, a peak assignment was made as shown in the Table 3.4. It should be noted that the H atoms ortho to the nitrogen on the phen moiety (H-2 and H-9) are shifted significantly upfield upon coordination. The upfield shift (by ~ 0.95 ppm) of the peaks for H-2 and H-9 may seem unexpected since these are close to the coordinating Ru(II) center. However, literature values for the equivalent sites on bpy and $Ru(bpy)_3^{2+}$ in d_6-DMSO also show an almost identical upfield shift (~ 0.90 ppm).[32] Apparently the back bonding from the Ru(II) contributes to this shift in resonance.

Table 3.4 ^{1}H-NMR (in d_6-DMSO) comparison for phen-azo-phenol and [Ru^{II}(phen-azo-phenol)$_3$](PF$_6$)$_2$

a. phenanthroline moiety:

	Chemical shift (ppm)[a]							
	2	3	4	5	6	7	8	9
Phen-azo-phenol	9.23	7.92	9.31	—	8.16[b]	8.70	7.81	9.14
[Ru^{II}(phen-azo-phenol)$_3$](PF$_6$)$_2$	8.27	7.88	9.45	—	8.52[b]	8.96	7.80	8.20
Shift upon coordination	–0.96	–0.04	0.14	—	0.36	0.26	–0.01	–0.94

b. phenol moiety:

	Chemical shift (ppm)[a]					
	2′	3′	4′	5′	6′	7′
Phen-azo-phenol	7.03	8.04	—	8.04	7.03	10.52[c]
[Ru^{II}(phen-azo-phenol)$_3$](PF$_6$)$_2$	7.05	8.09	—	8.09	7.05	10.73[c]
Shift upon coordination	0.02	0.05	—	0.05	0.02	0.21

[a] Unless otherwise noted, all chemical shifts reported from centers of multiplets.

[b] singlet.

[c] broad singlet.

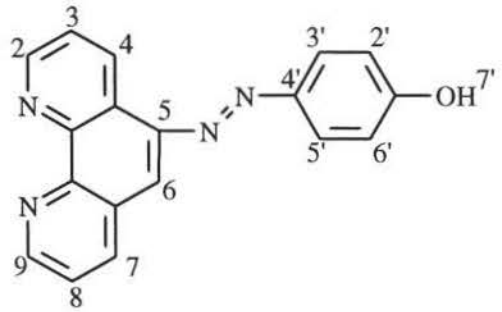

phen-azo-phenol

IR spectrum

***fac*-$Re^{I}(CO)_3Cl$(phen-azo-phenol)**

The IR spectrum (in KBr) of *fac*-$Re^{I}(CO)_3Cl$(phen-azo-phenol) is shown in Figure 3.5 and a summary of the carbonyl stretching frequencies for this complex is shown in Figure 3.6. A significant amount of water is present in the KBr pellet, the water originating from the KBr and probably also from the complex. Three intense carbonyl stretching peaks were observed at 2026.92 cm^{-1}, 1924.33 cm^{-1}, and 1895.40 cm^{-1}, which are quite close to those reported in a previous thesis (2026 cm^{-1}, 1920 cm^{-1}, and 1896 cm^{-1}).[24]

The three-peak pattern for the C≡O stretches appears to be typical for the facial geometries of tricarbonyl chloro-rhenium complexes of polypyridyl ligands.[28] Moreover, assuming a C_s local symmetry, one would expect three C≡O stretches (A″ + 2A′) with two stretches being close to degenerate.

A comparison of the C≡O stretching frequencies of *fac*-$Re^{I}(CO)_3Cl$(phen) and *fac*-$Re^{I}(CO)_3Cl$(phen-azo-phenol) might give some insight into the electron-donating properties of phen-azo-phenol compared to phen. A previous thesis[24] reported four C≡O stretching frequencies (in KBr; 2018, 1933, 1904, and 1879 cm^{-1}) for *fac*-$Re^{I}(CO)_3Cl$(phen), which appears to complicate comparisons. However, the 1879 cm^{-1} peak in that work was significantly less intense than the others. A comparison of the first three peaks would give 2018, 1933, and 1904 cm^{-1} for the phen complex and 2027, 1924, and 1895 cm^{-1} for the phen-azo-phenol complex. The most straightforward comparison would be 2018 cm^{-1} (phen) and 2027 cm^{-1} (phen-azo-phenol), which is presumably the C≡O stretch trans to Cl^-. The +9 cm^{-1} shift for *fac*-$Re^{I}(CO)_3Cl$(phen-azo-phenol) is consistent with the expectation that phen-azo-phenol is expected to be more electron-deficient than phen.

Electrochemistry

Cyclic voltammograms of phen-azo-phenol and its metal complexes as well as some comparison compounds in DMSO or CH_3CN with 0.1 M TBAH (tetrabutylammonium hexafluorophosphate) as the supporting electrolyte are shown in

Figures 3.7 – 3.14. A summary of the electrochemical data is presented in Table 3.5. $E_{1/2}$ values were calculated from the average of the anodic and cathodic peak potentials; $E_{1/2} = (E_{pc} + E_{pa})/2$. Peak separations ($\Delta E_p$) were measured in millivolts (mV); $\Delta E_p = |E_{pc} - E_{pa}|$. Scan rates were 100 mV/s. All potentials are reported versus the saturated sodium chloride calomel electrode (SSCE). DMSO was chosen to be the predominant solvent because it is one of the few solvents found to be able to sufficiently dissolve both the free phen-azo-phenol ligand and the metal complexes.

1. Phen-azo-phenol

The cyclic voltammograms of phen-azo-phenol in DMSO is shown in Figure 3.7. A single irreversible reduction wave at –0.92 V and a single, quasi-reversible (ΔE_p = 83 mV) wave at $E_{1/2} = -1.50$ V were observed. These are assigned as reductions of the azo group and the phen moiety, respectively. It should be noted that a very weak prewave at about –1.46 V was also observed, and this prewave was also observed in the cyclic voltammograms of the phen-azo-phenol metal complexes. The reason for this prewave is not clear. Two quasi-reversible oxidation waves at +0.96 V (ΔE_p = 102 mV) and +1.10 V (ΔE_p = 144 mV) were also observed. These are thought to be multi-electron oxidations of the phenol moiety. In addition, there is a reduction peak at about +0.20 V which appears on the return scan. This must be due to reduction of a species generated during the oxidative sweep out to +1.5 V. The identity of this species was not determined.

2. *fac*-$Re^{I}(CO)_3Cl$(phen) and *fac*-$Re^{I}(CO)_3Cl$(phen-azo-phenol)

The cyclic voltammograms of *fac*-$Re^{I}(CO)_3Cl$(phen) and *fac*-$Re^{I}(CO)_3Cl$(phen-azo-phenol) in DMSO are shown in Figures 3.8 and 3.9. A single, irreversible oxidation wave was observed at +1.18 V for *fac*-$Re^{I}(CO)_3Cl$(phen), which was assigned to be a one-electron oxidation of the Re(I) center. This assignment is based on a comparison to literature reports for the complex in CH_3CN.[33] It was expected that $Re^{I}(CO)_3Cl$(phen-azo-phenol) would give an oxidation wave at a similar potential (possibly anodically shifted somewhat due to the electron-withdrawing azo group on the phen). As shown in Figure 3.9, an irreversible wave was observed at +1.21 V. However, the peak height was

much larger than anticipated for a one-electron oxidation of Re(I). This multi-electron wave probably consists of an oxidation wave from the phenol moiety of the phen-azo-phenol overlapping a smaller wave from the oxidation of Re(I). It should be noted that, given this assignment, the phenol moiety appears slightly harder to oxidize when the phen-azo-phenol is coordinated to the Re(I) (compared to free phen-azo-phenol). Very weak irreversible waves at +0.88 V (in the anodic direction) and ~ +0.15 V (in the cathodic direction) were also observed. The wave at +0.15 V is very close to that previously observed for free phen-azo-phenol.

A quasi-reversible reduction wave ($E_{1/2}$ = –1.22 V; ΔE_p = 110 mV) was observed for *fac*-$Re^{I}(CO)_3Cl$(phen) in DMSO, and this was assigned to a phen ligand-based reduction, based on literature data in CH_3CN.[33] For the *fac*-$Re^{I}(CO)_3Cl$(phen-azo-phenol), an irreversible reduction wave at –0.76 V and a quasi-reversible wave at –1.23 V (ΔE_p = 94 mV, with a prewave at –1.16 V) were observed. These look quite similar to the –0.92 V and –1.50 V (with a prewave at –1.46 V) waves of the free ligand, respectively. Based on this comparison and comparison to the CV of *fac*-$Re^{I}(CO)_3Cl$(phen), these were thought to be ligand-based reductions of the diazo group and the phen moiety, respectively. The phen-azo-phenol reductions in *fac*-$Re^{I}(CO)_3Cl$(phen-azo-phenol) are shifted positively compared to the free ligand reductions. This was thought to be due to the positive charge on the metal center and the three strong π^*-accepting carbonyl groups, which reduce the overall electron density of the coordinated phen-azo-phenol ligand, making the reductions of the ligand easier upon coordination. Another almost irreversible reduction wave was observed for both *fac*-$Re^{I}(CO)_3Cl$(phen) ($E_{1/2}$ = –1.63 V) and *fac*-$Re^{I}(CO)_3Cl$(phen-azo-phenol) ($E_{1/2}$ = –1.69 V), which were probably further reductions of the phen and phen-azo-phenol ligands, based on literature reports for *fac*-$Re^{I}(CO)_3Cl$(phen).[33]

3. $[Ru^{II}(bpy)_3]Cl_2$ and $[Ru^{II}(bpy)_2$(phen-azo-phenol)$](PF_6)_2$

The cyclic voltammograms of $[Ru^{II}(bpy)_3]Cl_2$ and $[Ru^{II}(bpy)_2$(phen-azo-phenol)$](PF_6)_2$ in DMSO and CH_3CN are shown in Figures 3.10 – 3.13.

Oxidation of Ru(II) polypyridyl complexes usually involves a metal centered (π_M (t_{2g}) in octahedral symmetry) orbital, with formation of Ru(III) complexes (low spin $4d^5$ configuration) which are inert to ligand substitution.[2] The cyclic voltammogram usually shows one reversible Ru(II)/Ru(III) oxidation wave at positive potentials vs. SSCE for $Ru^{II}(bpy)_2(LL)^{2+}$ complexes.[34, 35]

The oxidation waves for $[Ru^{II}(bpy)_3]Cl_2$ in CH_3CN are shown in Figure 3.12. This well-characterized compound was used as a standard to aid in peak assignments for $[Ru^{II}(bpy)_2(phen\text{-}azo\text{-}phenol)](PF_6)_2$. $[Ru^{II}(bpy)_3]Cl_2$ does show a fairly reversible, metal-centered one-electron oxidation at $E_{1/2}$ = +1.29 V (ΔE_p = 68 mV). The early oxidation in this spectrum (E_{pa} = +1.05 V) and the later return wave (E_{pc} = +0.71 V) are simply due to the presence of Cl^- in the $[Ru^{II}(bpy)_3]Cl_2$ sample.

The oxidation of $[Ru^{II}(bpy)_2(phen\text{-}azo\text{-}phenol)](PF_6)_2$ in CH_3CN is shown in Figure 3.13. Instead of a single, reversible, one-electron oxidation, a large multi-electron oxidation wave was observed with small return waves. As with the $Re^{I}(CO)_3Cl(phen\text{-}azo\text{-}phenol)$, it appears that the metal-centered oxidation is buried under a multi-electron oxidation of the phenol portion of the coordinated phen-azo-phenol ligand. The sharp (but small) return wave at +1.27 V is most likely the return wave from the oxidation of Ru(II). Assuming a $\Delta E_p \cong 60$ mV, the $E_{1/2}$ for the "buried" Ru(II)/Ru(III) oxidation would be around +1.3 V, close to that for $[Ru^{II}(bpy)_3]Cl_2$ in CH_3CN and to the range of potentials expected for $[Ru^{II}(LL)_3]^{2+}$ oxidations.[2] It is also possible that the "shoulders" recorded at ~ +1.46 V and ~ +1.41 V represent the Ru(II)/Ru(III) couple. In this case, $E_{1/2}$ (Ru(II/III)) would be around 1.43 V. This would also seem reasonable if the phen-azo-phenol ligand was significantly electron deficient.

The oxidation of $[Ru^{II}(bpy)_2(phen\text{-}azo\text{-}phenol)](PF_6)_2$ was also measured in DMSO (Figure 3.11). The oxidation portion of the voltammogram in DMSO looks quite similar to that of *fac*-$Re^{I}(CO)_3Cl(phen\text{-}azo\text{-}phenol)$. The oxidation of Ru(II) center seems to be irreversible in DMSO and overlapped with the overwhelming oxidations of phen-azo-phenol ligand for $[Ru^{II}(bpy)_2(phen\text{-}azo\text{-}phenol)](PF_6)_2$ in DMSO. A very weak, irreversible wave was observed at +0.89 V, similar the +0.88 V wave for *fac*-$Re^{I}(CO)_3Cl(phen\text{-}azo\text{-}phenol)$.

In principle, reduction of Ru(II) polypyridyl complexes may involve either a metal-centered or a ligand-centered orbital, depending on the relative energy ordering. However, ligand-based reduction (on a π_L^* orbital) is the commonly observed behavior.[2] The reference complex, $[Ru^{II}(bpy)_3]Cl_2$, showed three fairly reversible reductions in DMSO that were similar in peak current, wave shape, and peak area: –1.22 V (ΔE_p = 67 mV), –1.40 V (ΔE_p = 68 mV), and –1.65 V (ΔE_p = 68 mV). These were assigned to one-electron reductions of each of the three coordinated bpy ligands based on comparisons with the cyclic voltammograms in CH_3CN.[2] For $[Ru^{II}(bpy)_2(phen\text{-}azo\text{-}phenol)](PF_6)_2$ in DMSO, as is shown in Figures 3.11, an irreversible, a quasi-reversible, and two fairly reversible reduction waves were observed at –0.69 V, –1.18 V (ΔE_p = 99 mV, with a prewave at –1.09 V), –1.31 V (ΔE_p = 65 mV), and –1.53 V (ΔE_p = 71 mV). Based on a comparison to the reductions observed for *fac*-$Re^{I}(CO)_3Cl$(phen-azo-phenol) in DMSO, the waves at E_{pc} = –0.69 V and at $E_{1/2}$ = –1.18 V are assigned as reductions of the azo group and the phen moiety, respectively, of the coordinated phen-azo-phenol ligand. The waves at $E_{1/2}$ = –1.31 V and –1.53 V are assigned as sequential reductions of the bpy ligands based on comparison to the data obtained for $[Ru^{II}(bpy)_3]Cl_2$ in DMSO.

The reduction of $[Ru^{II}(bpy)_2(phen\text{-}azo\text{-}phenol)](PF_6)_2$ was also measured in CH_3CN as shown in Figure 3.13. Reduction waves at E_{pc} = –0.75 V and $E_{1/2}$ = –1.17 V (ΔE_p = 85 mV, with a prewave at –1.10 V), –1.24 V (ΔE_p = 65 mV), and –1.43 V (ΔE_p = 92 mV) are assigned to the same sequence of reductions as noted above for the DMSO solution.

4. $[Ru^{II}(phen\text{-}azo\text{-}phenol)_3](PF_6)_2$

The cyclic voltammograms of $[Ru^{II}(phen\text{-}azo\text{-}phenol)_3](PF_6)_2$ in DMSO are shown in Figure 3.14. The oxidation process looks similar (but with less distinct shoulders) to the other two complexes containing one phen-azo-phenol ligand. Since three phen-azo-phenol ligands are coordinated, it would be expected that the irreversible oxidation wave assigned as phenol oxidation would be significantly larger than for either $[Ru^{II}(bpy)_2(phen\text{-}azo\text{-}phenol)](PF_6)_2$ or *fac*-$Re^{I}(CO)_3Cl$(phen-azo-phenol). From the data shown in Figures 3.9 to 3.14, it does not appear that this is the case. However, since the exact

concentrations of the complexes were not ever known during each CV experiment, it is not possible to exactly compare current amplitudes. Moreover, the oxidation waves were always "shoulders" on an increasing background current, at least in DMSO.

The reduction of $[Ru^{II}(phen\text{-}azo\text{-}phenol)_3](PF_6)_2$ was quite similar in features to that of the free ligand and the *fac*-$Re^{I}(CO)_3Cl$(phen-azo-phenol) complex. An irreversible wave and a quasi-reversible (with a weak prewave) wave were observed at –0.73 V and –1.20 V (ΔE_p = 152 mV, with a prewave at –1.16 V), respectively. These were assigned to the reductions of the azo group and phen moiety in the coordinated phen-azo-phenol fragment. These reduction potentials decreased by 0.19 and 0.30 V, respectively, compared to those of free phen-azo-phenol, and are quite close to the potential changes observed for *fac*-$Re^{I}(CO)_3Cl$(phen-azo-phenol).

Table 3.5 Electrochemical data for phen-azo-phenol, Re(I) and Ru(II) complexes, and related compounds

Compound	Solvent	$E_{1/2}$ (V) (ΔE_p (mV))	
		Oxidation	reduction
Phen-azo-phenol	DMSO	+0.96 (102) +1.10 (144) +0.20 (irr, E_{pc})	–0.92 (irr) –1.46 (irr, prewave) –1.50 (83)
fac-$Re^{I}(CO)_3Cl$(phen)	DMSO	+1.18 (irr)	–1.22 (110) –1.63 (irr)
fac-$Re^{I}(CO)_3Cl$(phen-azo-phenol)	DMSO	+0.88 (irr, E_{pa}) +1.21 (irr) +0.15 (irr, E_{pc})	–0.76 (irr) –1.16 (irr, prewave) –1.23 (94) –1.69 (irr)
$Ru^{II}(bpy)_3Cl_2$	DMSO		–1.22 (67) –1.40 (68) –1.65 (68)
	CH_3CN	+1.05 (irr, E_{pa}) +1.29 (68) +0.71 (irr, E_{pc})	
$[Ru^{II}(bpy)_2$(phen-azo-phenol)$](PF_6)_2$	DMSO	+0.89 (irr, E_{pa}) +1.21 (irr)	–0.69 (irr) –1.09 (irr, prewave) –1.18 (99) –1.31 (65) –1.53 (71)
	CH_3CN	+1.31 (irr) +1.46 (shoulder, E_{pa}) +1.41 (shoulder, E_{pc}) +1.27 (irr, E_{pc}) +0.21 (irr, E_{pc})	–0.75 (irr) –1.10 (irr, prewave) –1.17 (85) –1.24 (65) –1.43 (92)
$[Ru^{II}$ (phen-azo-phenol)$_3](PF_6)_2$	DMSO		–0.73 (irr) –1.16 (irr, prewave) –1.20 (152)

irr = irreversible

E_{pa} = peak recorded in anodic scan direction

E_{pc} = peak recorded in cathodic scan direction

UV-Vis spectra

1. Phen-azo-phenol

The UV-Vis spectra of phen-azo-phenol in methanol and DMSO are shown in Figures 3.15 and 3.17, respectively, and the λ_{max} and ε values are summarized in Table 3.7. The spectrum in methanol is similar to that reported in a previous thesis.[24] In the methanol solution, the longest wavelength absorption was observed at 379 nm with a molar extinction coefficient $\varepsilon = 2.87 \times 10^4\ M^{-1}\ cm^{-1}$ (obtained from Beer-Lambert plotting as shown in Figure 3.16). This absorption corresponds to ligand centered $n \rightarrow \pi^*$ or $\pi \rightarrow \pi^*$ transitions. This assignment is in agreement with literature on azo compounds containing an electron-releasing group with lone pairs.[23] For example, the extinction coefficient of the longest wavelength band ($\lambda_{max} = 408$ nm) of dimethylaminophenylazo-benzene is known to be $\varepsilon = 2.75 \times 10^4\ M^{-1}\ cm^{-1}$ in 95 % ethanol.[23]

As shown in Figure 3.17, phen-azo-phenol (1.928×10^{-5} M) shows an extra absorption band in DMSO at about 544 nm. The ratio of the intensity of this peak to the intensity of the shorter wavelength absorption at 387 nm increased as the concentration of phen-azo-phenol decreased. It was suspected that this behavior was due to the deprotonation of the –OH group in the phenol moiety:

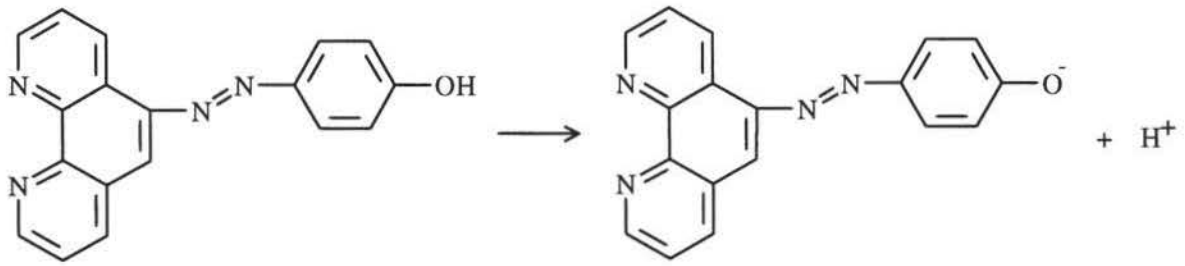

This was confirmed by intentional addition of small amounts of acid or base. With the addition of a fraction of a drop[a] of conc. H_2SO_4 to ~ 2.5 mL of a DMSO solution of phen-azo-phenol, the color of the solution changed from yellowish pink to light yellow, the absorption at 544 nm disappeared, and the 387 nm peak ($\varepsilon = 2.25 \times 10^4\ M^{-1}\ cm^{-1}$)

[a] The DMSO/phen-azo-phenol solution was simply touched with a narrowed capillary pipet (used for spotting TLC plates) containing a very small amount of conc. H_2SO_4.

increased and red-shifted to 396 nm ($\varepsilon = 2.52 \times 10^4$ M^{-1} cm^{-1}). The spectrum is shown in Figure 3.18. With the addition of about half a drop[b] of a 10% aqueous solution of NaOH to ~ 2.5 mL of a fresh DMSO solution of phen-azo-phenol, the color changed to pink-violet, the 387 nm peak almost disappeared, and the intensity of the 544 nm peak (originally $\varepsilon = 9.34 \times 10^3$ M^{-1} cm^{-1}) increased dramatically (to $\varepsilon = 5.51 \times 10^4$ M^{-1} cm^{-1}). The spectrum is shown in Figure 3.19. If the low energy transitions on phen-azo-phenol originate from orbitals centered on the –OH group, deprotonation should red-shift these absorptions. This is in fact what occurs.

2. *fac*-$Re^I(CO)_3Cl$(phen-azo-phenol)

Spectroscopic comparisons of *fac*-$Re^I(CO)_3Cl$(phen-azo-phenol) with the well-characterized analog *fac*-$Re^I(CO)_3Cl$(phen) and with free phen-azo-phenol in methanol were reported in a previous thesis.[24] The intense absorption of *fac*-$Re^I(CO)_3Cl$(phen-azo-phenol) at 390 nm ($\varepsilon = 3.35 \times 10^4$ M^{-1} cm^{-1})[24] was thought to be a mixture of MLCT and LC transitions. The spectrum of the *fac*-$Re^I(CO)_3Cl$(phen-azo-phenol) sample synthesized in this thesis is nearly identical to the previously reported compound, as shown in Figure 3.20.

The UV-Vis spectrum of *fac*-$Re^I(CO)_3Cl$(phen-azo-phenol) in DMSO is shown in Figure 3.21. A strong absorption was observed at 400 nm ($\varepsilon = 2.14 \times 10^4$ M^{-1} cm^{-1}), and it was assigned as a mixture of MLCT and LC bands. In addition, an intense long-wavelength band was also observed at 588 nm ($\varepsilon = 2.02 \times 10^4$ M^{-1} cm^{-1}). The ratio of the intensity of the absorption at 588 nm to that at 400 nm increased as the concentration decreased. As with the free ligand, the long-wavelength band was thought to be the result of deprotonation of the –OH group in the phenol moiety of the coordinated phen-azo-phenol ligand. This was confirmed by an experiment analogous to that performed with the free ligand. Figures 3.22 and 3.23 show the UV-Vis spectra of the completely protonated (DMSO + H_2SO_4) and deprotonated (DMSO + NaOH) forms of *fac*-$Re^I(CO)_3Cl$(phen-azo-phenol). Upon addition of conc. H_2SO_4 to a DMSO solution of the complex, the

[b] The DMSO/phen-azo-phenol solution was simply touched with a capillary tube containing a small amount of 10% NaOH; approximately half of a drop.

color of the solution changed from light navy to light yellow, the 400 nm absorption increased in intensity (to $\varepsilon = 2.80 \times 10^4\ M^{-1}\ cm^{-1}$) and the absorption at 588 nm disappeared. Upon addition of 10% NaOH to a fresh DMSO solution of the complex, the color changed to cobalt blue, the absorption at ~ 400 nm decreased significantly (403 nm, $\varepsilon = 7.64 \times 10^3\ M^{-1}\ cm^{-1}$), and the absorption at 588 nm increased dramatically and blue-shifted slightly ($\lambda_{max} = 583$ nm, $\varepsilon = 5.58 \times 10^4\ M^{-1}\ cm^{-1}$). The residual absorption at 403 nm is probably an MLCT transition arising from excitation of an electron from a Re(I) HOMO π_M (t_{2g}) orbital to the LUMO π_L^* phen orbital. The MLCT transition would thus be red-shifted from that of *fac*-$Re^I(CO)_3$(phen) ($\lambda_{max} = 370$ nm in methanol;[24] $\lambda_{max} = 377$ nm in CH_2Cl_2[36]) as would be expected for the presence of the more electron deficient azo linkage on position # 5 of the phenanthroline ring. This MLCT band does overlap on the tail of the strong peak at 583 nm. There is a noticeable shift in the λ_{max} of deprotonated phen-azo-phenol between the free ($\lambda_{max} = 544$ nm) and Re(I)-coordinated ($\lambda_{max} = 588$ nm) forms. In the previous section, it was stated that the long-wavelength absorption of the deprotonated phen-azo-phenol arose from transitions arising from the $-O^-$ group. The acceptor orbitals in this transition appear to be lowered in energy by Re(I) coordination, since the transition is red-shifted upon coordination of the ligand to the metal. Those acceptor orbitals are most likely centered on the electron deficient azo linkage.

3. $[Ru^{II}(bpy)_2$(phen-azo-phenol)$](PF_6)_2$

The UV-Vis spectrum of $[Ru^{II}(bpy)_2$(phen-azo-phenol)$](PF_6)_2$ in CH_3CN is shown in Figure 3.24[c]. The intense absorption band at 286 nm ($\varepsilon = 6.27 \times 10^4\ M^{-1}\ cm^{-1}$) is assigned to a ligand-based (LC) $\pi \rightarrow \pi^*$ transition by comparisons with the spectra of the $Ru^{II}(bpy)_3^{2+}$ and $Ru^{II}(phen)_3^{2+}$ complexes.[2, 37, 38] Based on the same comparisons, the absorption maximum at 448 nm ($\varepsilon = 2.30 \times 10^4\ M^{-1}\ cm^{-1}$) is assigned to spin-allowed charge transfer from the metal π_M (t_{2g}) orbitals to the π_L^* orbitals of the phen-azo-phenol ligand (MLCT transition). As shown in Figure 3.24, an intense absorption at 386 nm was

[c] Among the metal complexes synthesized in this work, only the $[Ru^{II}(bpy)_2$(phen-azo-phenol)$](PF_6)_2$ was soluble enough in CH_3CN to measure ε values.

also observed in CH_3CN ($\varepsilon = 2.73 \times 10^4\ M^{-1}\ cm^{-1}$). This band is probably due to $n \rightarrow \pi^*$ or $\pi \rightarrow \pi^*$ transitions arising from the phen-azo-phenol ligand, based on comparisons with the UV-Vis spectra of the free phen-azo-phenol ligand (λ_{max} = 375 nm in CH_3CN), $Ru^{II}(bpy)_3^{2+}$, and $Ru^{II}(phen)_3^{2+}$. The LC band at 386 nm and the MLCT band at 448 nm overlap to enhance the intensity of the high energy shoulder typically seen on the MLCT bands of $Ru^{II}(LL)_3^{2+}$ complexes. Here, this shoulder appears as a band at 418 nm ($\varepsilon = 2.50 \times 10^4\ M^{-1}\ cm^{-1}$).

As shown in Figure 3.25, a long wavelength absorption at ~ 595 nm was observed for $[Ru^{II}(bpy)_2(phen\text{-}azo\text{-}phenol)](PF_6)_2$ in DMSO. The intensity of this absorption relative to that around 450 nm increased with decreasing concentration. This behavior is very similar to that already described for the free ligand and its Re(I) complex in DMSO, and therefore is thought to be due to the deprotonation equilibrium of the coordinated phen-azo-phenol ligand. The spectrum of the fully protonated form (DMSO + H_2SO_4) is shown in Figure 3.26. Here the MLCT absorption (~ 452 nm) appears as a shoulder on the more intense LC absorption of the phen-azo-phenol ligand (~ 395 nm). The deprotonated form of $[Ru^{II}(bpy)_2(phen\text{-}azo\text{-}phenol)](PF_6)_2$ has the spectra shown in Figure 3.27. The intense absorption at ~ 590 nm overshadows the smaller MLCT absorption at ~ 452 nm.

Since this complex is partially water soluble, an experiment was carried out to determine the pKa of the phenol moiety of coordinated phen-azo-phenol in aqueous solution. In this experiment, 0.1 mL of a 2.94×10^{-4} M solution of $[Ru^{II}(bpy)_2(phen\text{-}azo\text{-}phenol)](PF_6)_2$ in DMSO was added to 10 mL of an aqueous buffer solution. The buffers used were prepared from H_2SO_4, acetic acid, NaH_2PO_4, Na_2HPO_4, and Na_3PO_4 and the pH values were 0.46, 1.20, 2.66, 4.26, 5.84, 6.65, 7.44, 7.93, 8.29, 8.70, 9.59, 10.55, 11.38, and 12.28. A full spectrum was obtained for each solution.

Two interesting results were obtained from this experiment. First, the λ_{max} of the deprotonated form of the complex in aqueous solution (466 nm) was blue-shifted dramatically from that in DMSO. This was thought to be due to strong H-bonding from the water to the deprotonated phenol, minimizing the effect of the deprotonation. Secondly as shown in Figure 3.28, the pKa of the phenol moiety of phen-azo-phenol is

around 7.7 as measured by the growth of the absorption at 466 nm. This can be compared to the pKa of phenol (9.99) and 4-nitro-phenol (7.150),[39] and reflects the electron-withdrawing nature of the diazo linkage.

4. $[Ru^{II}(phen\text{-}azo\text{-}phenol)_3](PF_6)_2$

The UV-Vis spectrum of $[Ru^{II}(phen\text{-}azo\text{-}phenol)_3](PF_6)_2$ in DMSO is shown in Figure 3.29. As might be expected, the spectrum looks similar to that of $[Ru^{II}(bpy)_2(phen\text{-}azo\text{-}phenol)](PF_6)_2$ in DMSO (Figure 3.25) with the peaks due to the phen-azo-phenol being significantly enhanced in intensity. For example, absorptions around 403 nm and 598 nm, both previously identified as arising from coordinated phen-azo-phenol, show enhanced intensity relative to the MLCT transition (~ 461 nm) when compared to the analogous absorptions in the spectrum of $[Ru^{II}(bpy)_2(phen\text{-}azo\text{-}phenol)](PF_6)_2$.

As previously observed with free phen-azo-phenol and the other complexes in DMSO, the intensity of the long wavelength absorption increases relative to the absorption intensity at 403 nm as the concentration of the complex decreases. In addition, the $\pi \rightarrow \pi^*$ LC absorption at < 300 nm for $[Ru^{II}(phen\text{-}azo\text{-}phenol)_3](PF_6)_2$ does appear to be shifted to higher energy.

The spectra of $[Ru^{II}(phen\text{-}azo\text{-}phenol)_3](PF_6)_2$ with added H_2SO_4 and added NaOH in DMSO are shown in Figures 3.30 and 3.31, respectively. In the presence of acid, the 598 nm band disappeared and the intensities of the LC (λ_{max} = 269 nm, $\varepsilon = 6.08 \times 10^4$ M^{-1} cm^{-1}; λ_{max} = 400 nm, $\varepsilon = 4.82 \times 10^4$ M^{-1} cm^{-1}) and MLCT (λ_{max} = 461 nm, $\varepsilon = 3.40 \times 10^4$ M^{-1} cm^{-1}) bands all increased. The increased intensities for the absorptions at 269 nm and 461 nm are most likely the result of a significant increase in absorption at 400 nm (–OH form of phen-azo-phenol) and the overlap of this band with the other two. As expected, the –OH form of $[Ru^{II}(phen\text{-}azo\text{-}phenol)_3](PF_6)_2$ shows a significantly higher intensity absorption at ~ 400 nm compared to acidified $[Ru^{II}(bpy)_2(phen\text{-}azo\text{-}phenol)](PF_6)_2$ in DMSO. Likewise, the deprotonated form of $[Ru^{II}(phen\text{-}azo\text{-}phenol)_3](PF_6)_2$ shows a much more intense absorption at ~ 598 nm than the corresponding Ru(II) complex containing only one phen-azo-phenol ligand.

5. Additional Spectral Data in MeOH

Spectra for the free ligand and for *fac*-$Re^{I}(CO)_3Cl$(phen-azo-phenol) previously obtained in methanol initially appeared to be free of deprotonated product. However, upon reexamination of the spectrum of phen-azo-phenol in methanol (Figure 3.15), a previously unnoticed weak shoulder at ~ 450 – 480 nm was observed. This absorption disappears upon addition of conc. H_2SO_4 (Figure 3.32) but became dominant (λ_{max} = 453 nm) upon addition of aqueous NaOH (Figure 3.33). A similar very weak shoulder at ~ 500 nm was found in the spectrum of *fac*-$Re^{I}(CO)_3Cl$(phen-azo-phenol) in methanol (Figure 3.20). In a manner similar to the free ligand, this absorption disappeared in methanol + H_2SO_4 and dominated in methanol + NaOH (Figures 3.34 and 3.35, respectively).

Additional UV-Vis spectra in methanol were obtained for both $[Ru^{II}(bpy)_2$(phen-azo-phenol)$](PF_6)_2$ and $[Ru^{II}$(phen-azo-phenol$)_3](PF_6)_2$. As seen in Figure 3.36, the spectrum of $[Ru^{II}(bpy)_2$(phen-azo-phenol)$](PF_6)_2$ did in fact still show evidence for some deprotonation (*i.e.* shoulder at ~ 515 nm). This was confirmed by addition of conc. H_2SO_4 to the methanol solution. The shoulder at ~ 515 nm disappeared and the spectrum resembled that obtained in CH_3CN, with the MLCT absorption at ~ 446 nm and the LC absorption of phen-azo-phenol at ~ 395 nm (see Figure 3.37). When aqueous 10% NaOH was added to a fresh solution of $[Ru^{II}(bpy)_2$(phen-azo-phenol)$](PF_6)_2$ in methanol, the absorption at 395 nm disappeared and a broad, intense band (λ_{max} = 504 nm; LC absorption of deprotonated phen-azo-phenol) appeared with a significant shoulder at ~ 463 nm (MLCT transition), as shown in Figure 3.38. The spectra of $[Ru^{II}$(phen-azo-phenol$)_3](PF_6)_2$ in methanol, methanol + conc. H_2SO_4, and methanol + aqueous 10% NaOH (Figures 3.39, 3.40, and 3.41, respectively) showed similar behavior.

6. Solvent dependence of coordinated phen-azo-phenol ionization

When the phen-azo-phenol is free in solution or coordinated to Re(I) or Ru(II), the ionization of the phenol moiety and the spectra of the deprotonated form are strongly solvent dependent. Using $[Ru^{II}(bpy)_2$(phen-azo-phenol$)](PF_6)_2$ as an example (soluble in the broadest range of solvents), the following summary can be examined.

Solvent	Relative extent of ionization of phenol moiety	λ_{max} of –OH form	λ_{max} of $-O^-$ form
CH_3CN	no ionization observed	~ 386 nm	—
MeOH	slightly ionization	~ 395 nm	504 nm
DMSO	significant ionization	~ 395 nm	590 nm
H_2O	(pH dependent)	~ 377 nm	466 nm

Table 3.6 Solvent dependence of ionization of coordinated phen-azo-phenol in $[Ru^{II}(bpy)_2(phen\text{-}azo\text{-}phenol)](PF_6)_2$

The relative extent of ionization of the phen-azo-phenol in various solvents should depend on the ability of those solvents to act as H^+ acceptors (basicity). The energy of the transitions of the deprotonated forms seems to correlate with the H-bonding capabilities of the solvents.

The very strong solvent dependence of the λ_{max} of deprotonated phen-azo-phenol is apparent in Table 3.6 and 3.7. As stated previously, if the visible absorption of phen-azo-phenol arises from a transition from an orbital localized on the –OH group to an orbital localized on the azo linkage, deprotonation of the –OH group would be expected to red-shift the absorption. This is in fact observed. Moreover, the extent of interaction between $-O^-$ and the solvent would be expected to be greater than between –OH group and the solvent. This also appears to be observed, as only the absorption of the deprotonated form seems strongly solvent dependent. Finally, strong H-bonding in MeOH and H_2O partially replaces the lost H^+ from the phenol moiety, lowering the absolute energies of the $-O^-$-centered orbitals, and blue-shifting the observed λ_{max} of the deprotonated form of phen-azo-phenol relative to DMSO.

Table 3.7 UV-Vis spectral data of phen-azo-phenol and related metal complexes

Compound	Solvent	λ_{max} (nm) (extinction coefficient $\varepsilon \times 10^{-4}$ M^{-1} cm^{-1})
Phen-azo-phenol	methanol	221 (3.22) 251 (2.20) 273 (2.18) 379 (2.87)
	methanol + acid	282 (2.26) 388 (2.53)
	methanol + base	274 (2.44) 453 (3.03)
	DMSO	278 (sh, 2.36) 387 (2.25) 544 (0.934)
	DMSO + acid	285 (2.26) 396 (2.52)
	DMSO + base	312 (1.18) 544 (5.51)
Fac-$Re^{I}(CO)_3Cl$(phen-azo-phenol)	Methanol	279 390 (3.35[a])
	Methanol + acid	248 (sh) 280 390
	methanol + base	274 497
	DMSO	284 (sh, 2.01) 400 (2.14) 588 (2.02)
	DMSO + acid	284 (2.04) 400 (2.80)
	DMSO + base	297 (sh, 1.94) 403 (0.764) 583 (5.58)

[a] reference 24.

Table 3.7 UV-Vis spectral data of phen-azo-phenol and related metal complexes (continued)

Compound	Solvent	λ_{max} (nm) (extinction coefficient $\varepsilon \times 10^{-4}$ M^{-1} cm^{-1})
$Ru^{II}(bpy)_3Cl^b$	methanol	454 (1.46)
$Ru^{II}(phen)_3Cl^b$	methanol	446 (1.90)
$[Ru^{II}(bpy)_2(phen\text{-}azo\text{-}phenol)](PF_6)_2$	CH_3CN	286 (6.27) 386 (2.73) 418 (2.50) 448 (2.30)
	DMSO	290 (6.67) 395 (sh, 1.84) 429 (2.26) 452 (2.23) 595 (3.74)
	DMSO + acid	290 (6.68) 395 (2.80) 423 (3.02) 452 (2.72)
	DMSO + base	292 (7.15) 460 (sh, 2.04) 590 (4.62)
	methanol	286 (6.92) 395 (sh, 2.26) 423 (sh, 2.75) 454 (3.14) 515 (sh, 2.14)
	methanol + acid	286 (6.74) 395 (3.14) 414 (3.22) 446 (2.82)
	methanol + base	286 (7.23) 463 (sh, 3.92) 504 (4.32)

[b] reference 38.

Table 3.7 UV-Vis spectral data of phen-azo-phenol and related metal complexes (continued)

Compound	Solvent	λ_{max} (nm) (extinction coefficient $\varepsilon \times 10^{-4}$ M^{-1} cm^{-1})
$[Ru^{II}(phen\text{-}azo\text{-}phenol)_3](PF_6)_2$	DMSO	268 (5.83) 403 (3.33) 461 (sh, 2.57) 598 (5.81)
	DMSO + acid	269 (6.08) 400 (4.82) 461 (sh, 3.40)
	DMSO + base	267 (5.87) 598 (12.8)
	methanol	267 (5.83) 403 (3.83) 465 (3.97) 512 (sh, 3.15)
	methanol + acid	266 (5.94) 398 (5.10) 454 (sh, 3.53)
	methanol + base	268 (5.80) 513 (7.42)

Conclusions and Future Work

An azo-phenol group has been introduced into 1,10-phenanthroline to form the phen-azo-phenol ligand. The phen-azo-phenol ligand coordinates to Re(I) and Ru(II) metal centers through the phenanthroline linkage. This is supported by both spectral and electrochemical data. The introduction of the azo group, which improves the absorption of the ligand itself in the visible region, enhances the absorption properties in the visible spectrum of the metal complexes containing one or more phen-azo-phenol ligands while retaining the stability and redox properties of traditional polypyridyl complexes. Such complexes might be useful in areas such as solar energy conversion and photosynthesis because of the broad absorption spectrum. The deprotonation of the –OH group on the phenol moiety of the phen-azo-phenol ligand changes the absorption properties of both the ligand and the metal complexes containing this ligand. This deprotonation equilibrium and the strong solvent dependence of the deprotonated species means that Re(I) and Ru(II) complexes of phen-azo-phenol can strongly absorb photons ranging in wavelength from < 300 nm to well over 600 nm.

Future work will involve comparing the emission properties of phen-azo-phenol and its Re(I) and Ru(II) complexes with the analogous phenanthroline derivatives. In addition, there will be an investigation into the efficiency of the population of the lowest energy excited states in the phen-azo-phenol complexes by visible light absorption and comparison to analogous complexes containing only bpy or phen ligands.

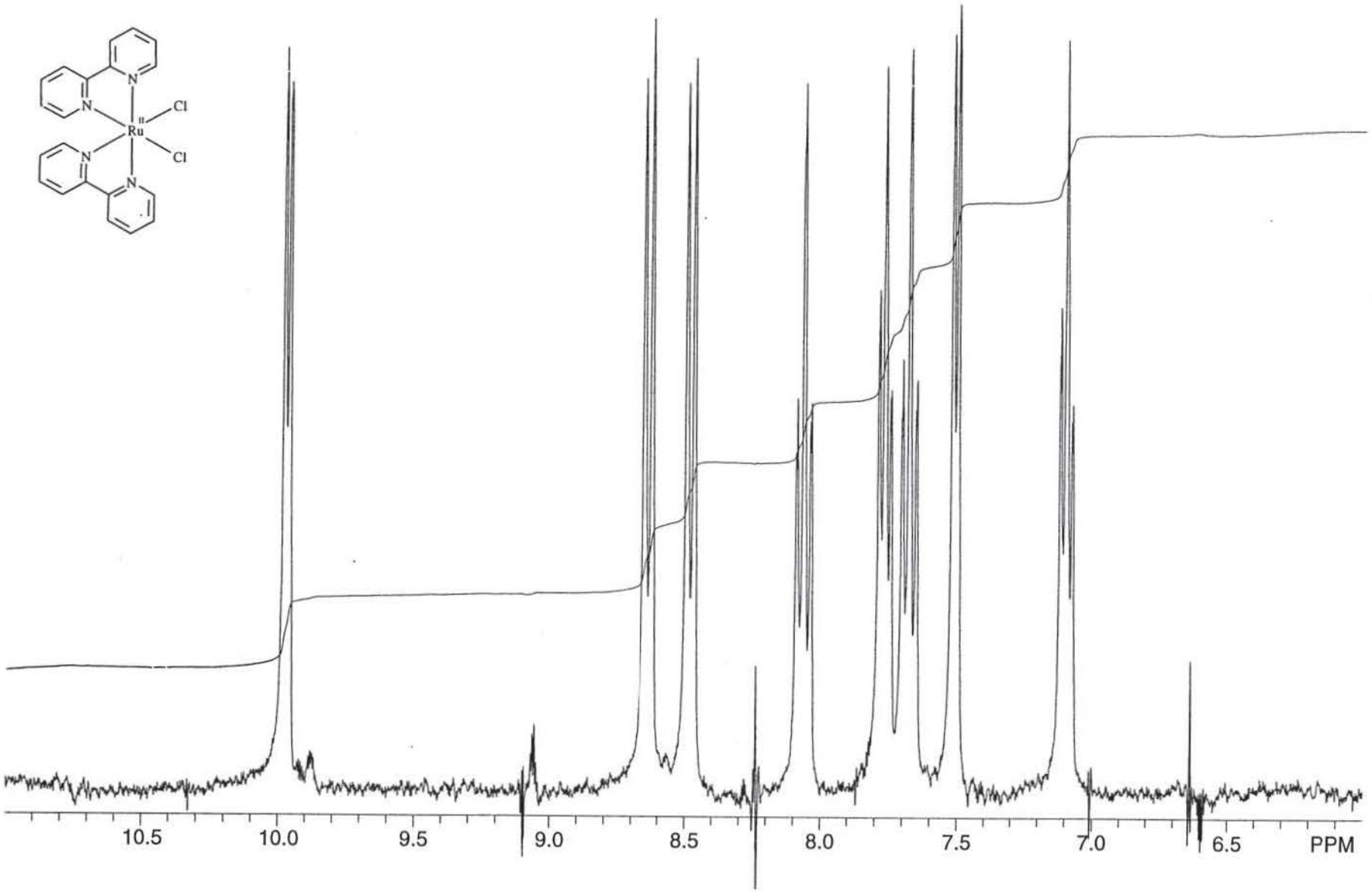

Figure 2.1 ^{1}H-NMR spectrum of *cis*-$Ru^{II}(bpy)_2Cl_2 \cdot 2H_2O$ in d_6-DMSO

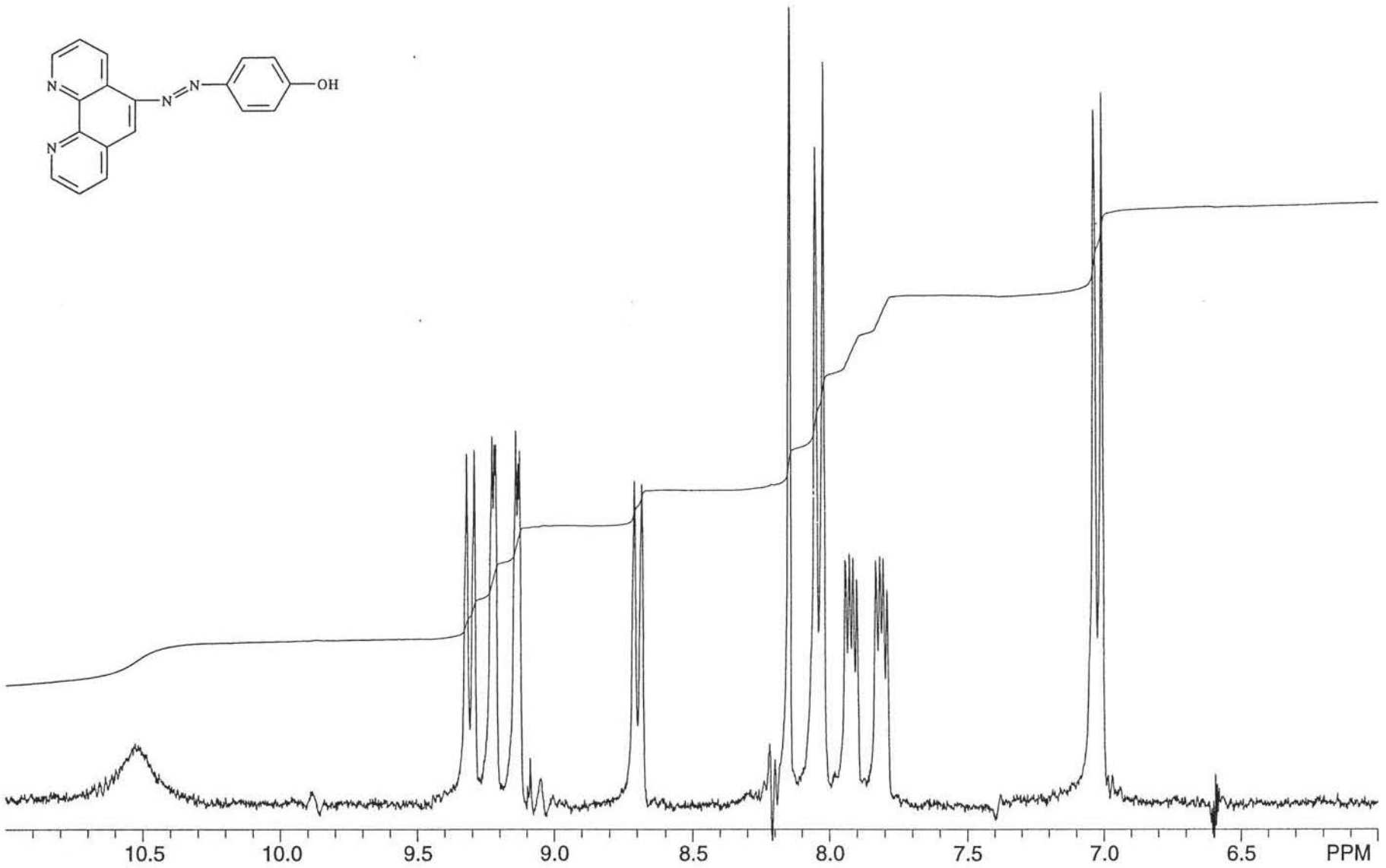

Figure 3.1 ^{1}H-NMR spectrum of phen-azo-phenol in d_6-DMSO

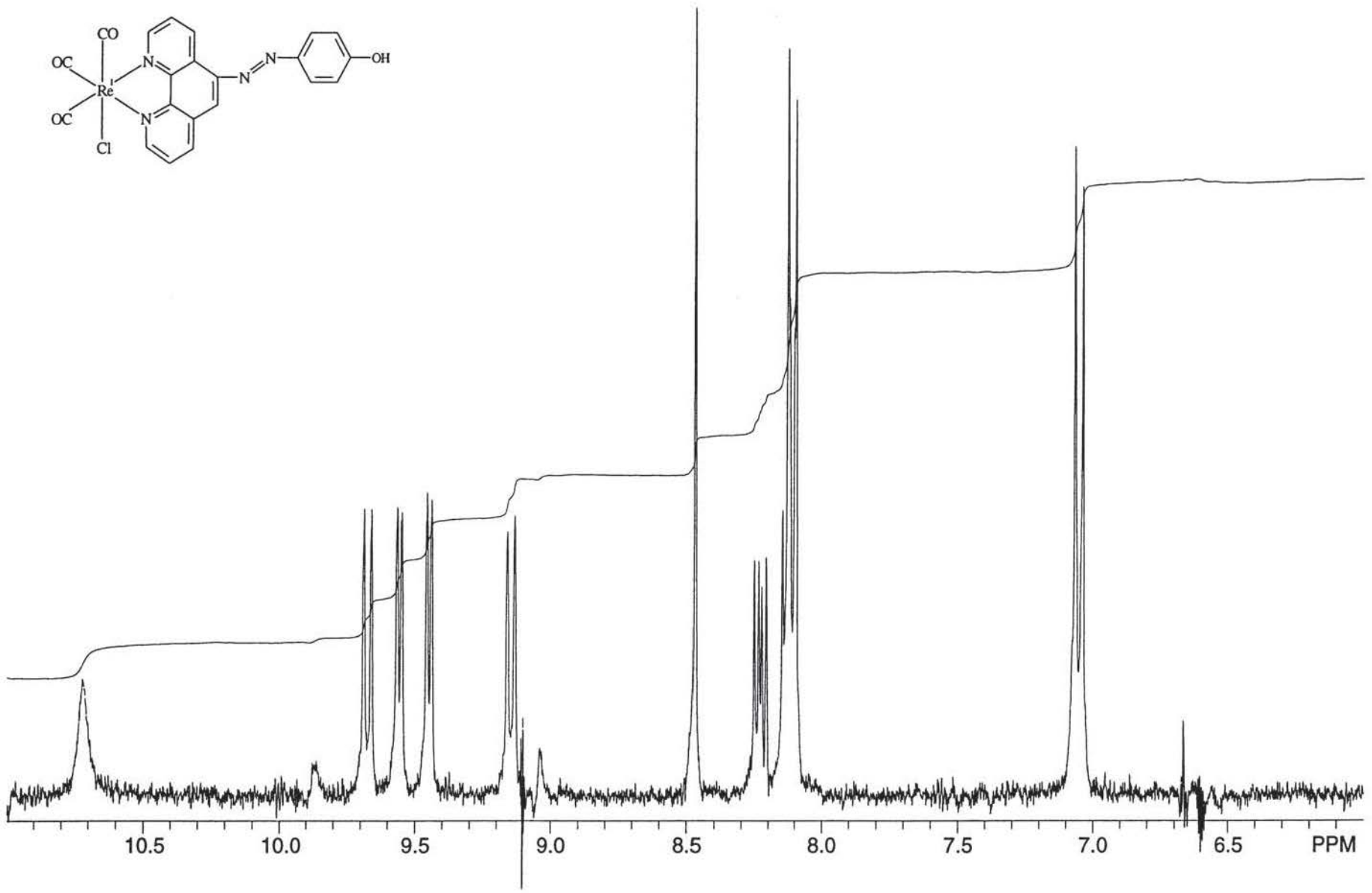

Figure 3.2a ^{1}H-NMR spectrum of *fac*-$Re^{I}(CO)_3Cl$(phen-azo-phenol) in d_6-DMSO (6 – 11 ppm)

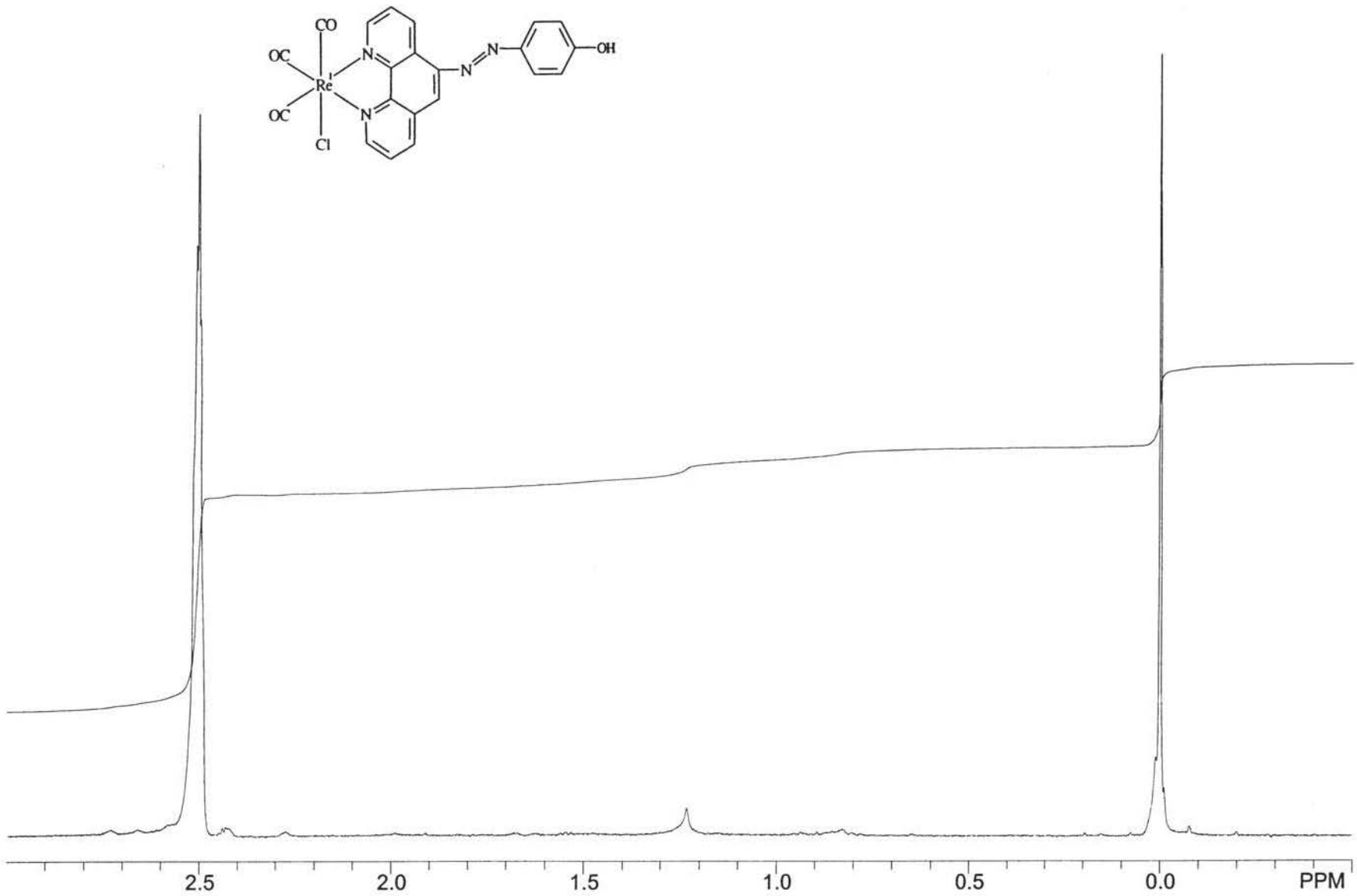

Figure 3.2b ^{1}H-NMR spectrum of *fac*-$Re^{I}(CO)_3Cl$(phen-azo-phenol) in d_6-DMSO (-0.5 – 3 ppm)

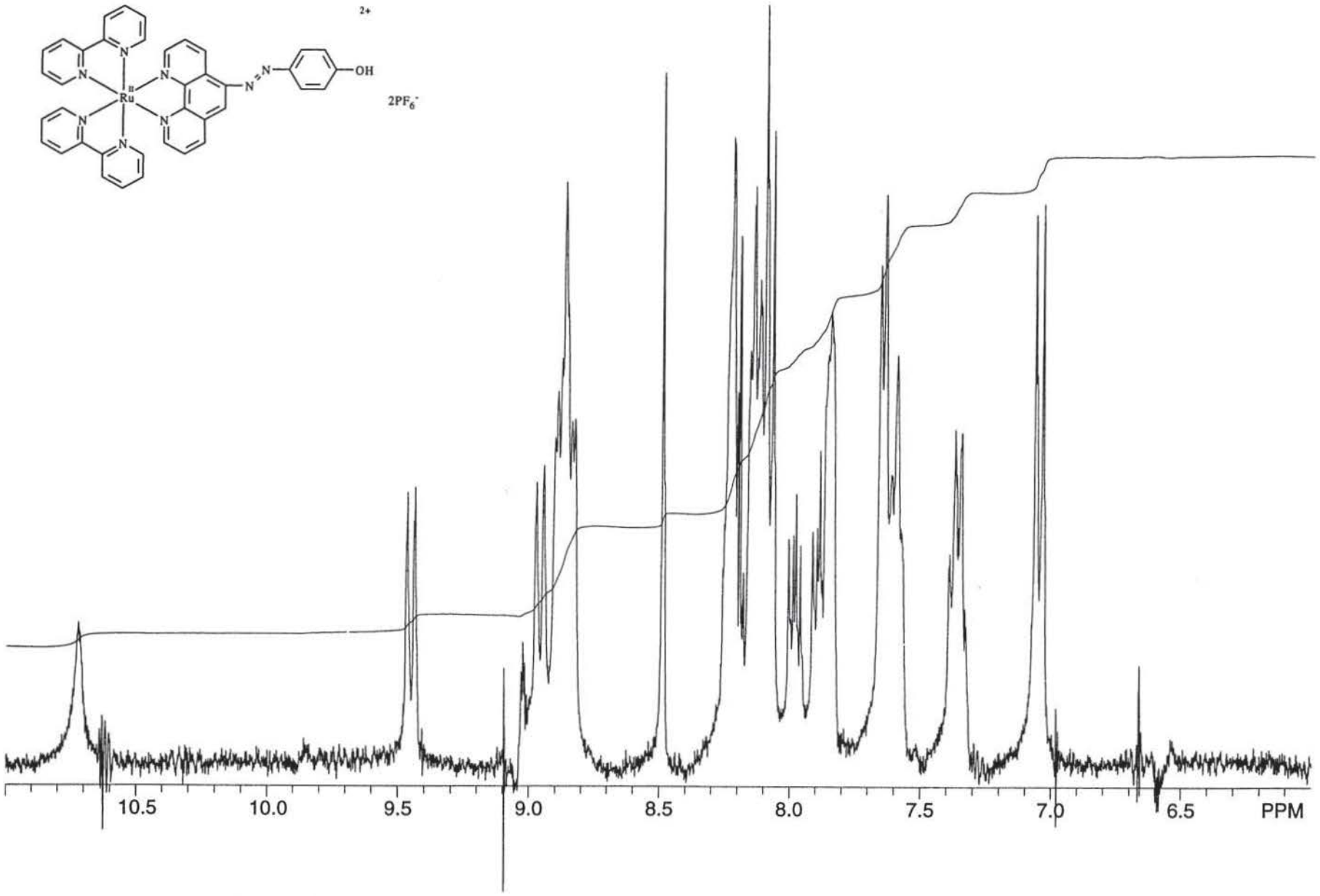

Figure 3.3a ^{1}H-NMR spectrum of $[Ru^{II}(bpy)_2(phen\text{-}azo\text{-}phenol)](PF_6)_2$ in d_6-DMSO

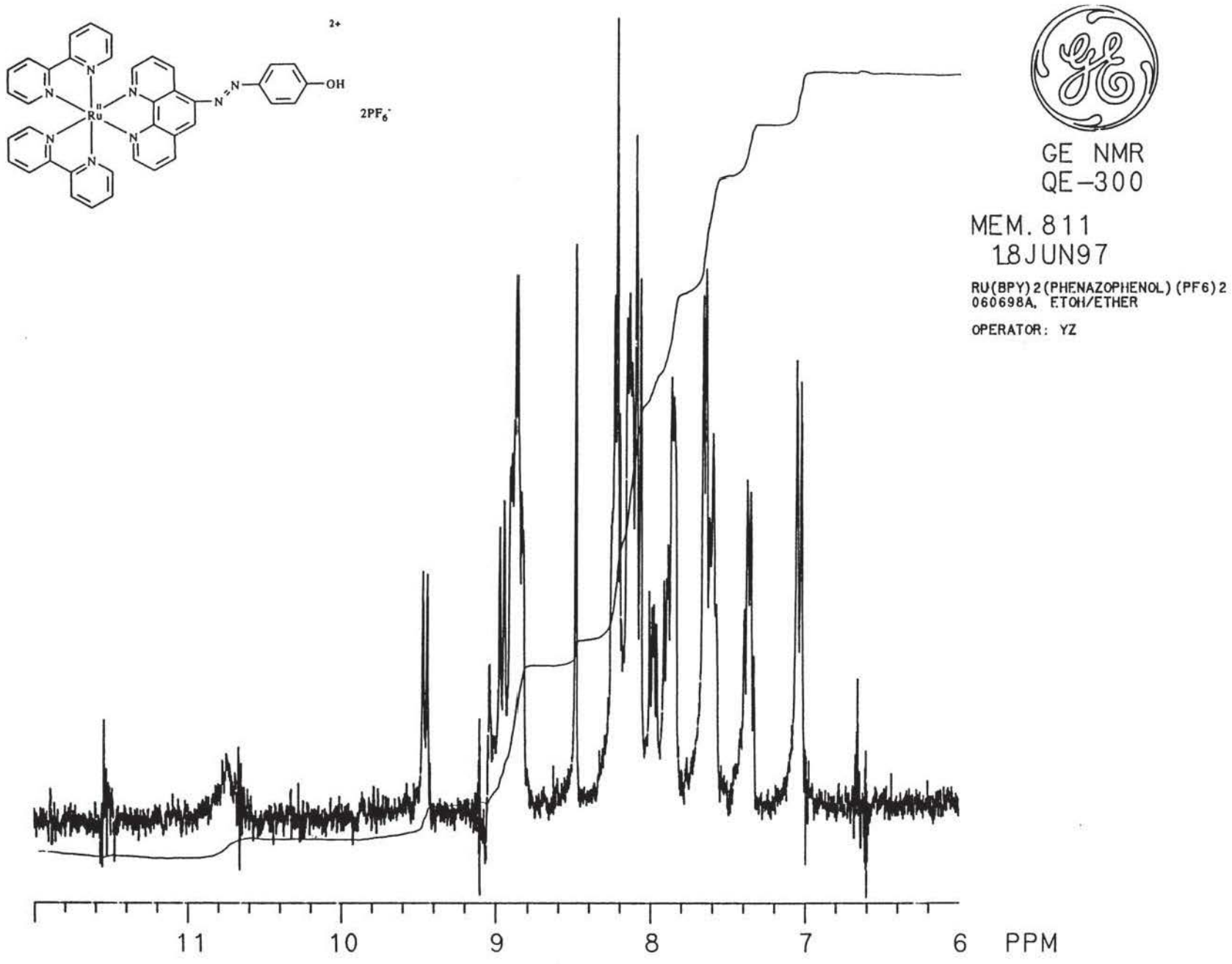

Figure 3.3b ^{1}H-NMR spectrum of $[Ru^{II}(bpy)_2(phen\text{-}azo\text{-}phenol)](PF_6)_2$ (second crop) in d_6-DMSO

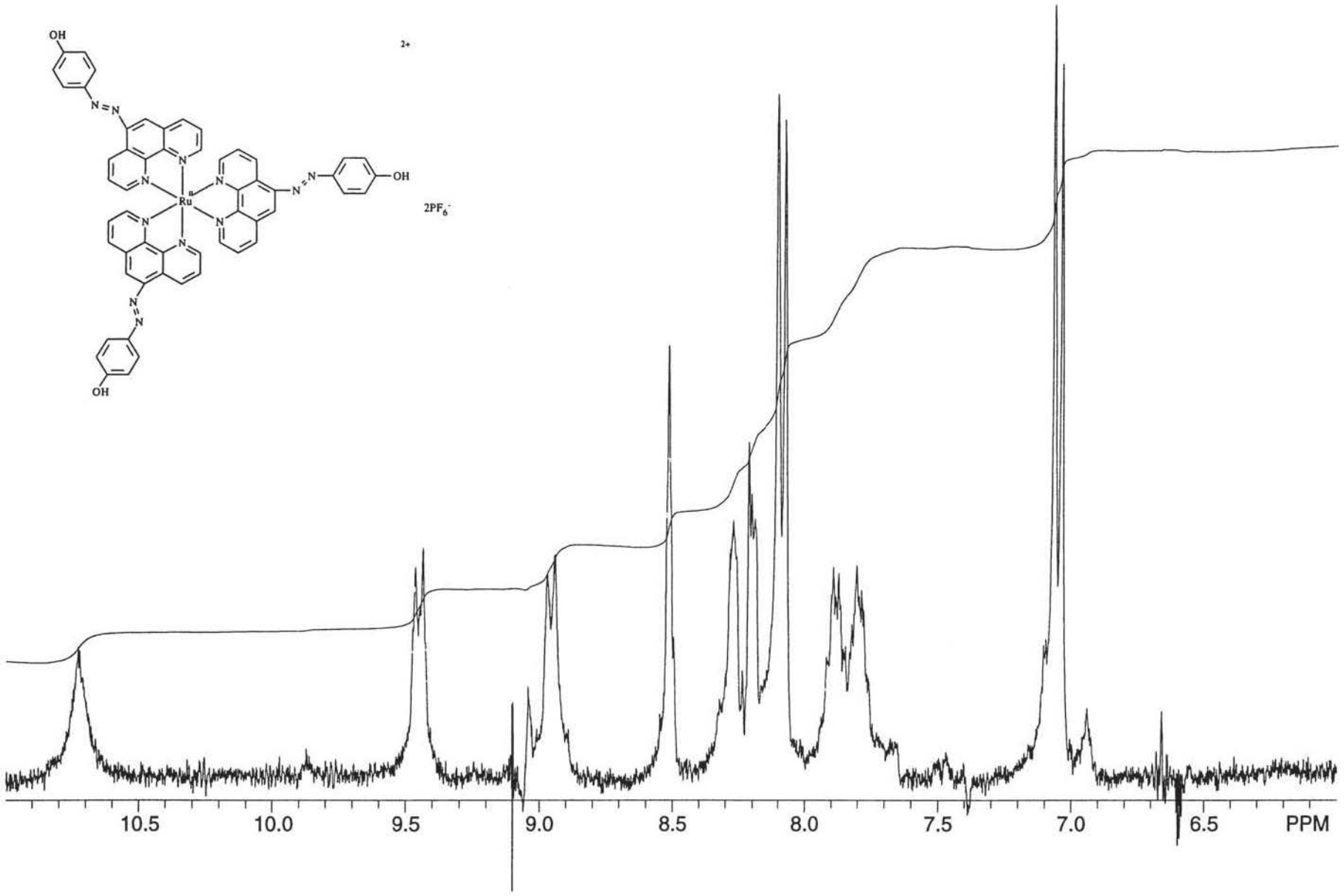

Figure 3.4a ^{1}H-NMR spectrum of $[Ru^{II}(phen\text{-}azo\text{-}phenol)_3](PF_6)_2$ in d_6-DMSO

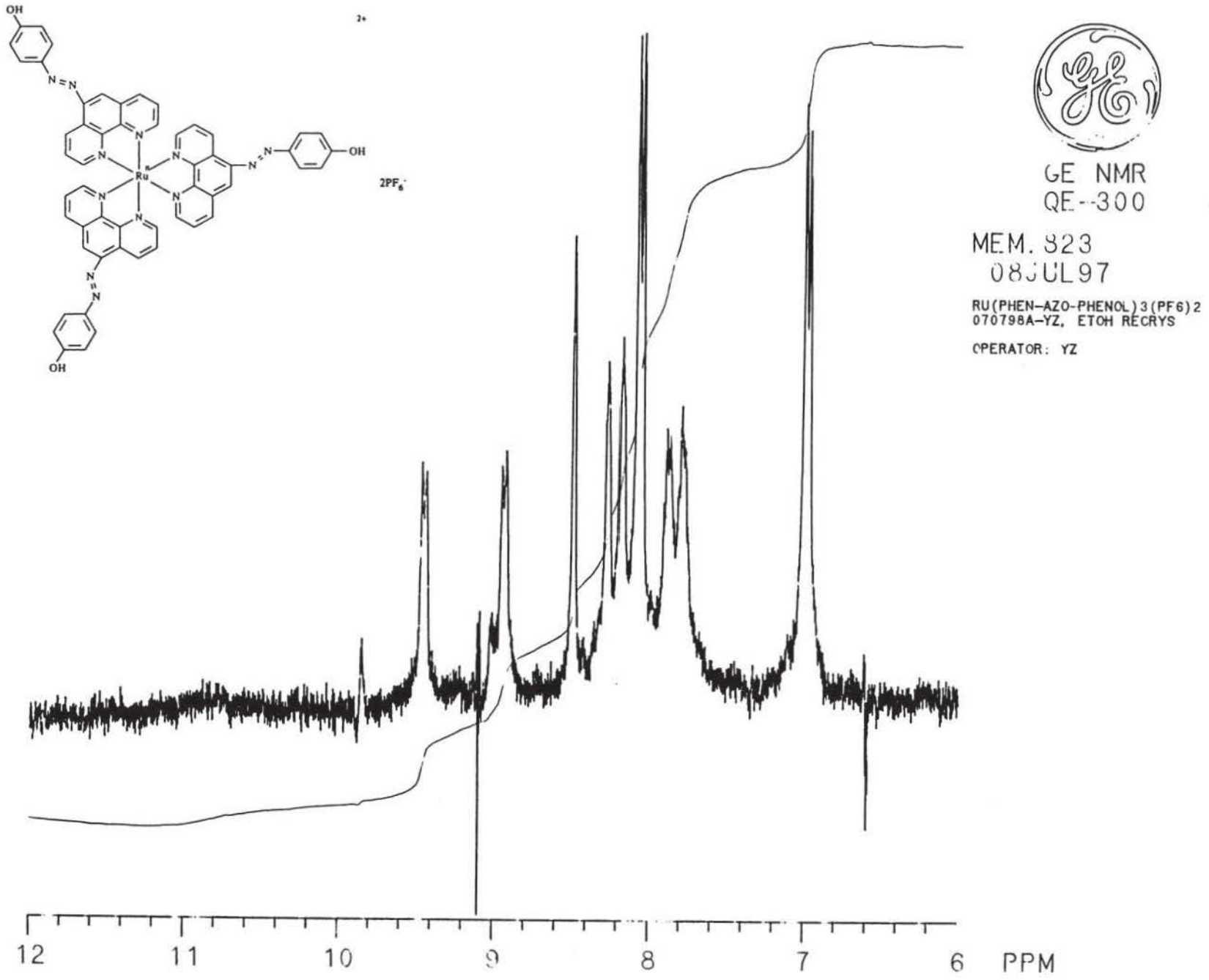

Figure 3.4b ^{1}H-NMR spectrum of $[Ru^{II}(phen\text{-}azo\text{-}phenol)_3](PF_6)_2$ (7.8 mg sample from neat ethanol) in d_6-DMSO

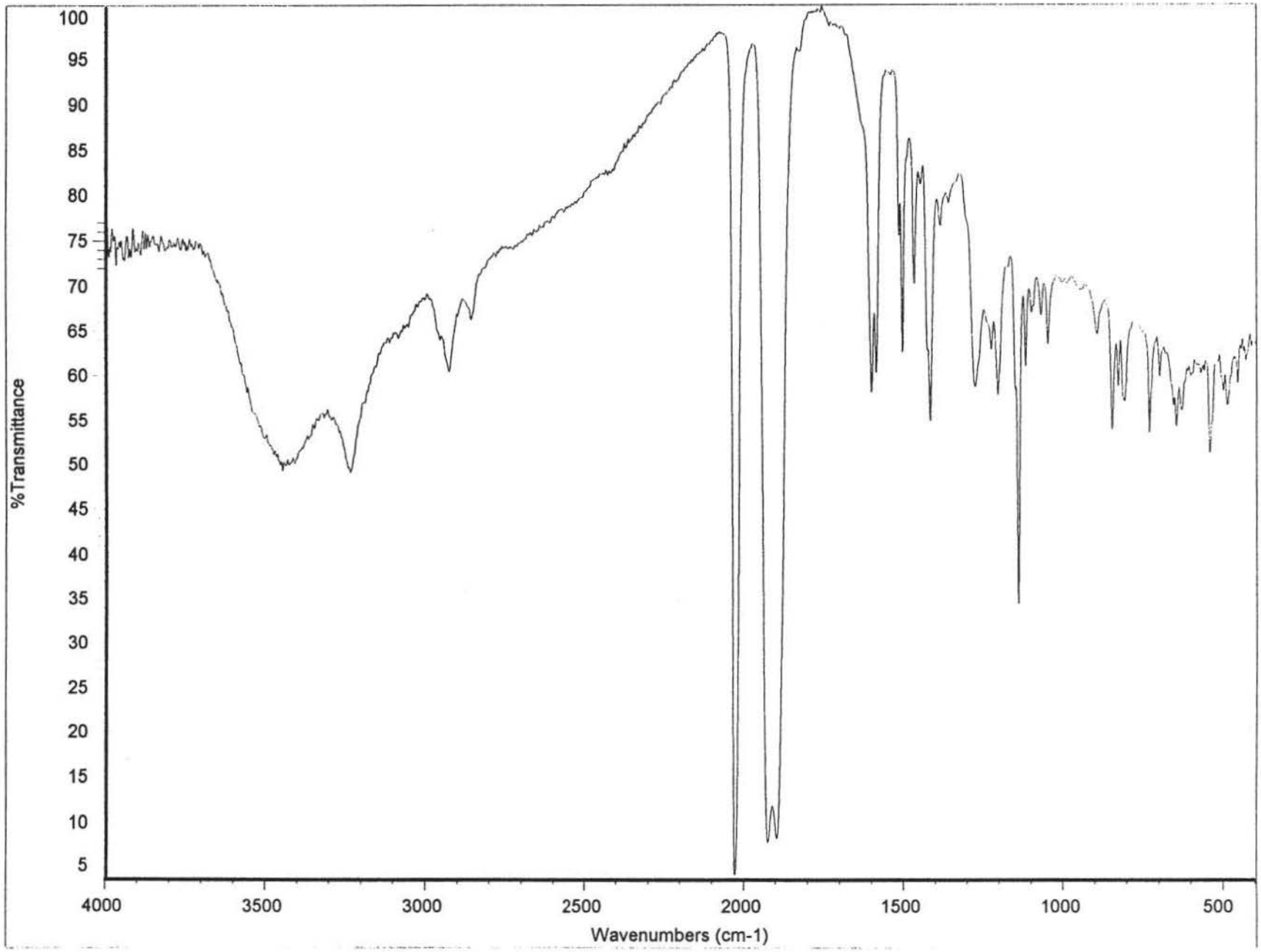

Figure 3.5 IR spectrum (in KBr) of *fac*-$Re^{I}(CO)_3Cl$(phen-azo-phenol)

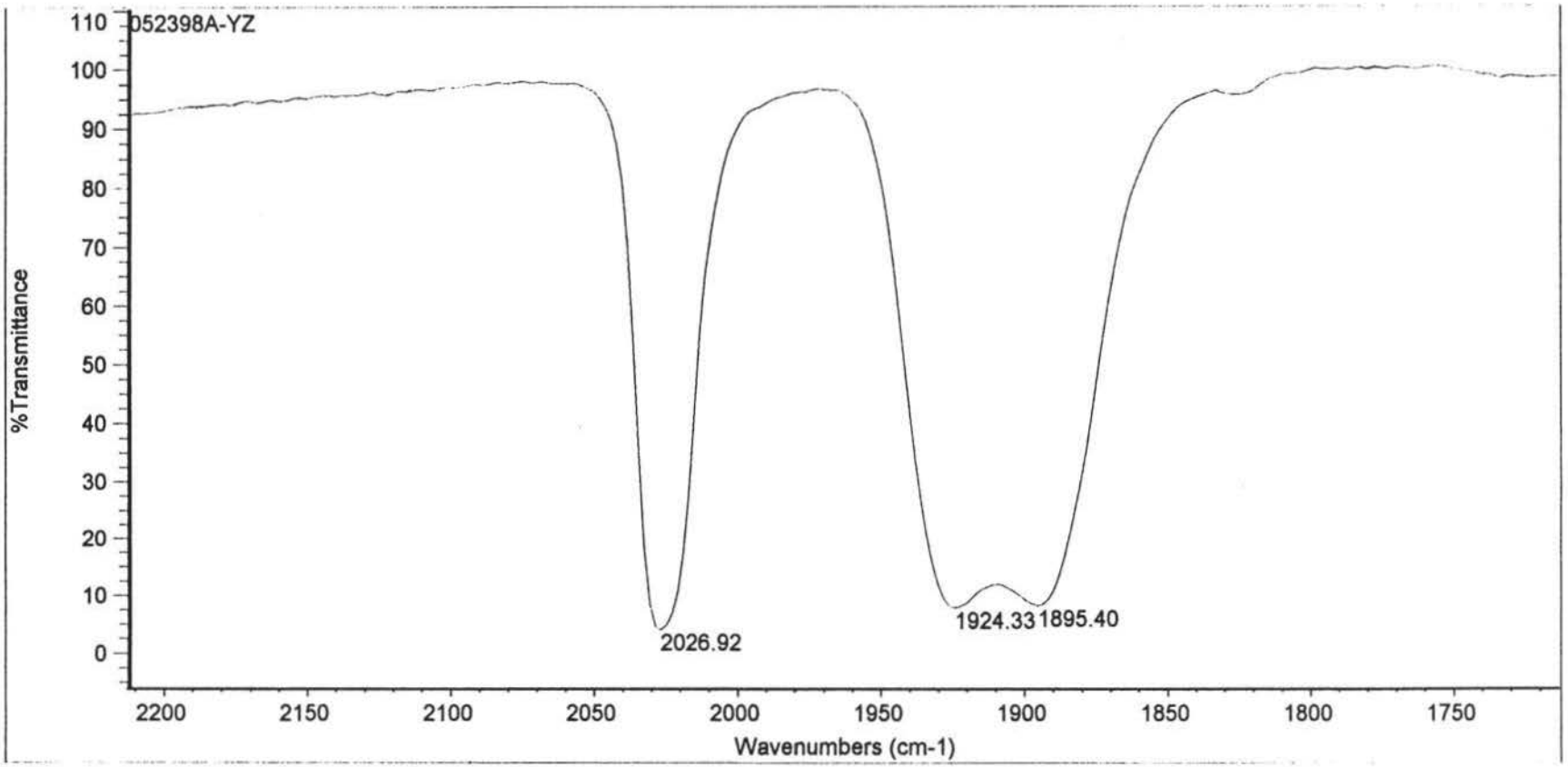

Tue Jul 14 16:45:20 1998
FIND PEAKS:

Spectrum:	052398A-YZ		
Region:	2212.67	1713.16	
Absolute threshold:	67.971		
Sensitivity:	50		
Peak list:			
Position:	2026.92	Intensity:	4.004
Position:	1924.33	Intensity:	7.724
Position:	1895.40	Intensity:	8.139

Figure 3.6 Carbonyl stretching of *fac*-$Re^{I}(CO)_3Cl$(phen-azo-phenol) in KBr

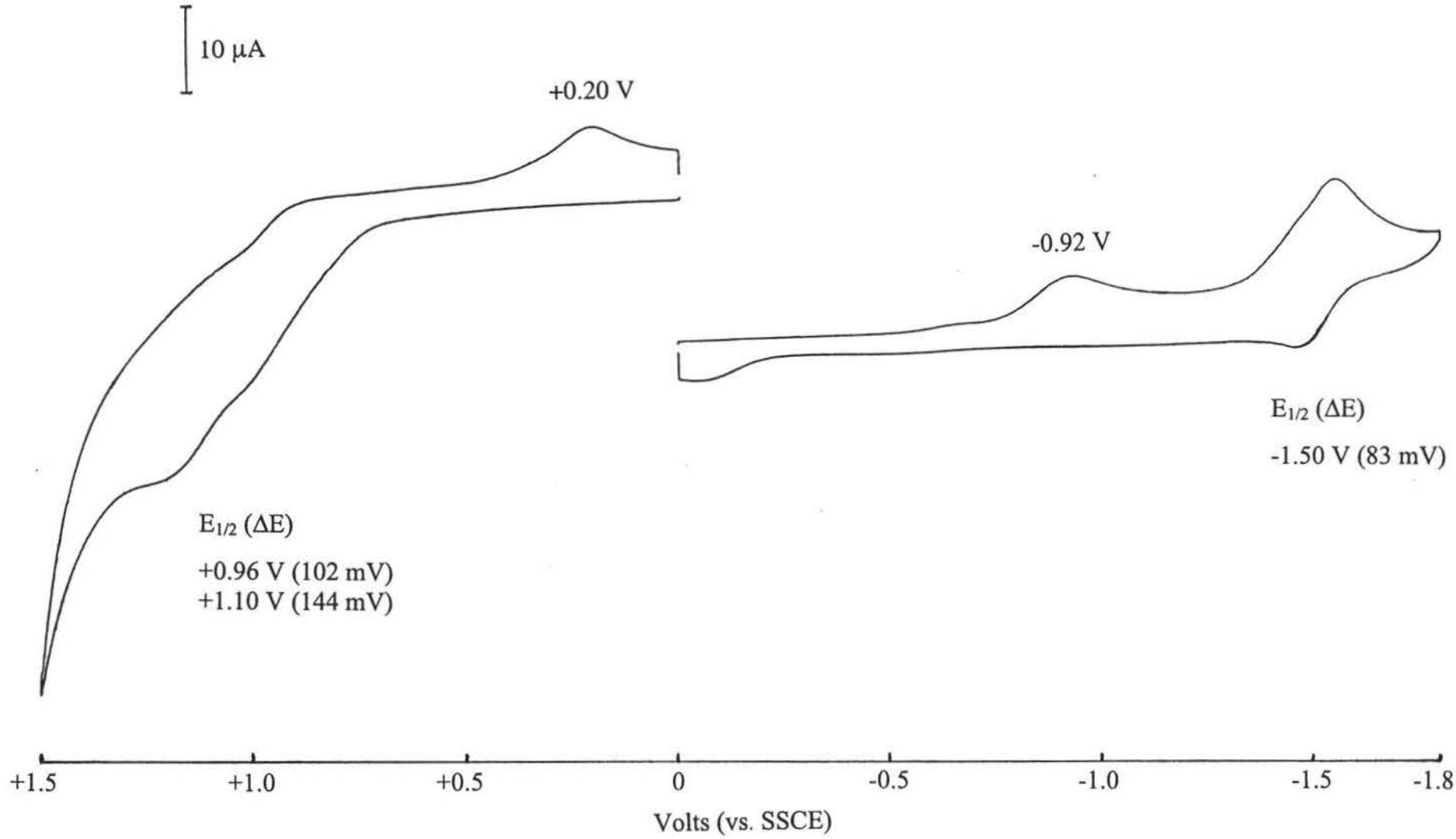

Figure 3.7 Cyclic voltammograms of phen-azo-phenol in DMSO

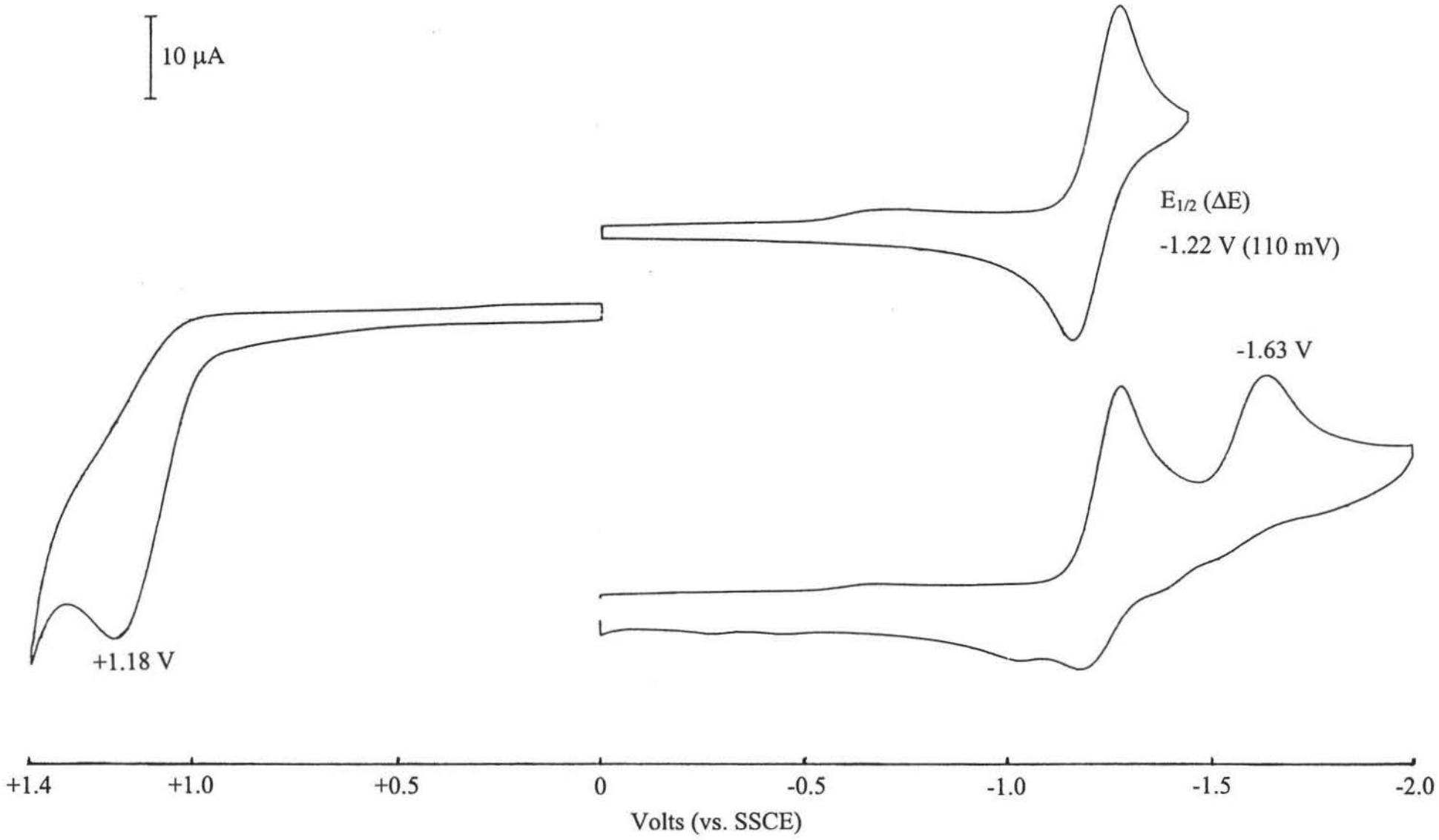

Figure 3.8 Cyclic voltammograms of *fac*-$Re^{I}(CO)_3Cl(phen)$ in DMSO

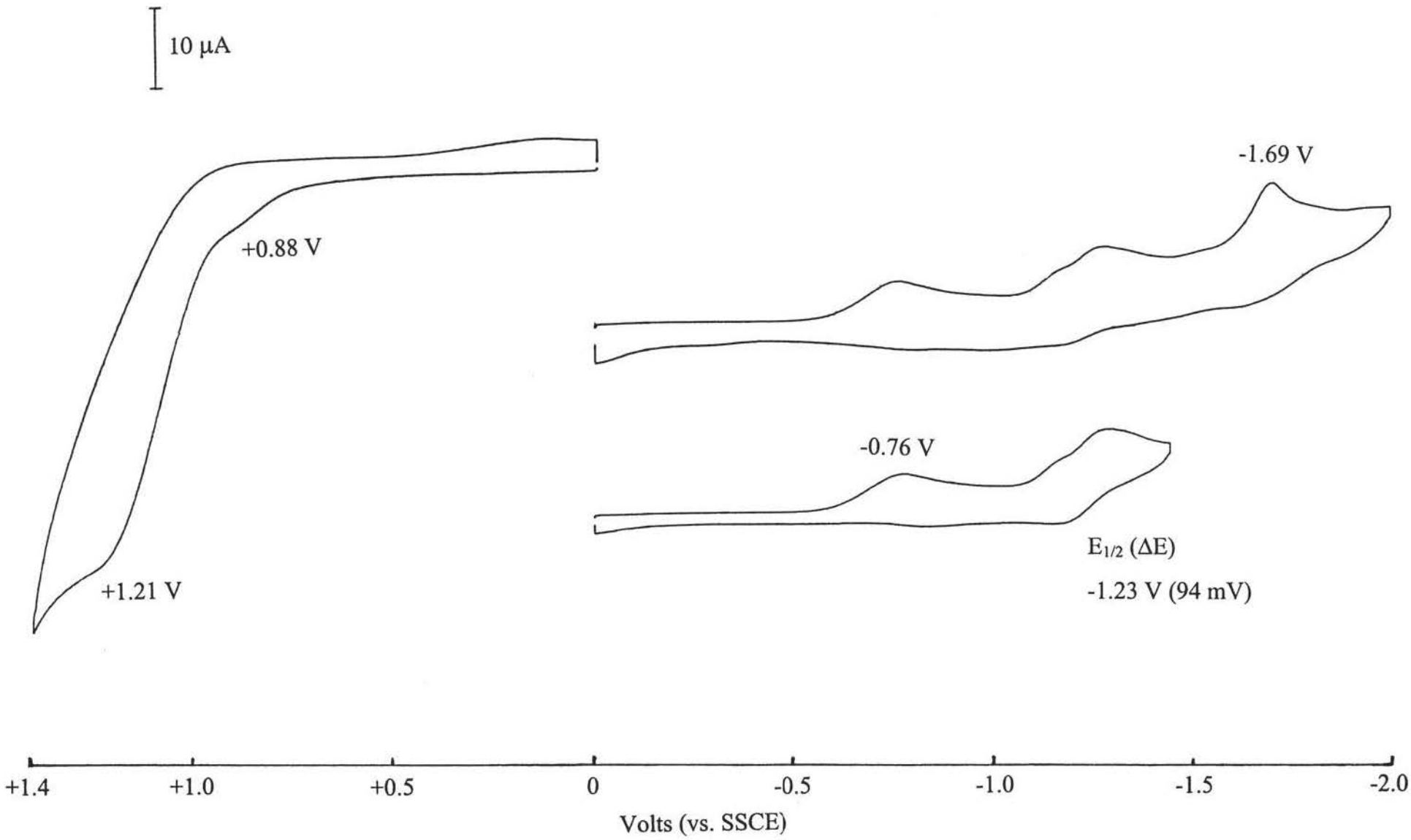

Figure 3.9 Cyclic voltammograms of *fac*-$Re^{I}(CO)_3Cl$(phen-azo-phenol) in DMSO

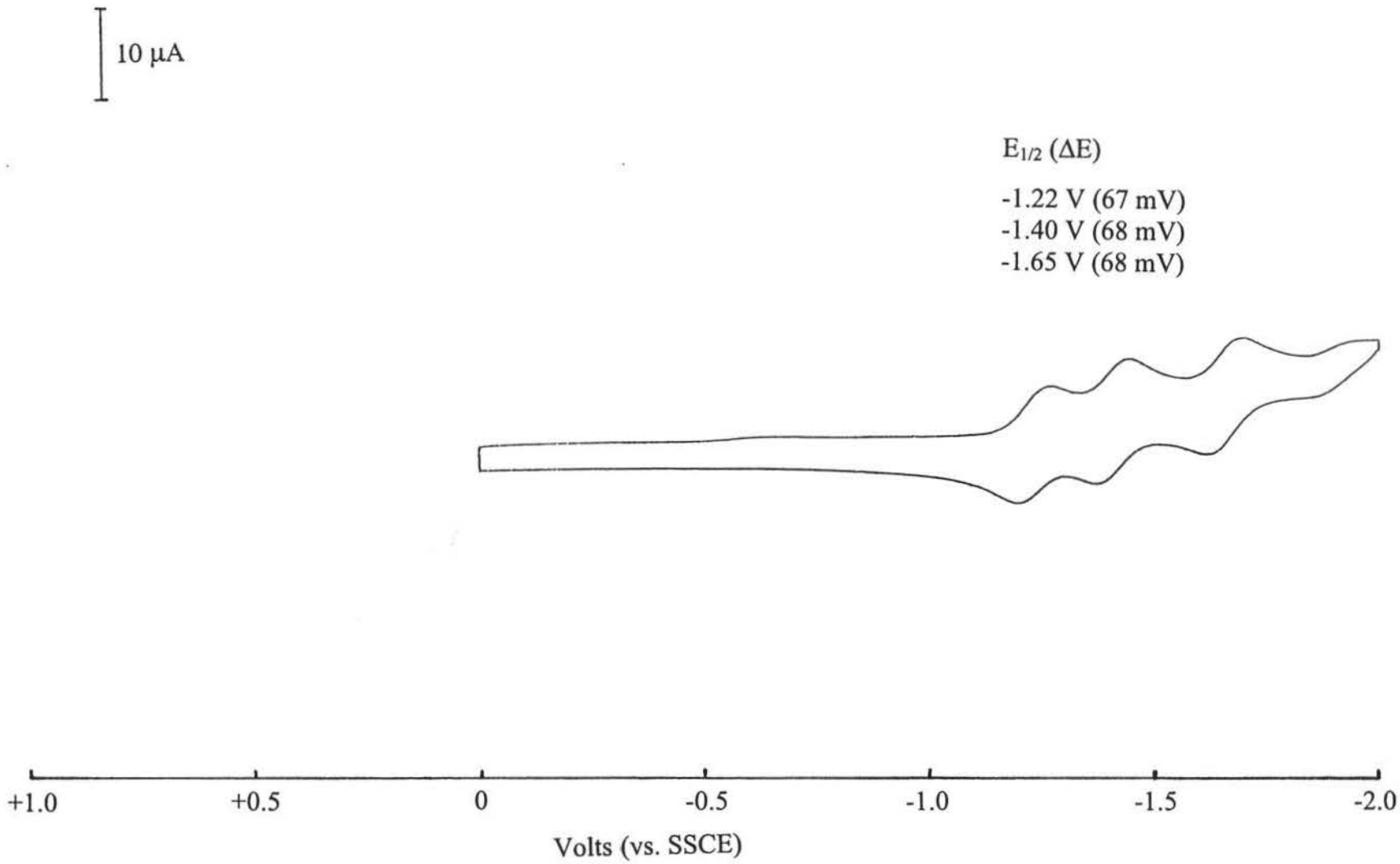

Figure 3.10 Cyclic voltammogram of $[Ru^{II}(bpy)_3]Cl_2$ in DMSO

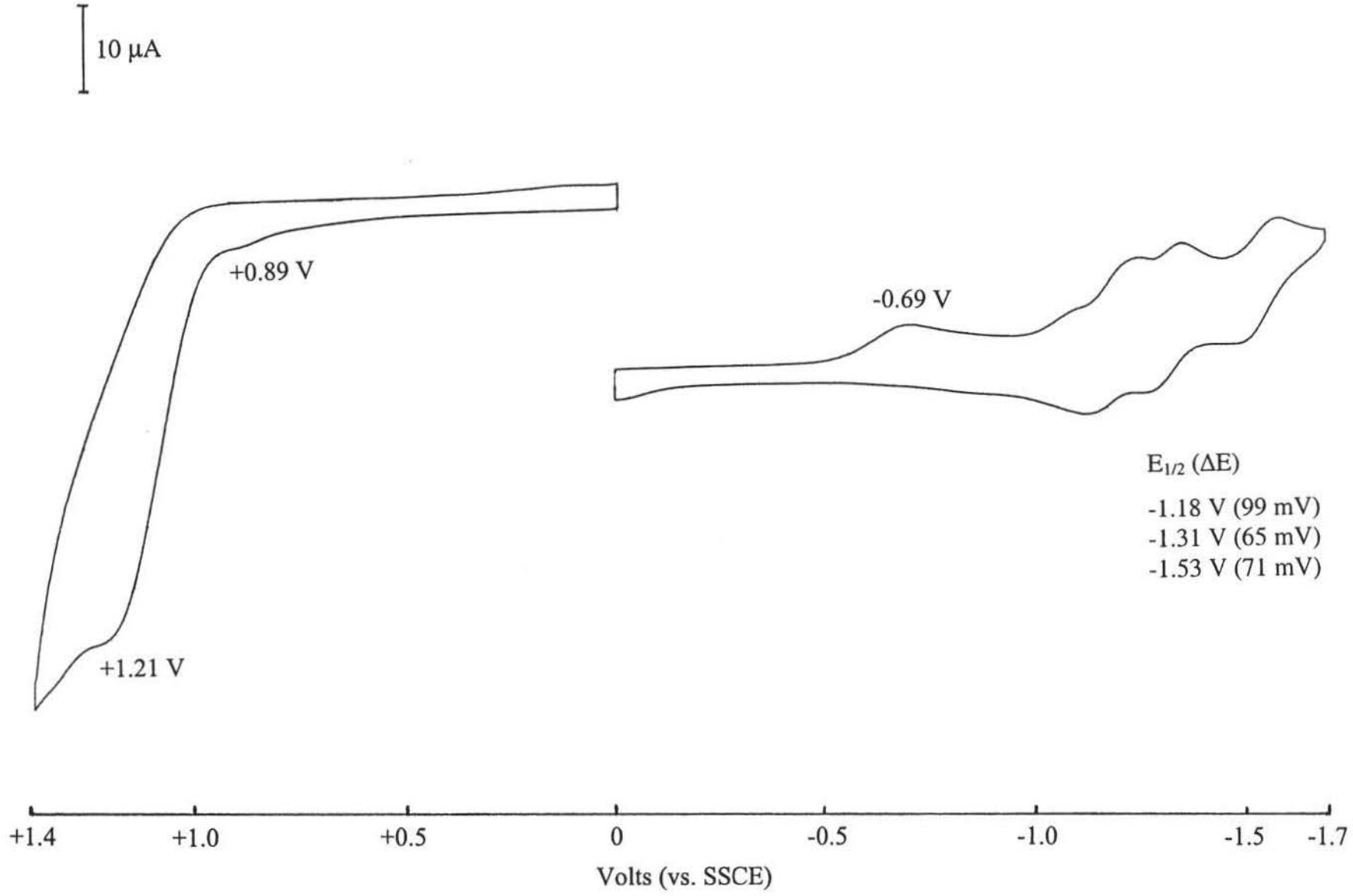

Figure 3.11 Cyclic voltammograms of $[Ru^{II}(bpy)_2(phen\text{-}azo\text{-}phenol)](PF_6)_2$ in DMSO

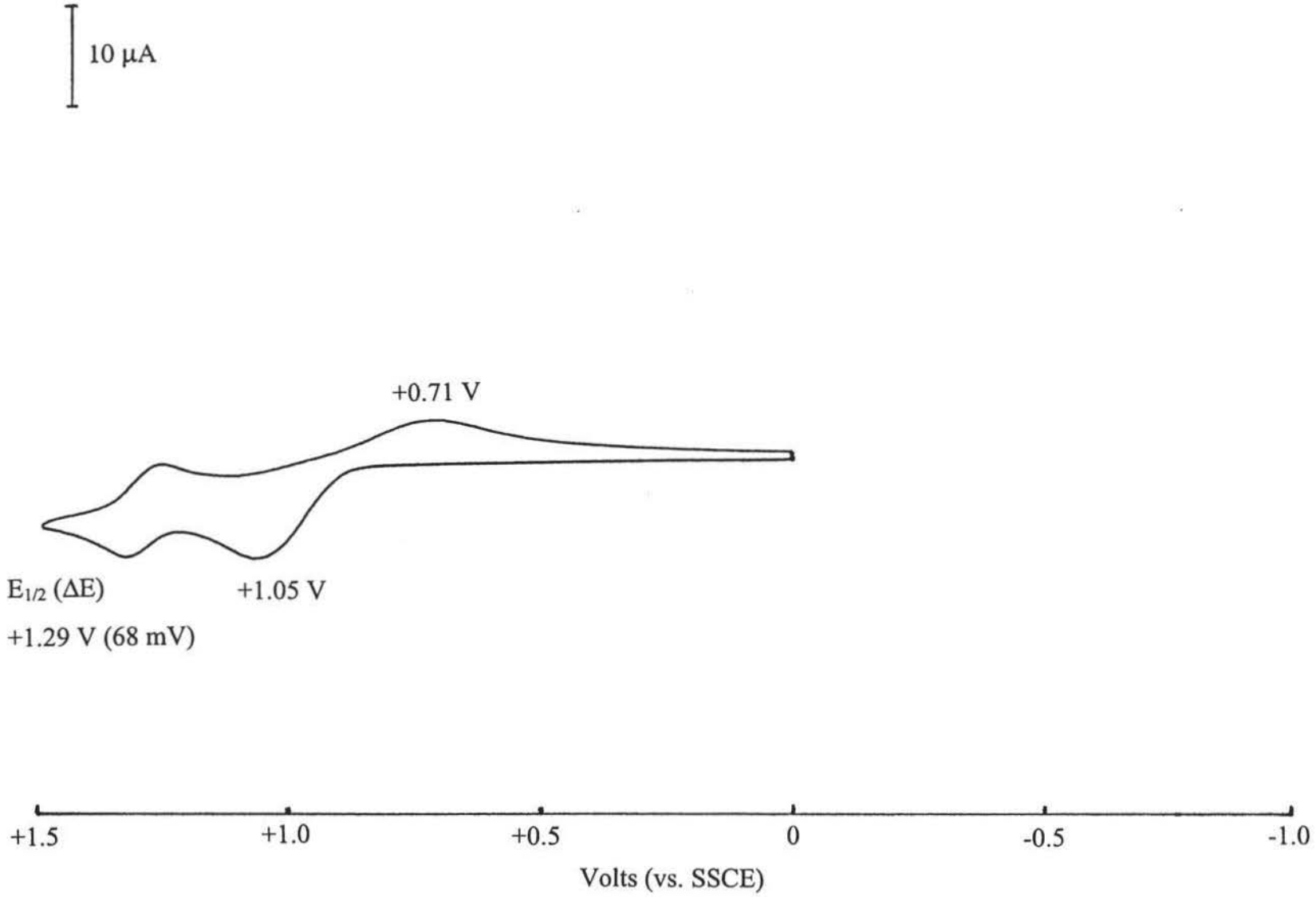

Figure 3.12 Cyclic voltammogram of $[Ru^{II}(bpy)_3]Cl_2$ in CH_3CN

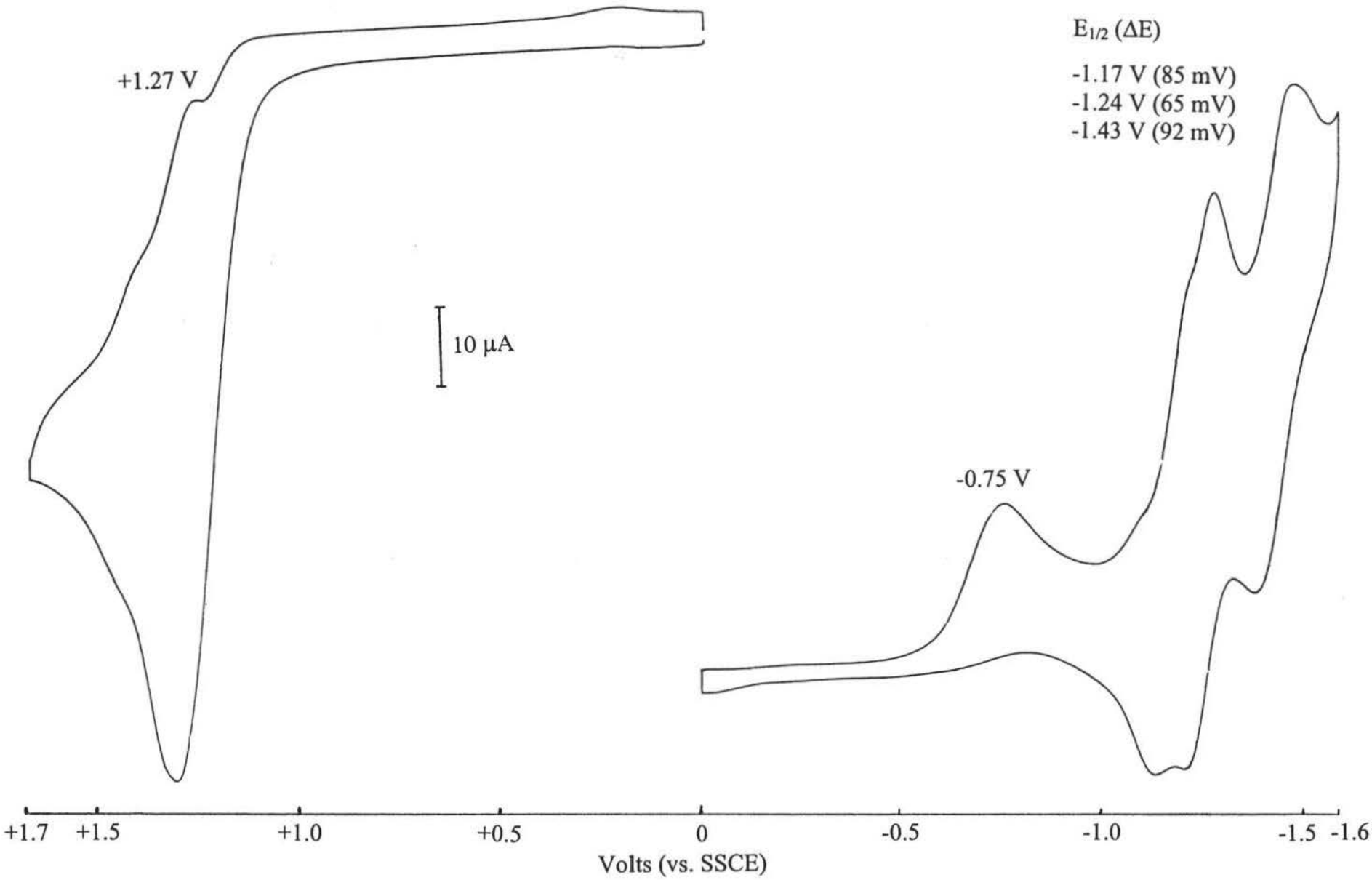

Figure 3.13 Cyclic voltammograms of $[Ru^{II}(bpy)_2(phen\text{-}azo\text{-}phenol)](PF_6)_2$ in CH_3CN

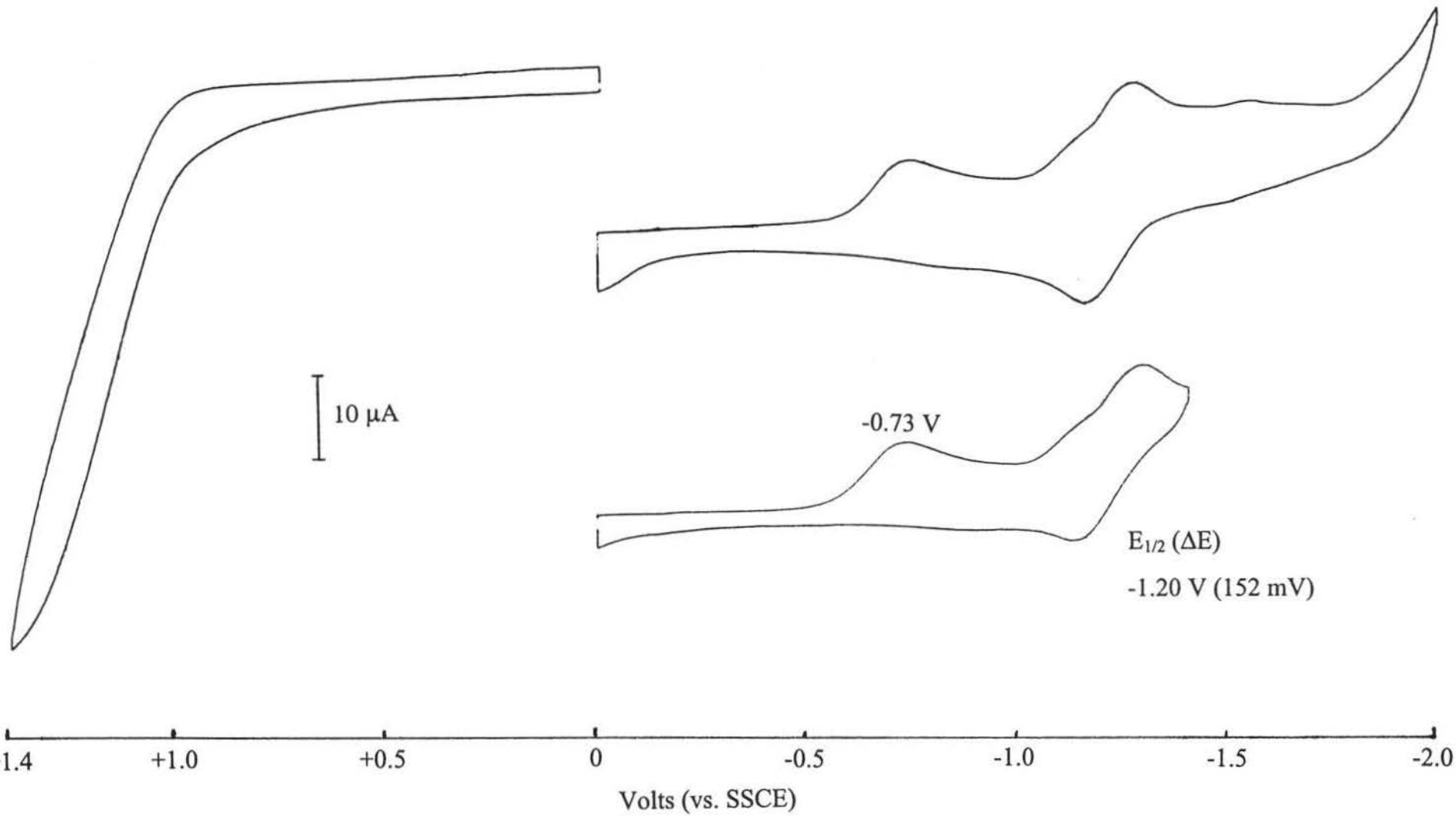

Figure 3.14 Cyclic voltammograms of $[Ru^{II}(phen\text{-}azo\text{-}phenol)_3](PF_6)_2$ in DMSO

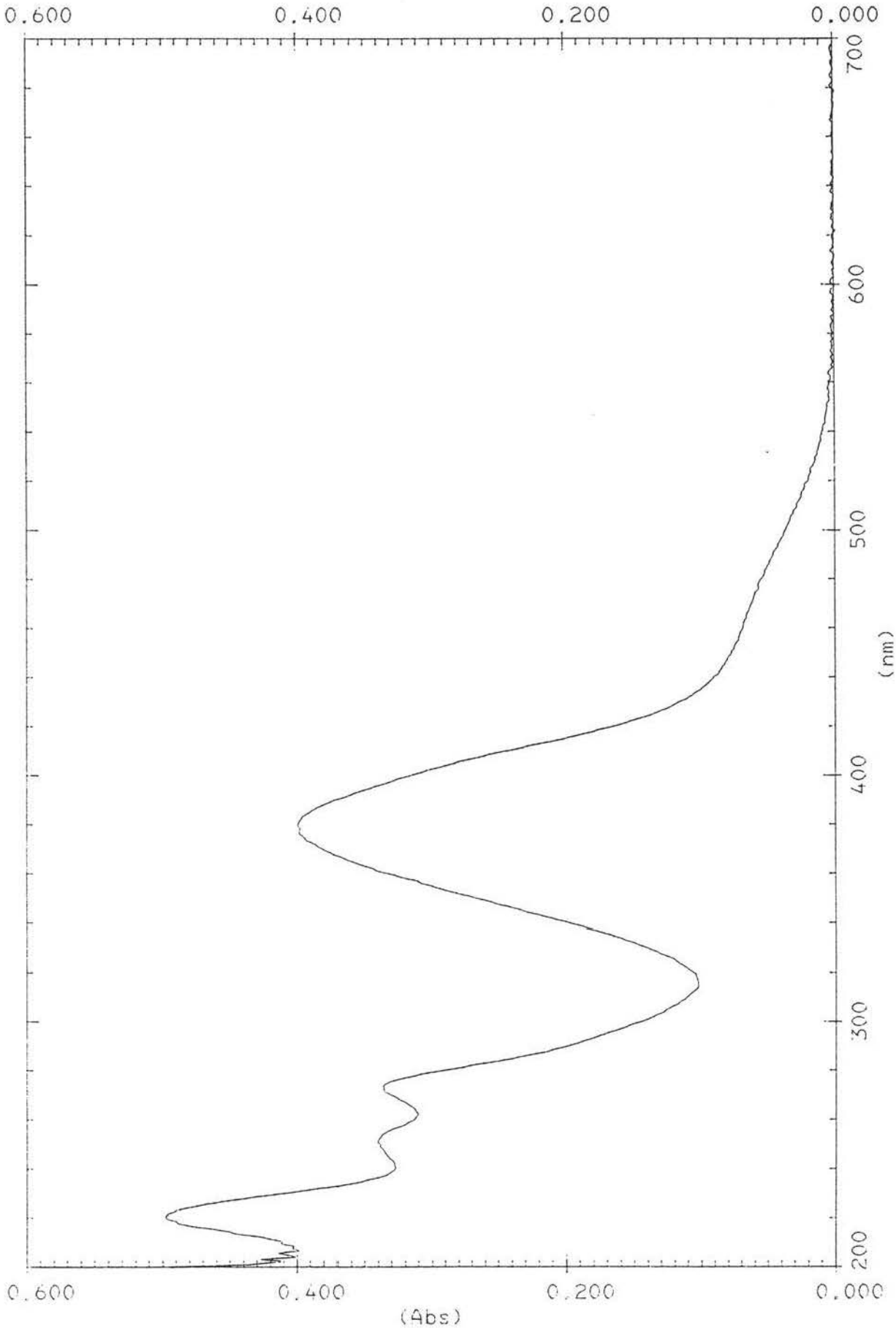

Figure 3.15 UV-Vis spectrum of phen-azo-phenol in methanol

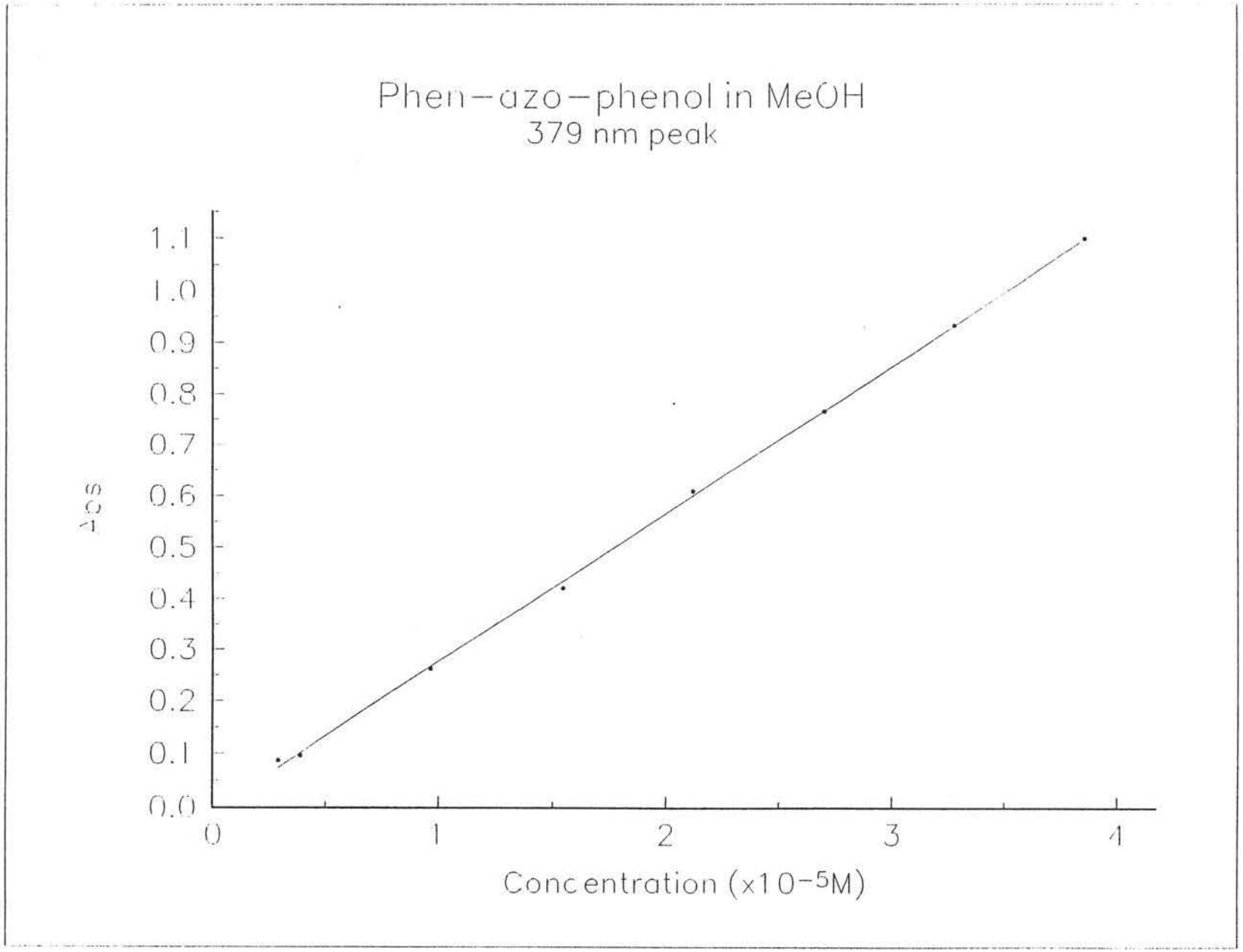

Figure 3.16 Beer-Lambert plotting of phen-azo-phenol in methanol (379 nm peak)

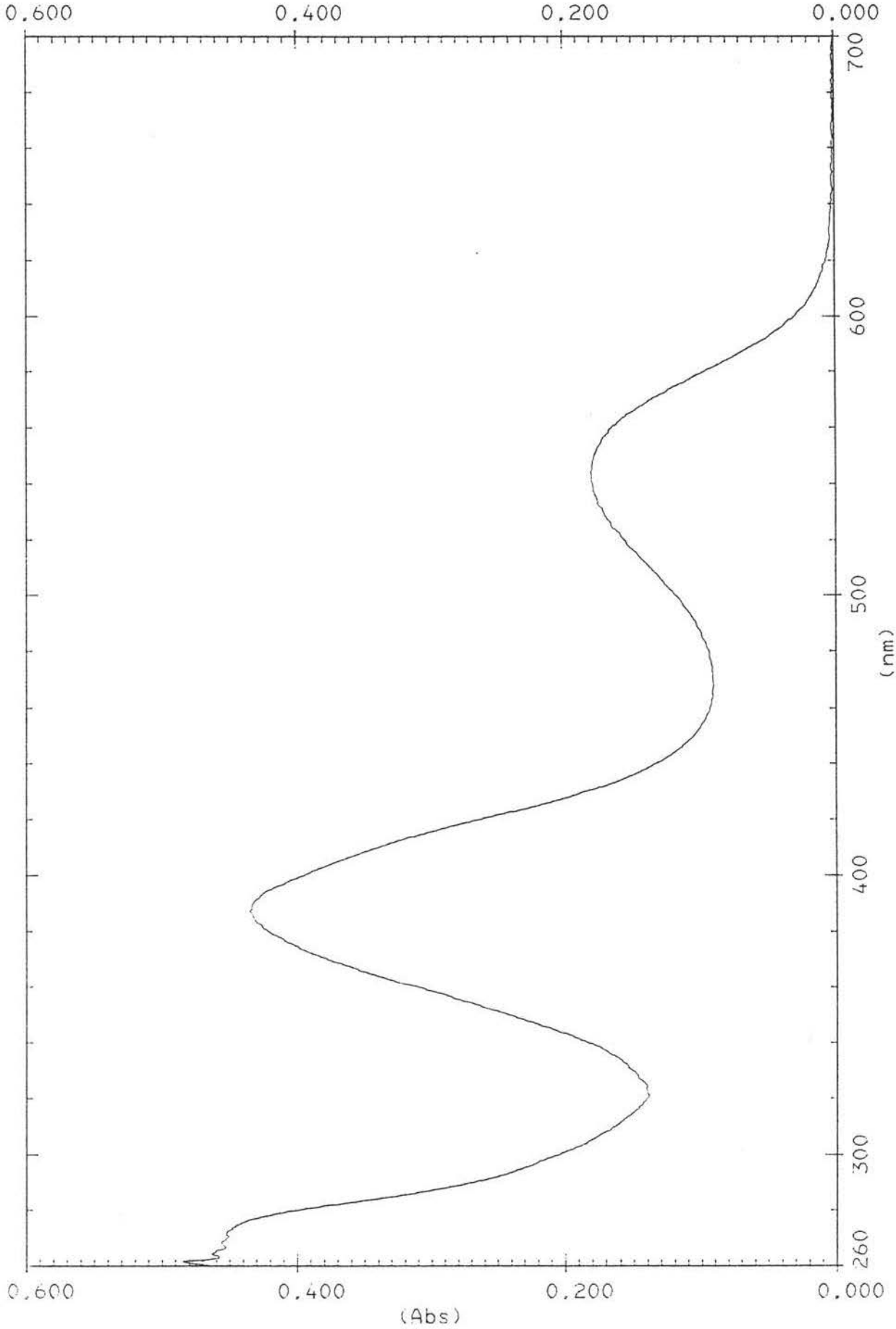

Figure 3.17 UV-Vis spectrum of phen-azo-phenol in DMSO

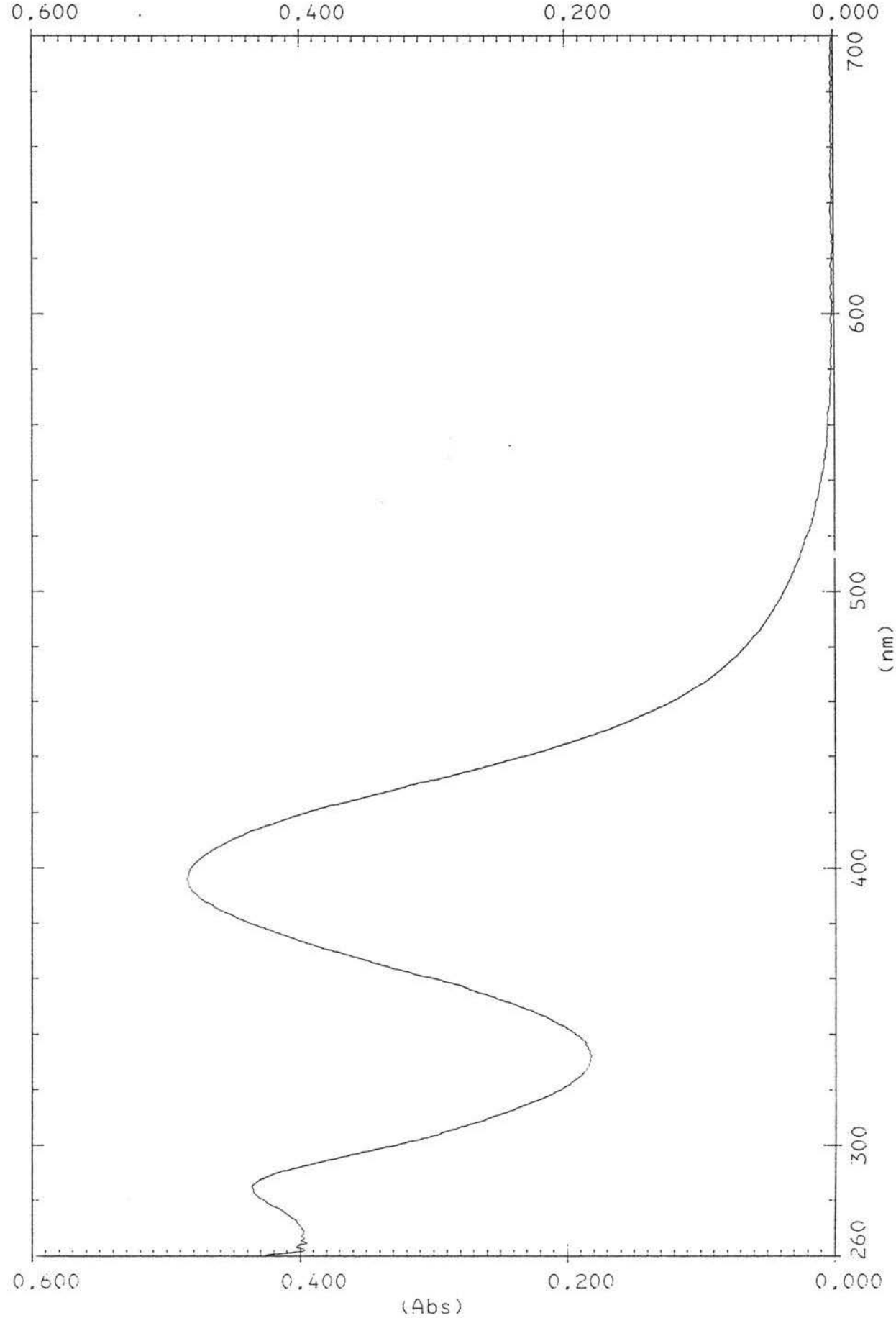

Figure 3.18 UV-Vis spectrum of phen-azo-phenol in DMSO with conc. H_2SO_4 added

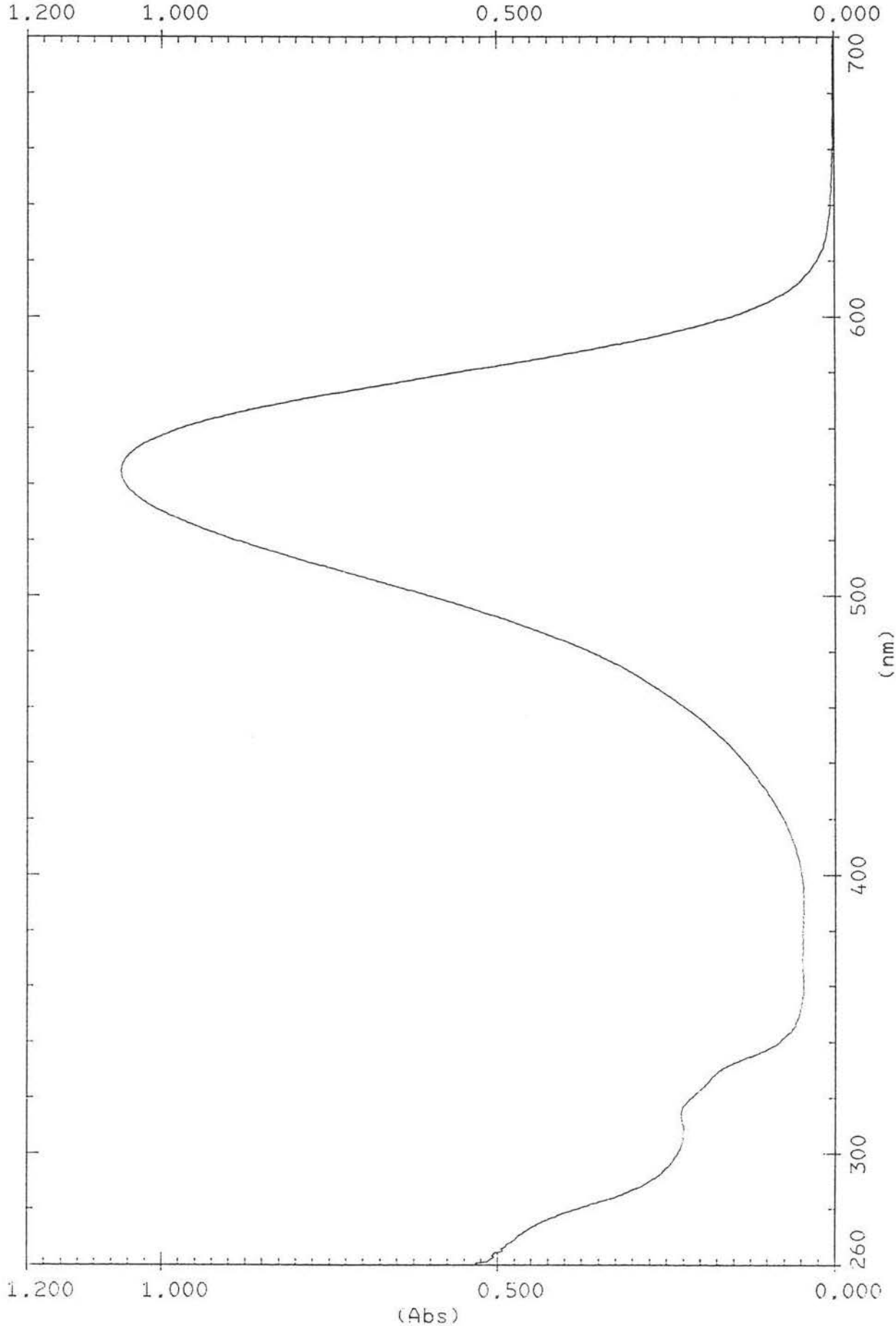

Figure 3.19 UV-Vis spectrum of phen-azo-phenol in DMSO with 10% NaOH (aq) added

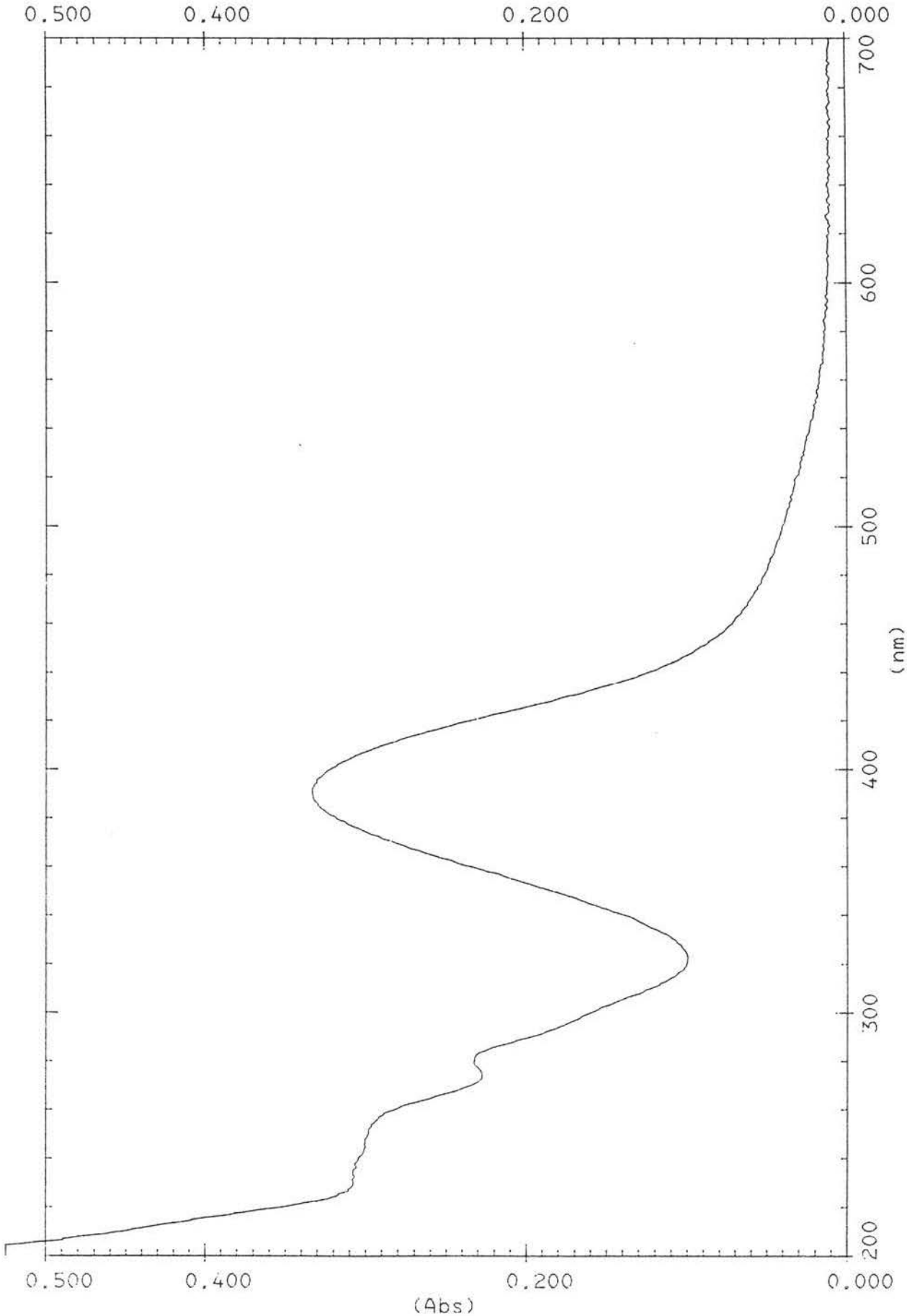

Figure 3.20 UV-Vis spectrum of *fac*-$Re^{I}(CO)_3Cl$(phen-azo-phenol) in methanol

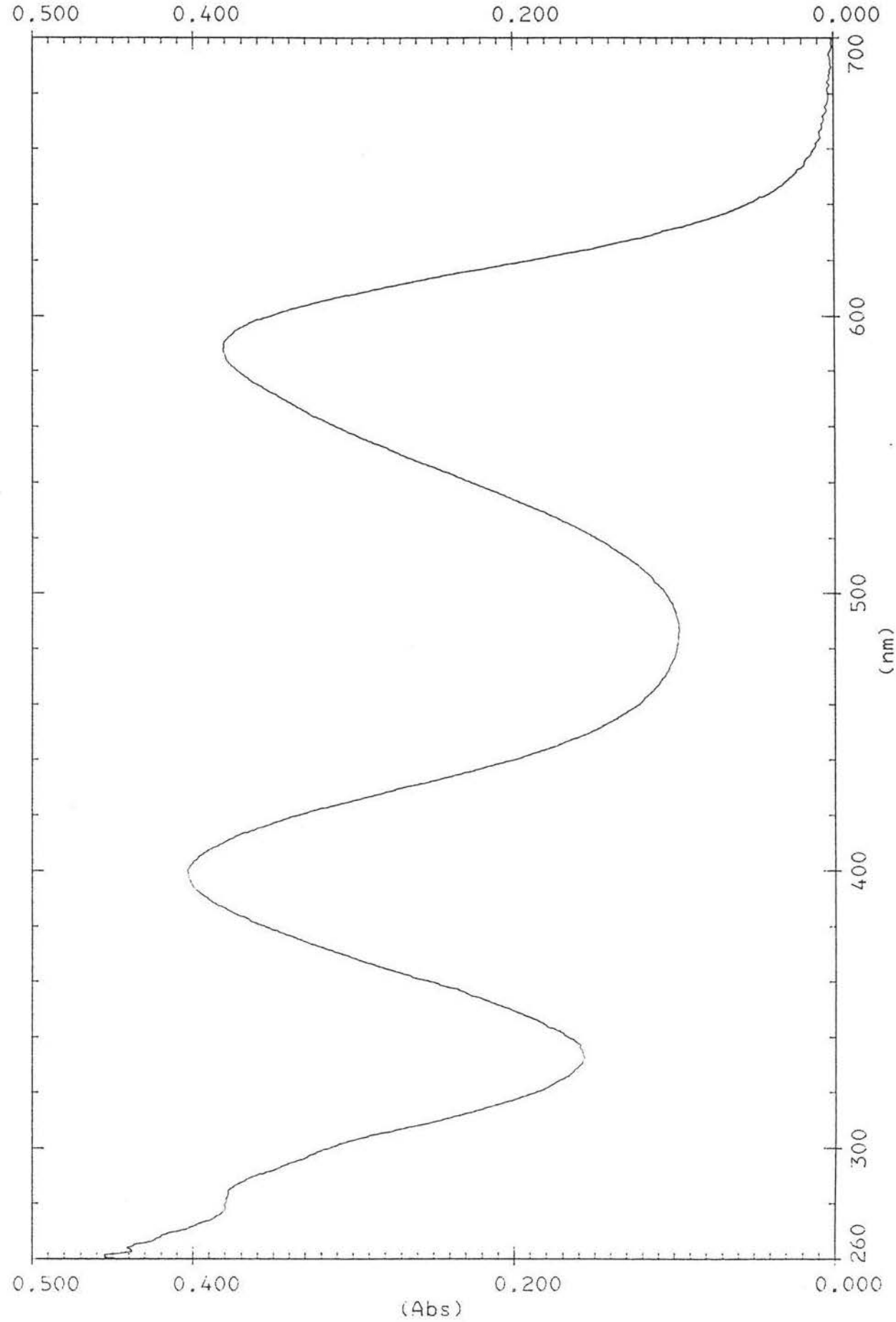

Figure 3.21 UV-Vis spectrum of *fac*-$Re^{I}(CO)_3Cl$(phen-azo-phenol) in DMSO

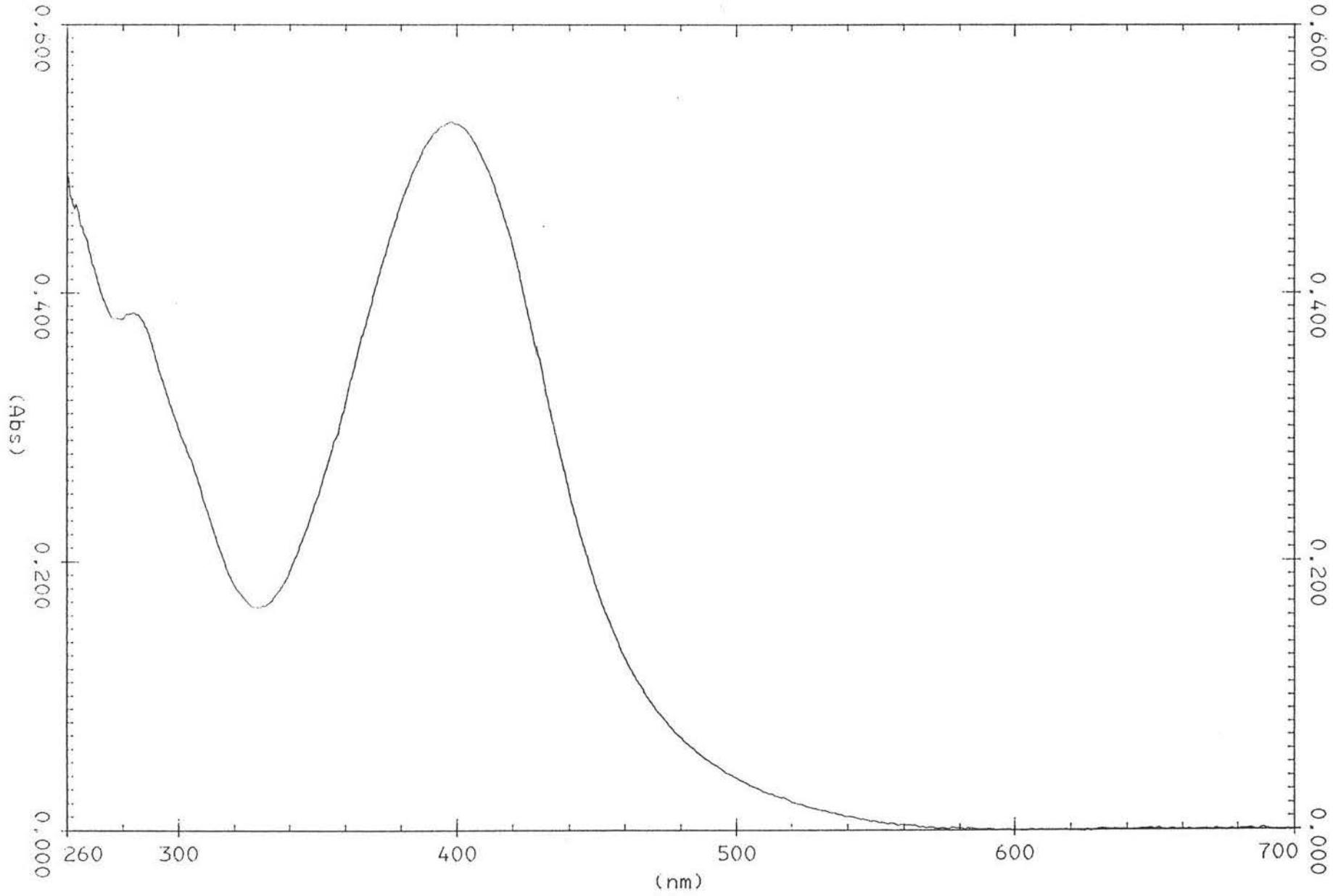

Figure 3.22 UV-Vis spectrum of *fac*-$Re^{I}(CO)_3Cl$(phen-azo-phenol) in DMSO with conc. H_2SO_4 added

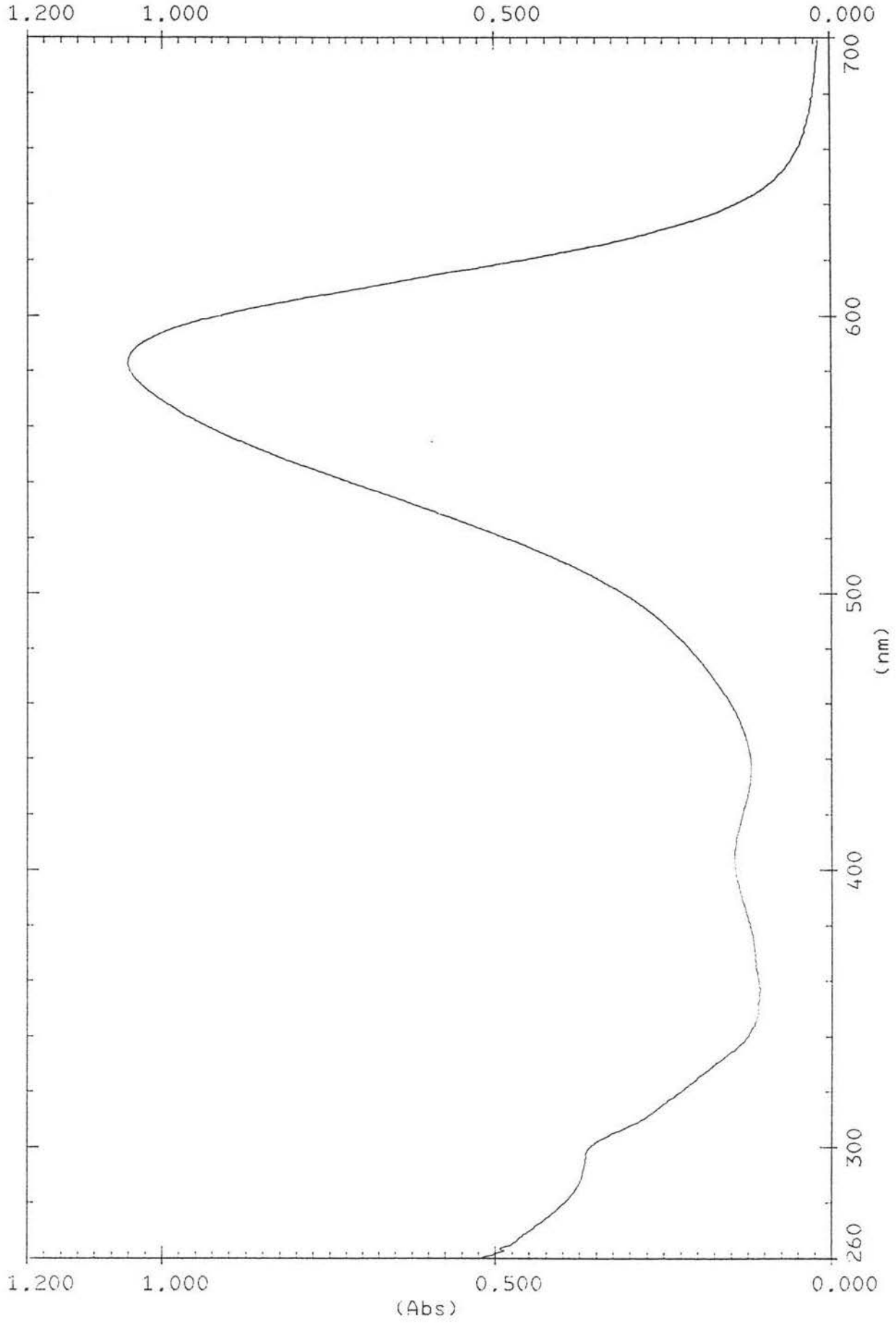

Figure 3.23 UV-Vis spectrum of *fac*-$Re^{I}(CO)_3Cl$(phen-azo-phenol) in DMSO with 10% NaOH (aq) added

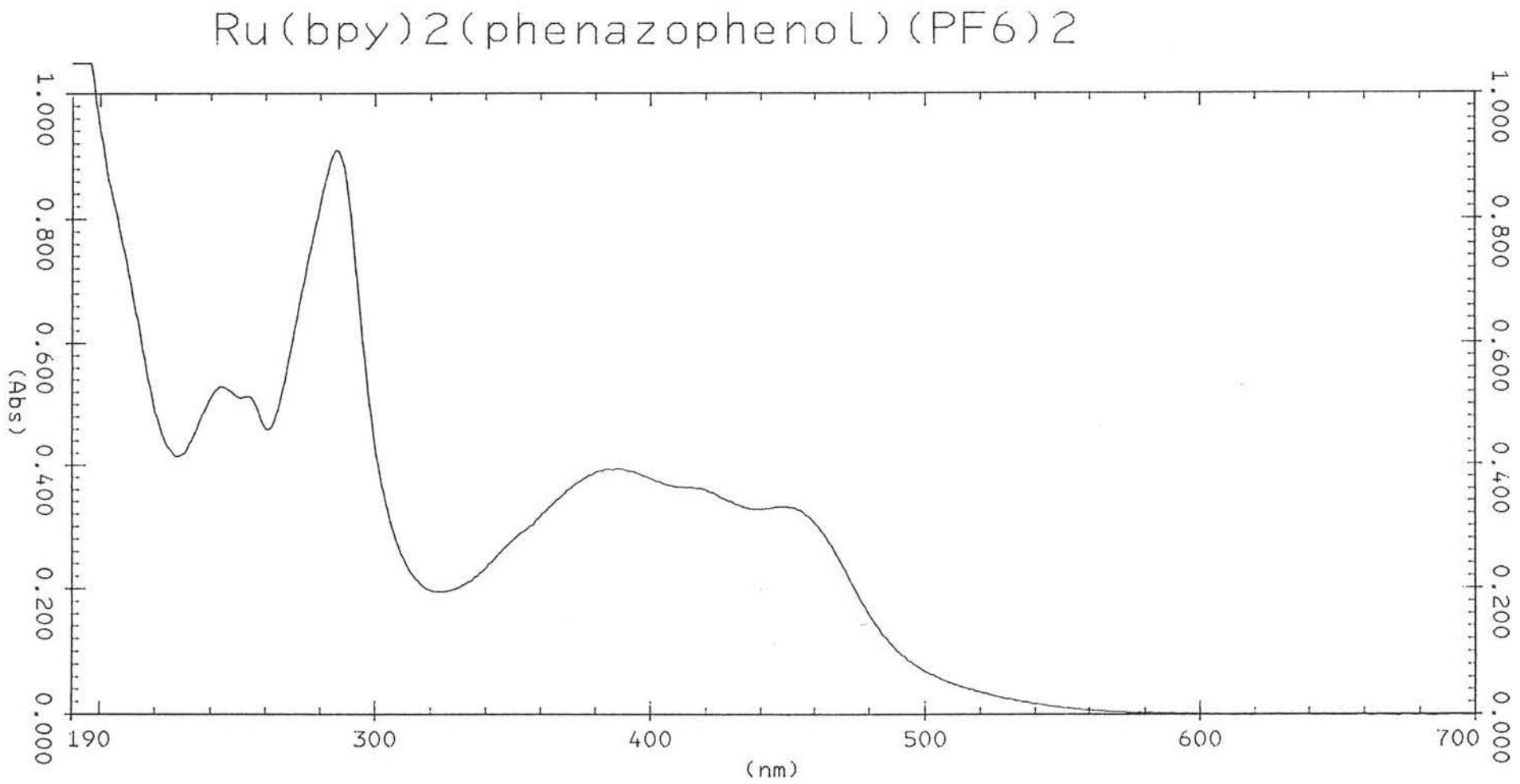

Figure 3.24 UV-Vis spectrum of $[Ru^{II}(bpy)_2(phen\text{-}azo\text{-}phenol)](PF_6)_2$ in CH_3CN

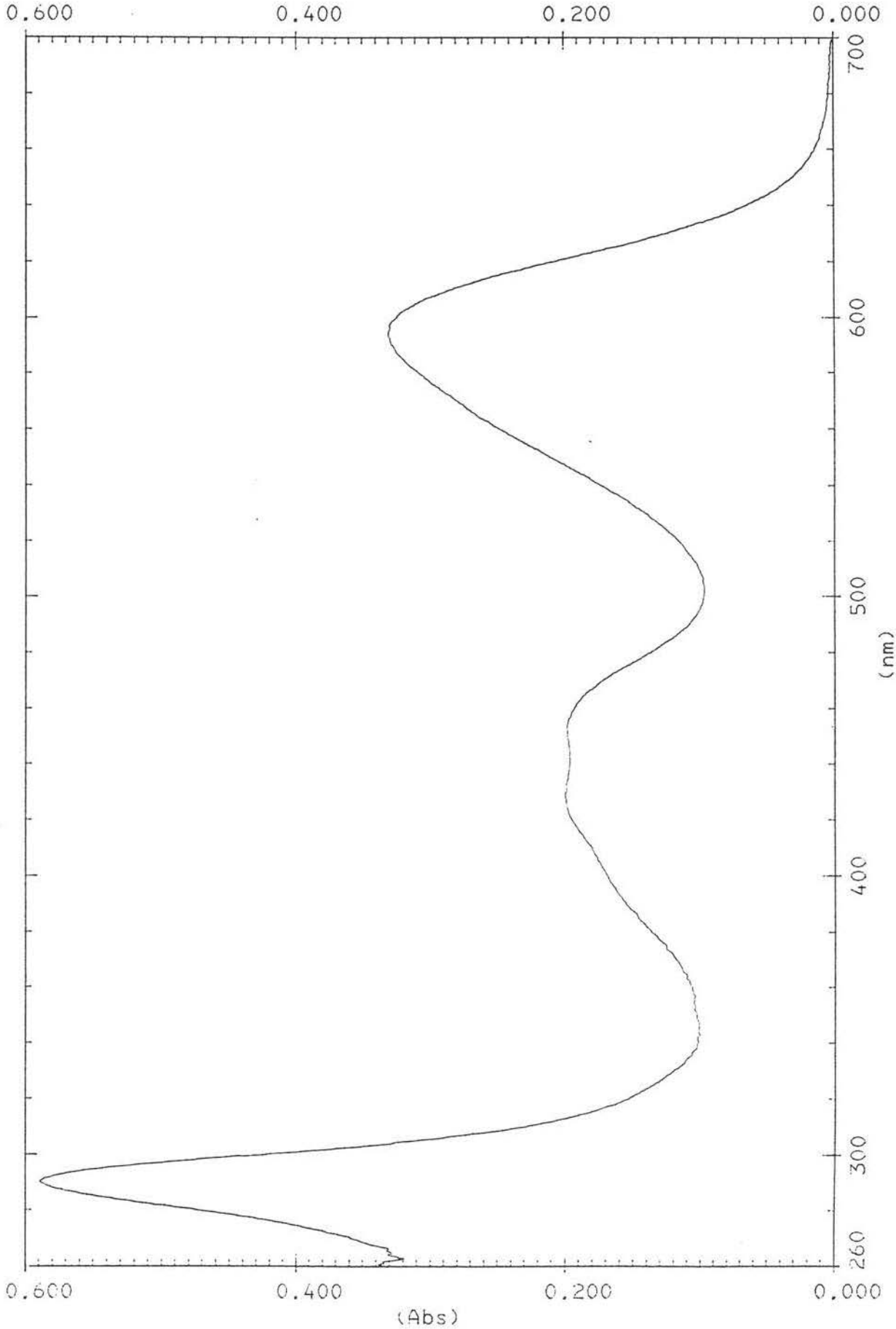

Figure 3.25 UV-Vis spectrum of $[Ru^{II}(bpy)_2(phen\text{-}azo\text{-}phenol)](PF_6)_2$ in DMSO

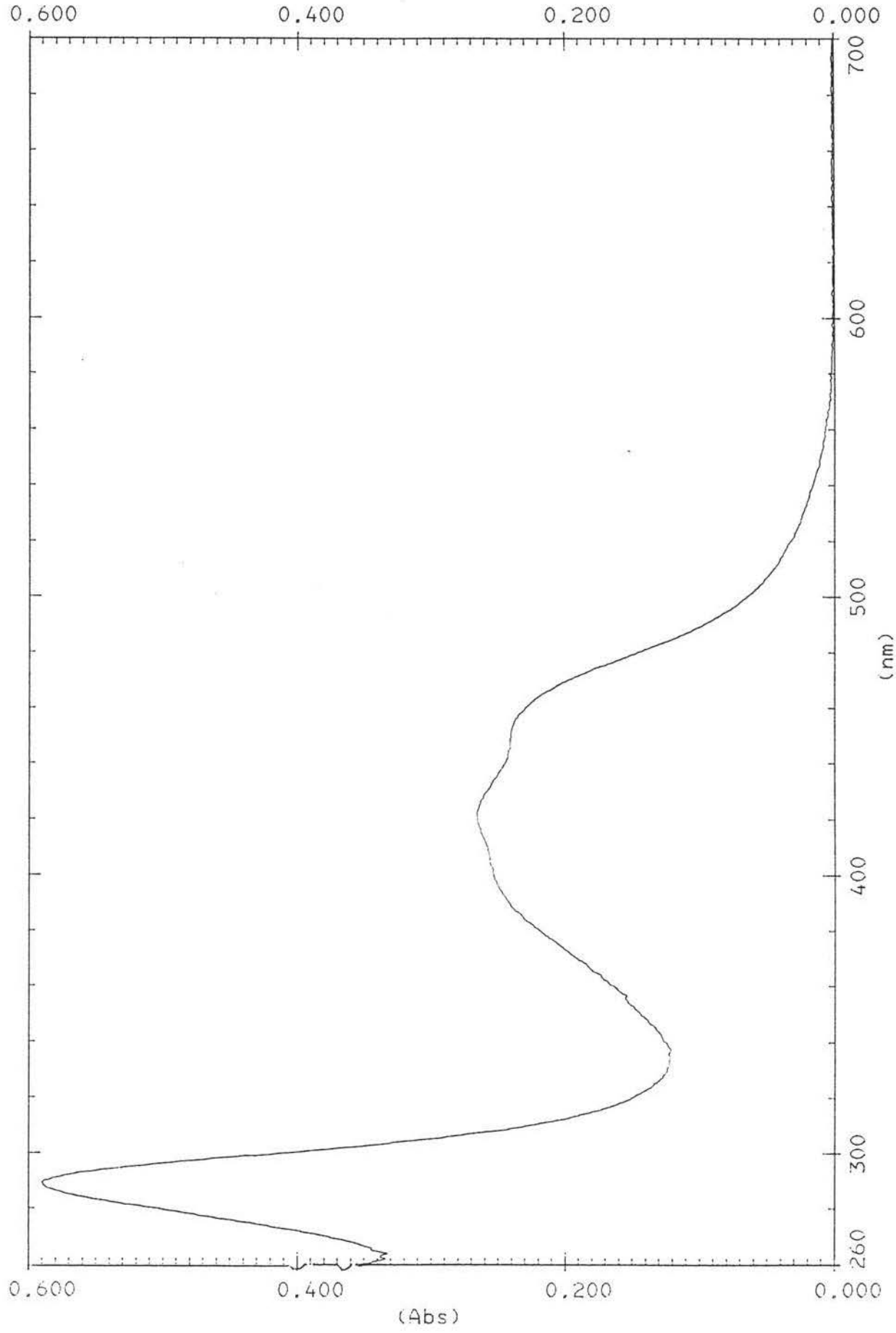

Figure 3.26 UV-Vis spectrum of $[Ru^{II}(bpy)_2(phen\text{-}azo\text{-}phenol)](PF_6)_2$ in DMSO with conc. H_2SO_4 added

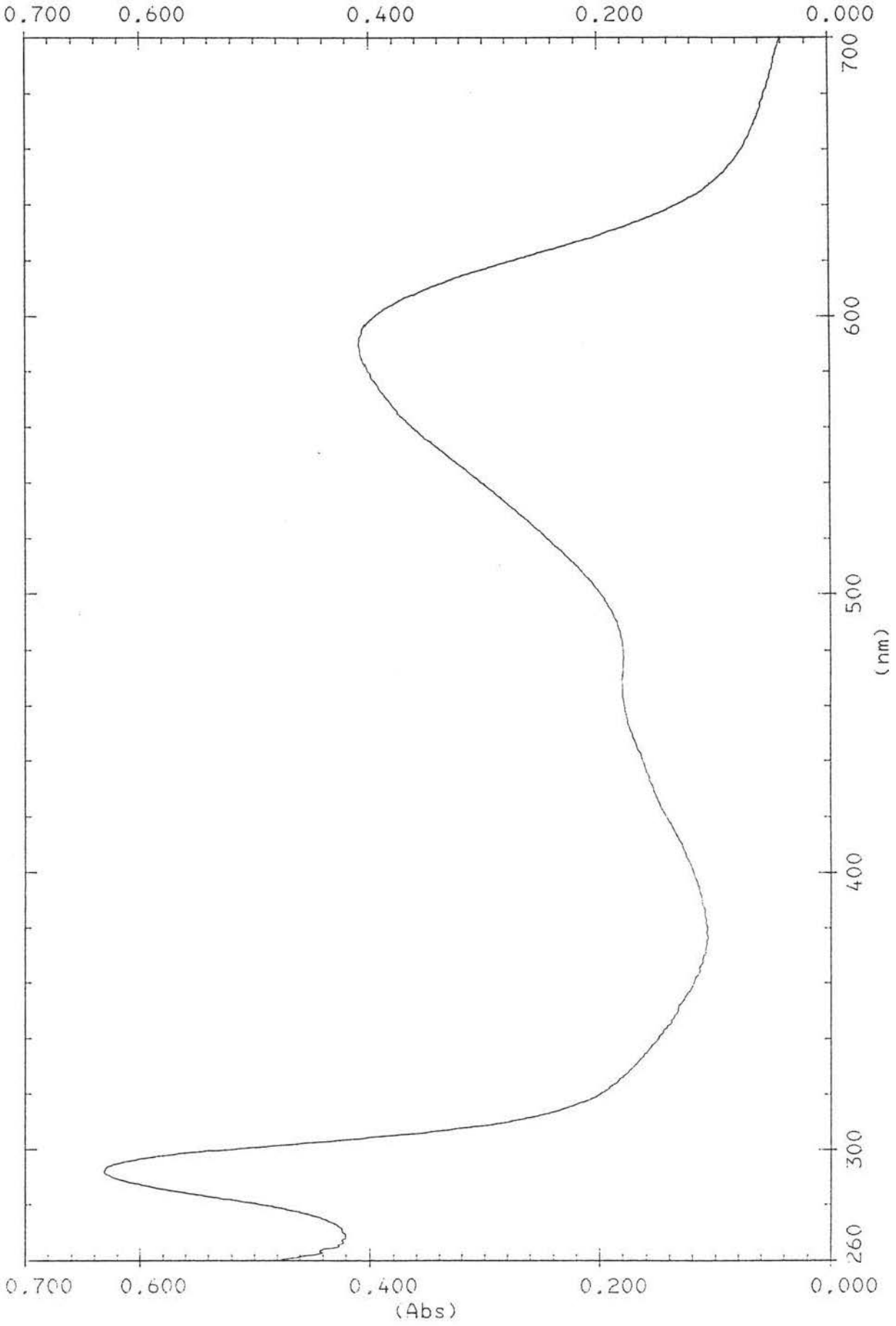

Figure 3.27 UV-Vis spectrum of $[Ru^{II}(bpy)_2(phen\text{-}azo\text{-}phenol)](PF_6)_2$ in DMSO with 10% NaOH (aq) added

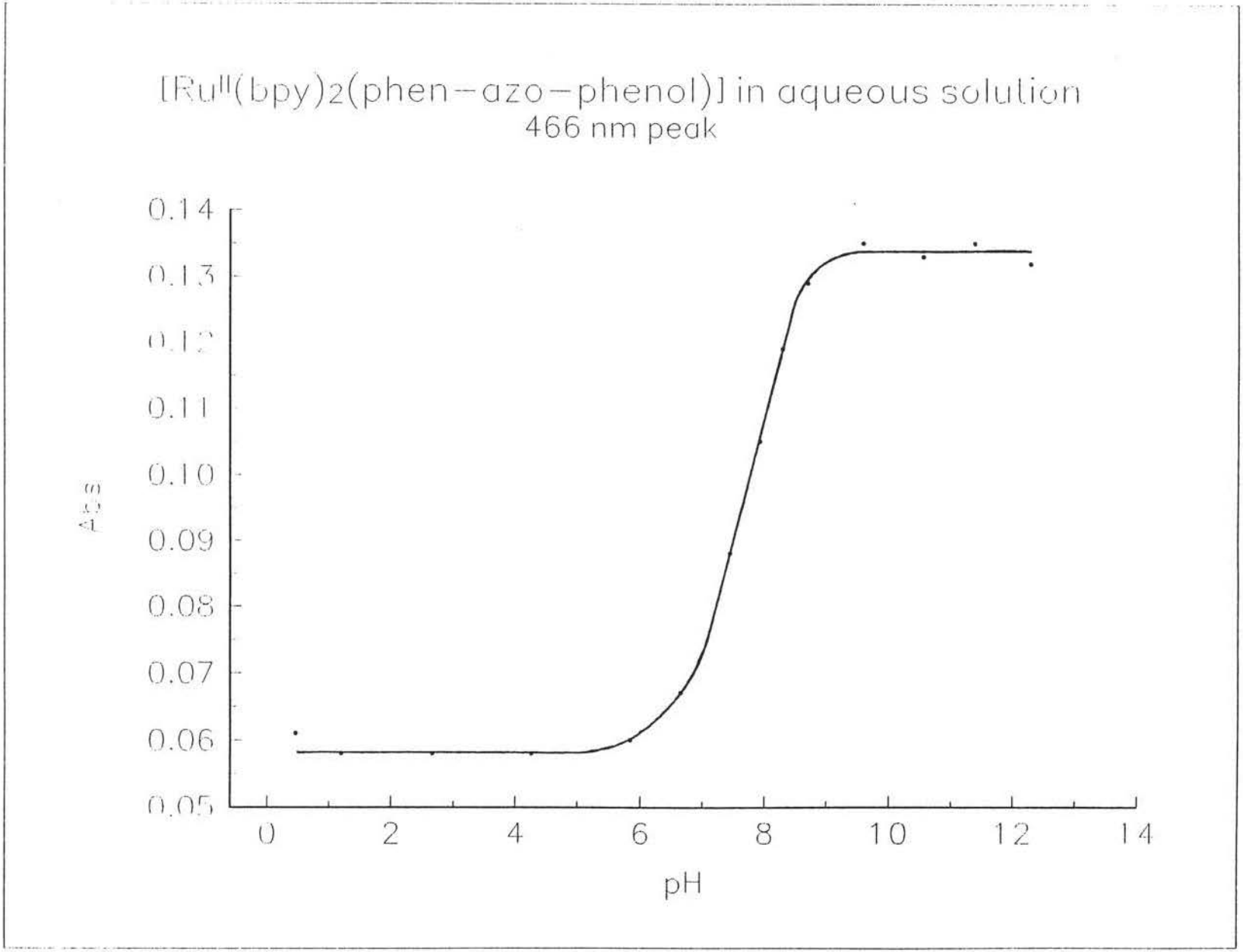

Figure 3.28 pKa determination of $[Ru^{II}(bpy)_2(phen\text{-}azo\text{-}phenol)](PF_6)_2$ in aqueous solution

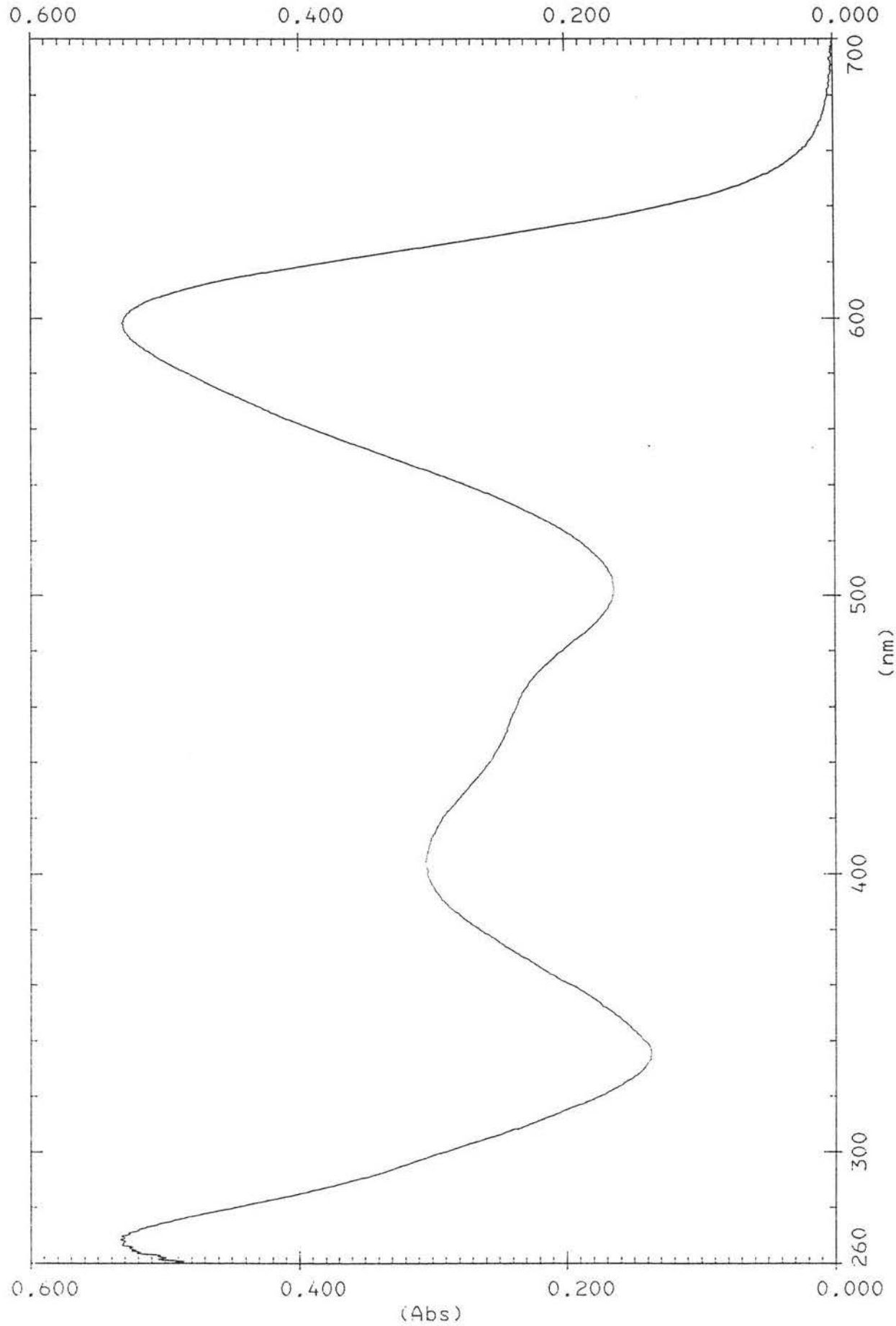

Figure 3.29 UV-Vis spectrum of $[Ru^{II}(phen\text{-}azo\text{-}phenol)_3](PF_6)_2$ in DMSO

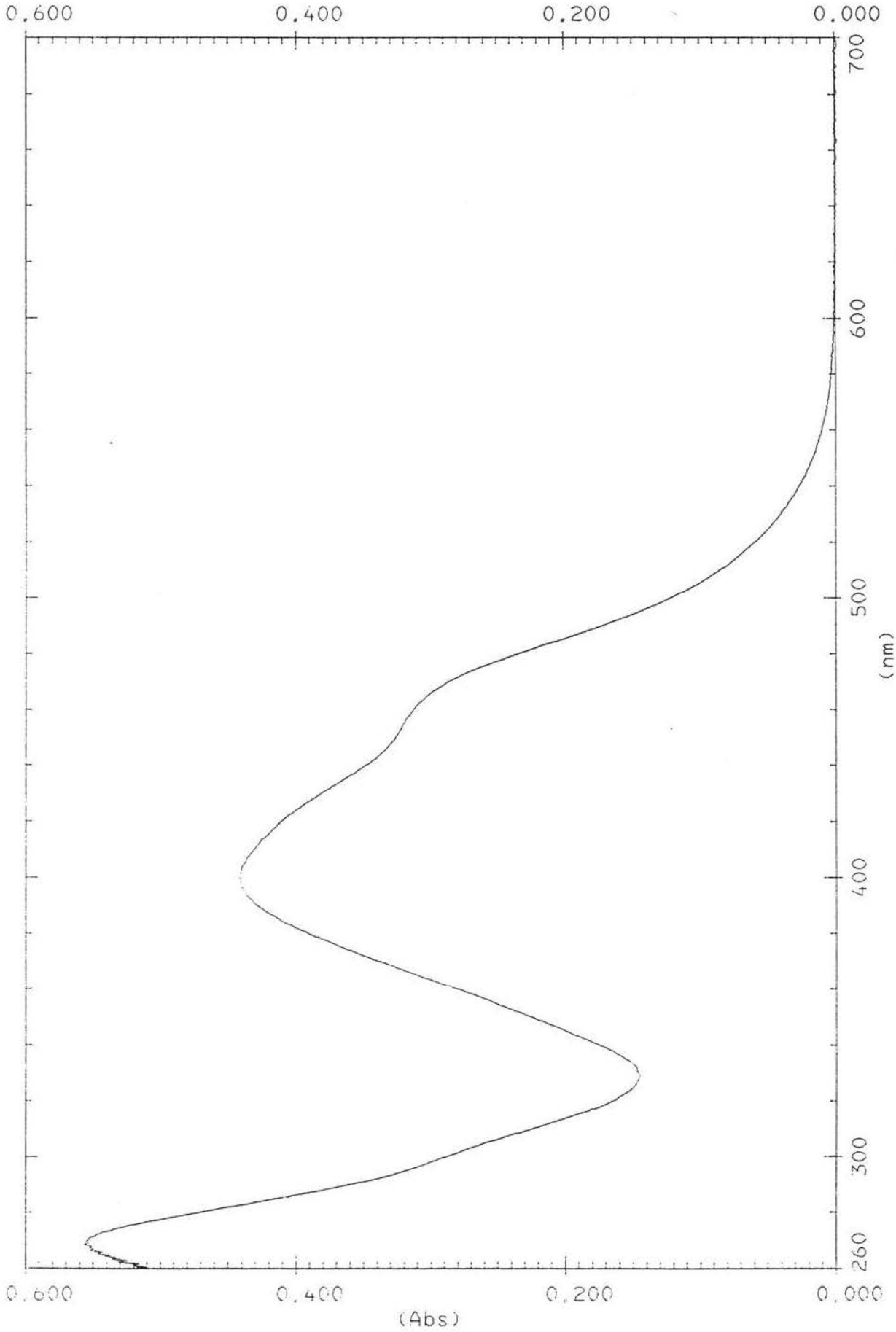

Figure 3.30 UV-Vis spectrum of $[Ru^{II}(phen\text{-}azo\text{-}phenol)_3](PF_6)_2$ in DMSO with conc. H_2SO_4 added

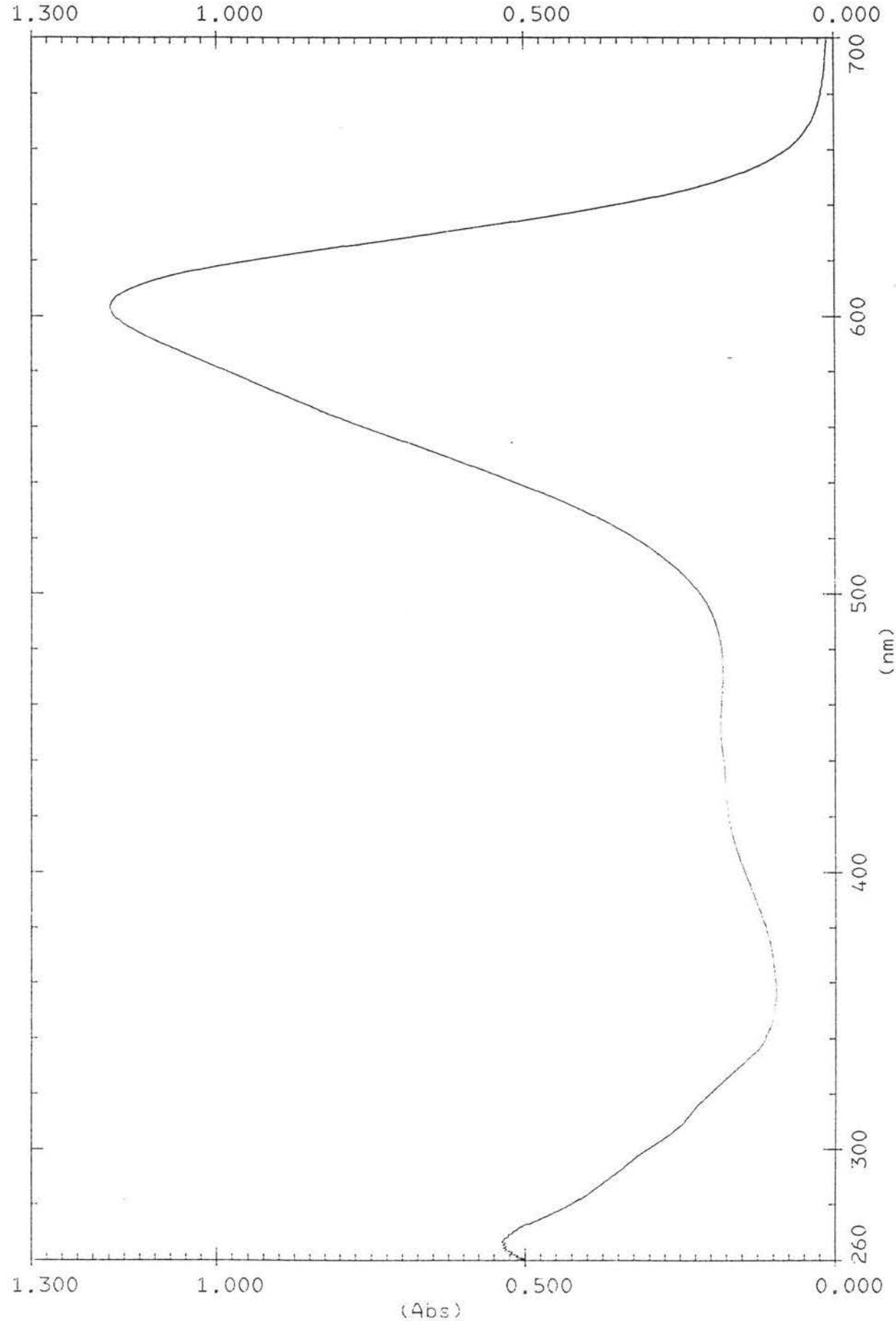

Figure 3.31 UV-Vis spectrum of $[Ru^{II}(phen\text{-}azo\text{-}phenol)_3](PF_6)_2$ in DMSO with 10% NaOH (aq) added

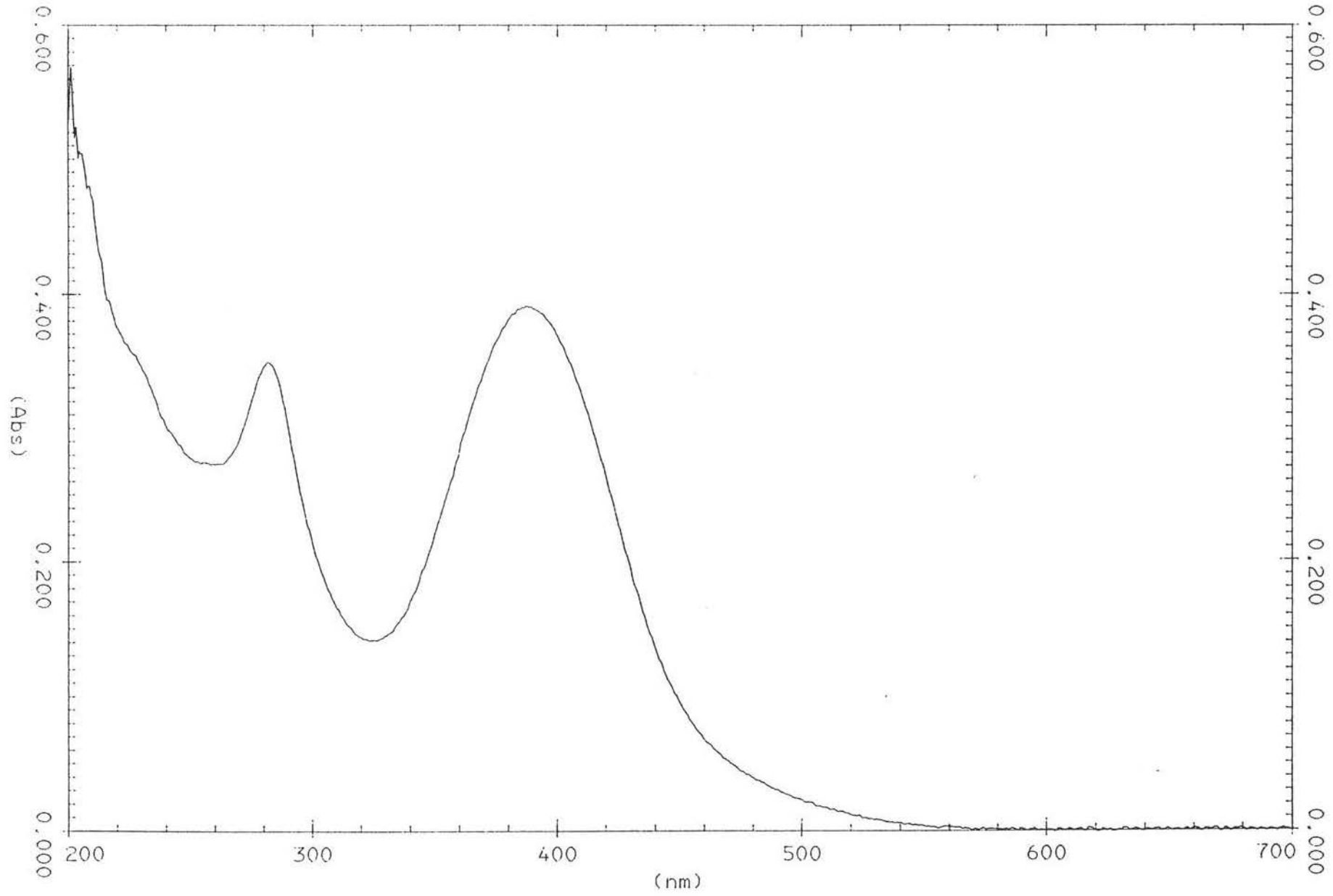

Figure 3.32 UV-Vis spectrum of phen-azo-phenol in methanol with conc. H_2SO_4 added

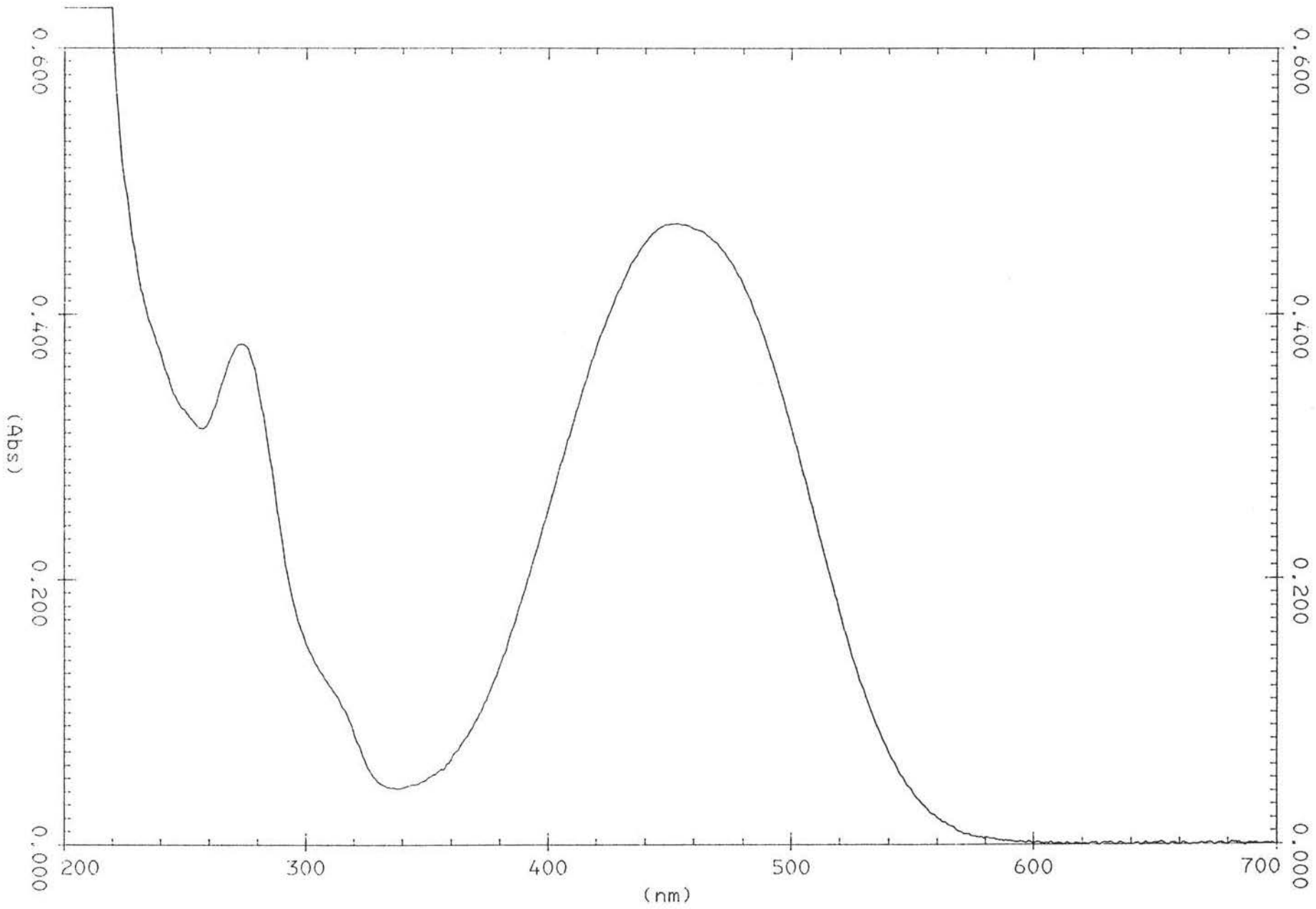

Figure 3.33 UV-Vis spectrum of phen-azo-phenol in methanol with 10% NaOH (aq) added

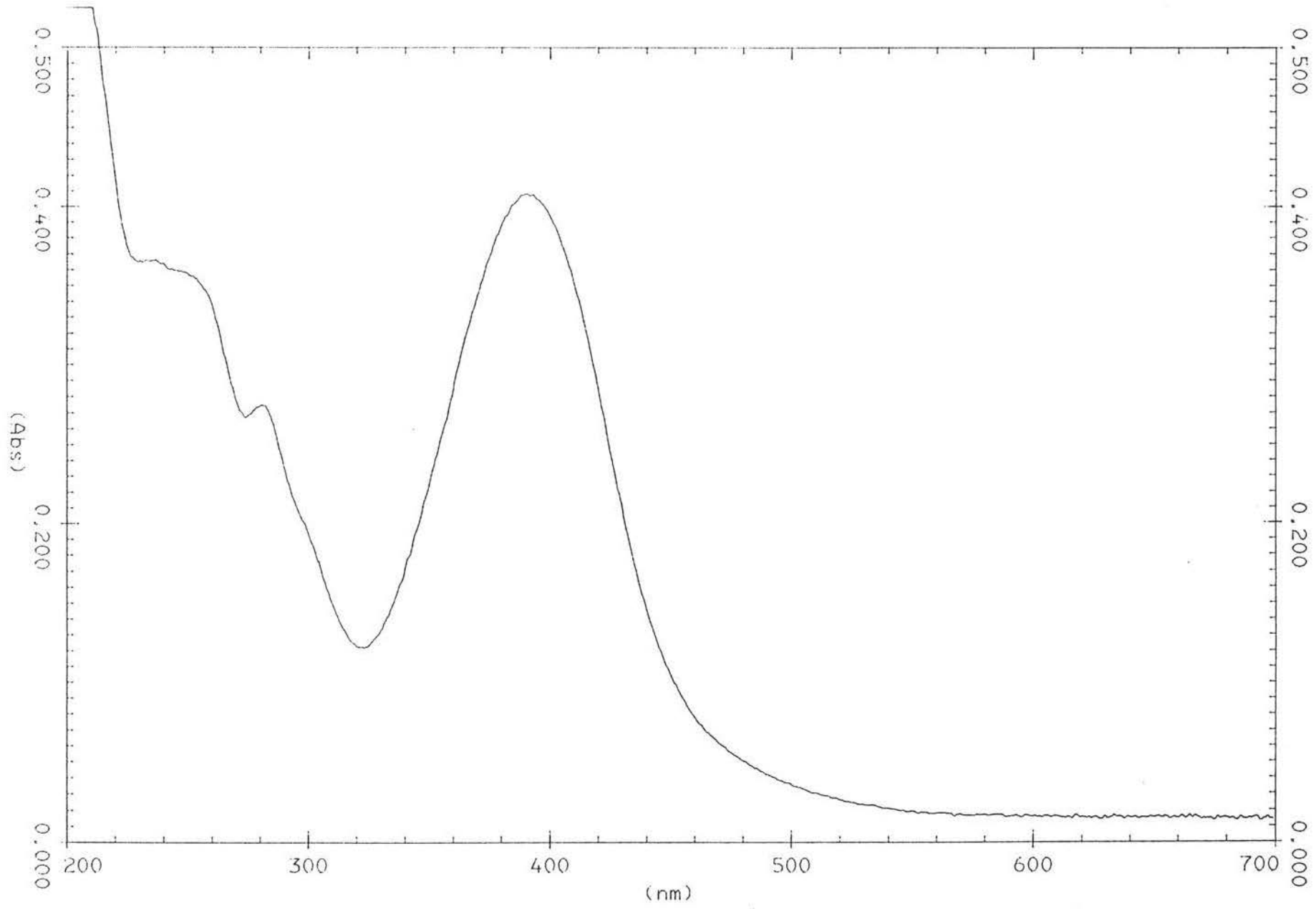

Figure 3.34 UV-Vis spectrum of *fac*-$Re^{I}(CO)_3Cl$(phen-azo-phenol) in methanol with conc. H_2SO_4 added

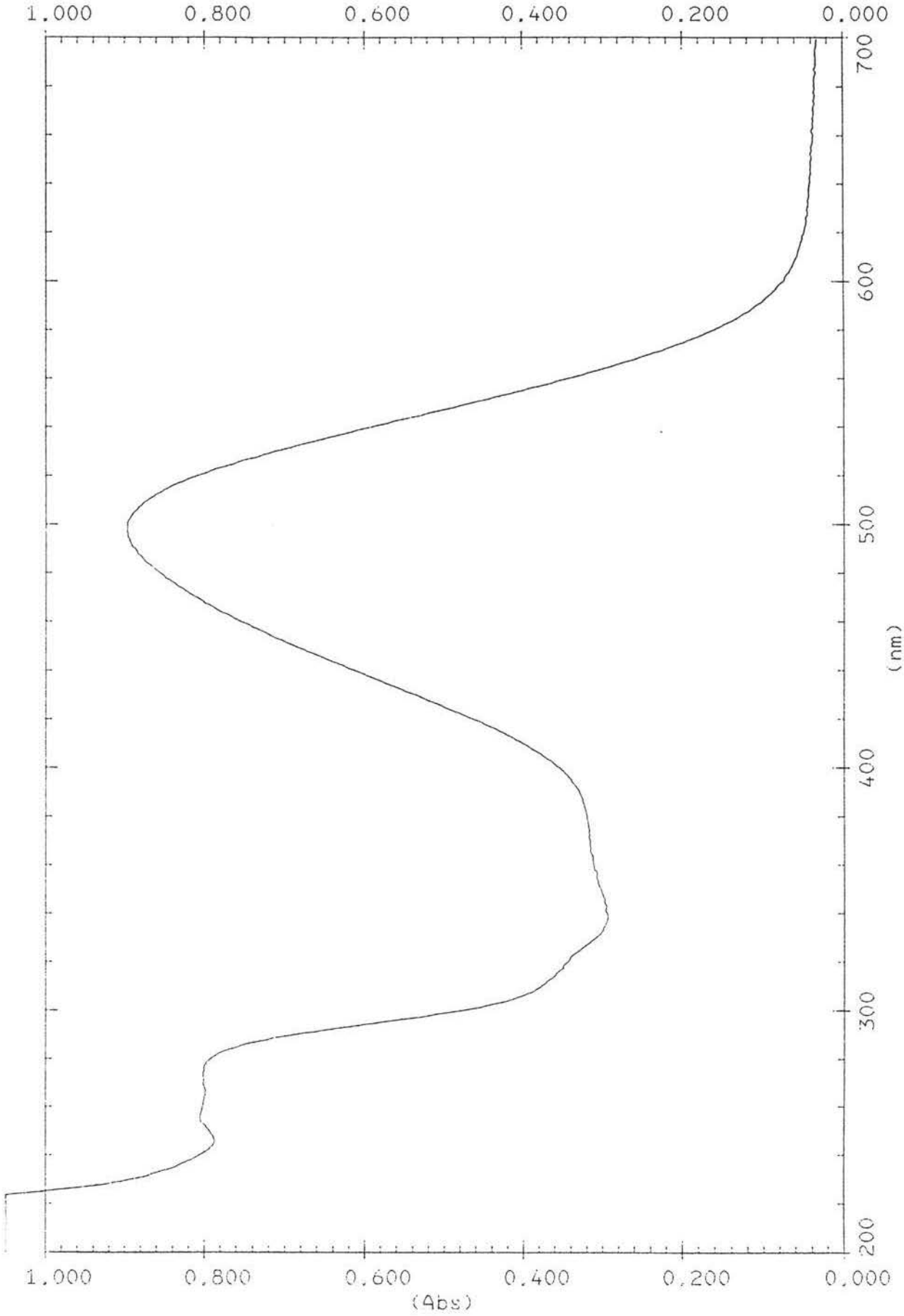

Figure 3.35 UV-Vis spectrum of *fac*-$Re^{I}(CO)_3Cl$(phen-azo-phenol) in methanol with 10% NaOH (aq) added

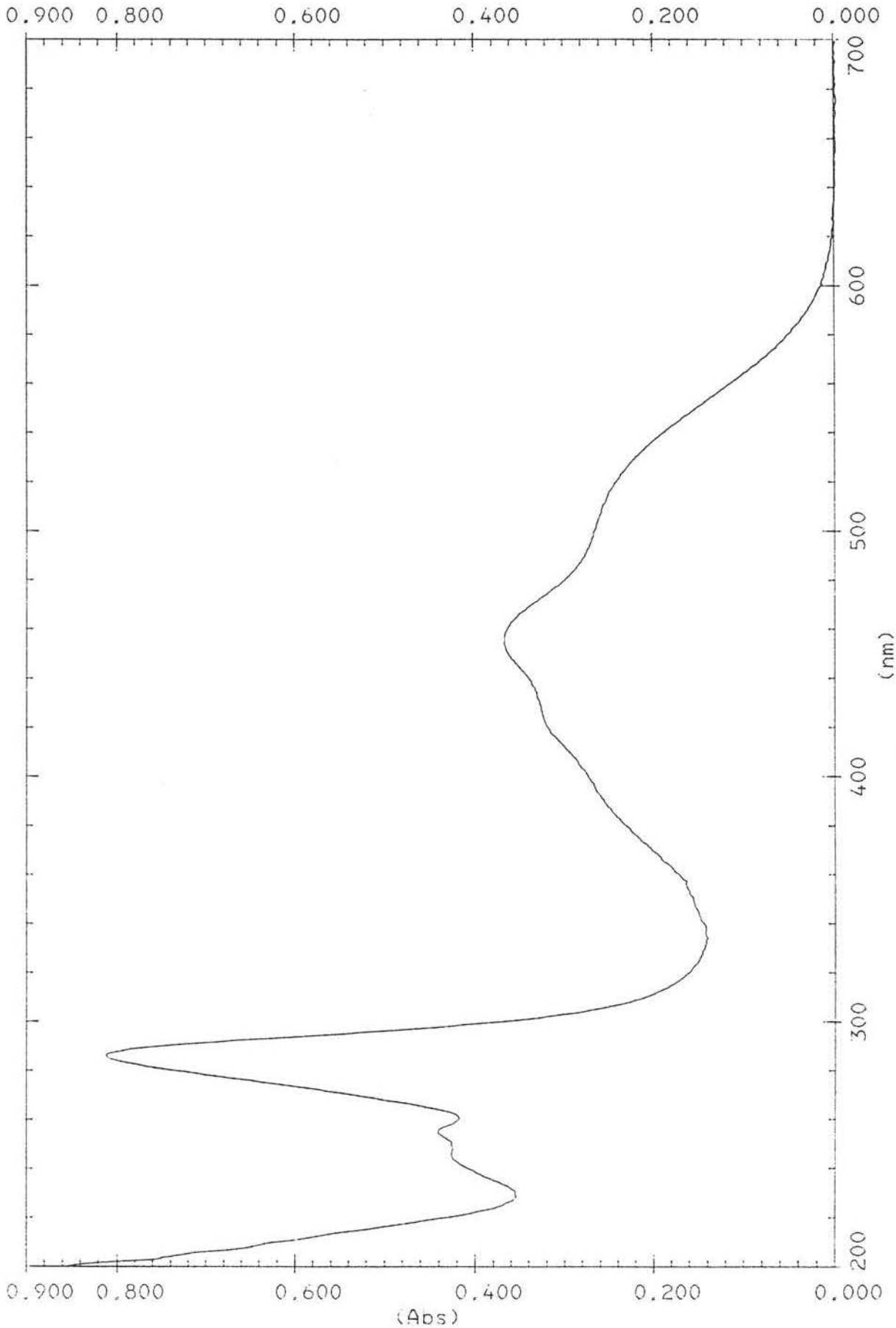

Figure 3.36 UV-Vis spectrum of $[Ru^{II}(bpy)_2(phen\text{-}azo\text{-}phenol)](PF_6)_2$ in methanol

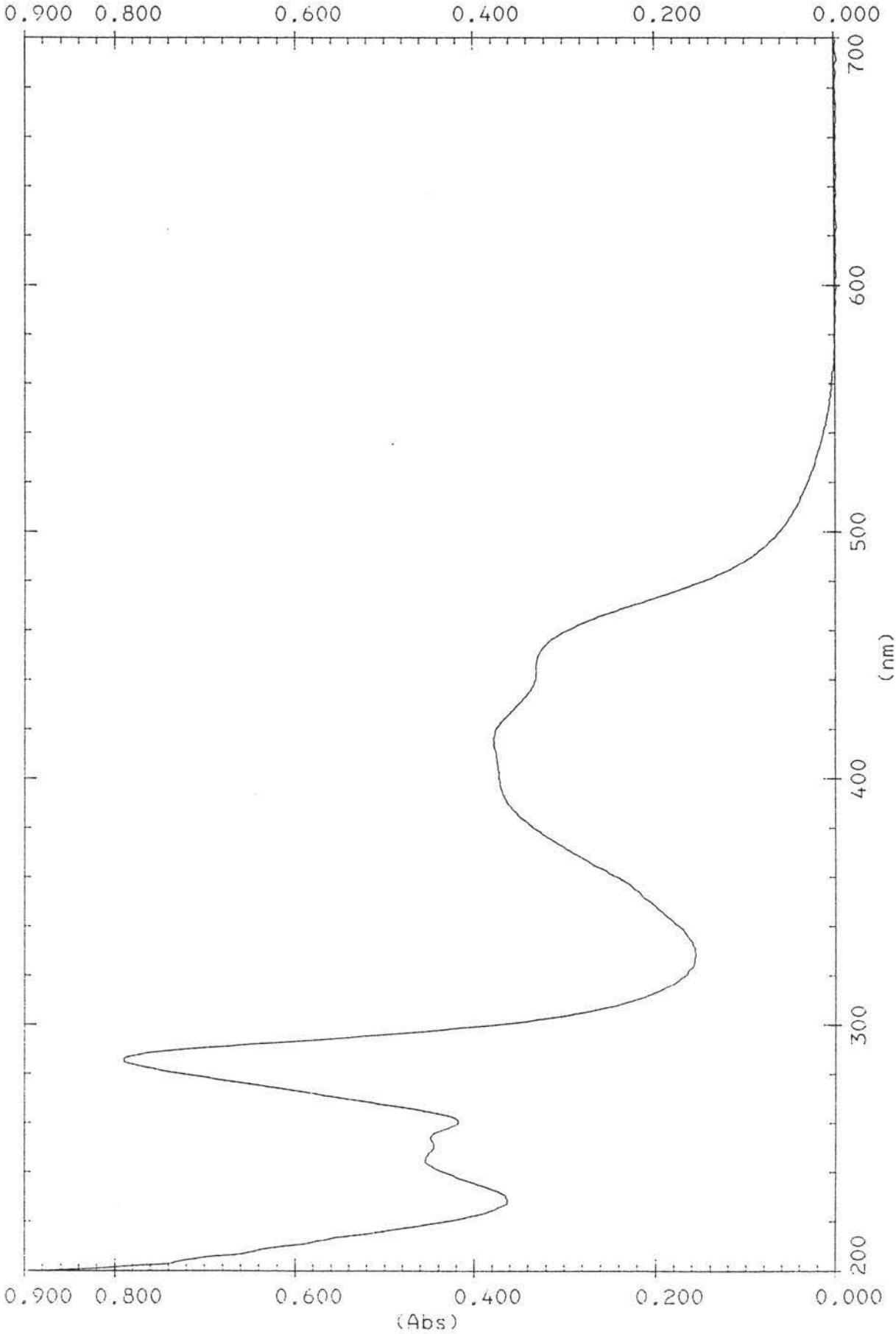

Figure 3.37 UV-Vis spectrum of $[Ru^{II}(bpy)_2(phen\text{-}azo\text{-}phenol)](PF_6)_2$ in methanol with conc. H_2SO_4 added

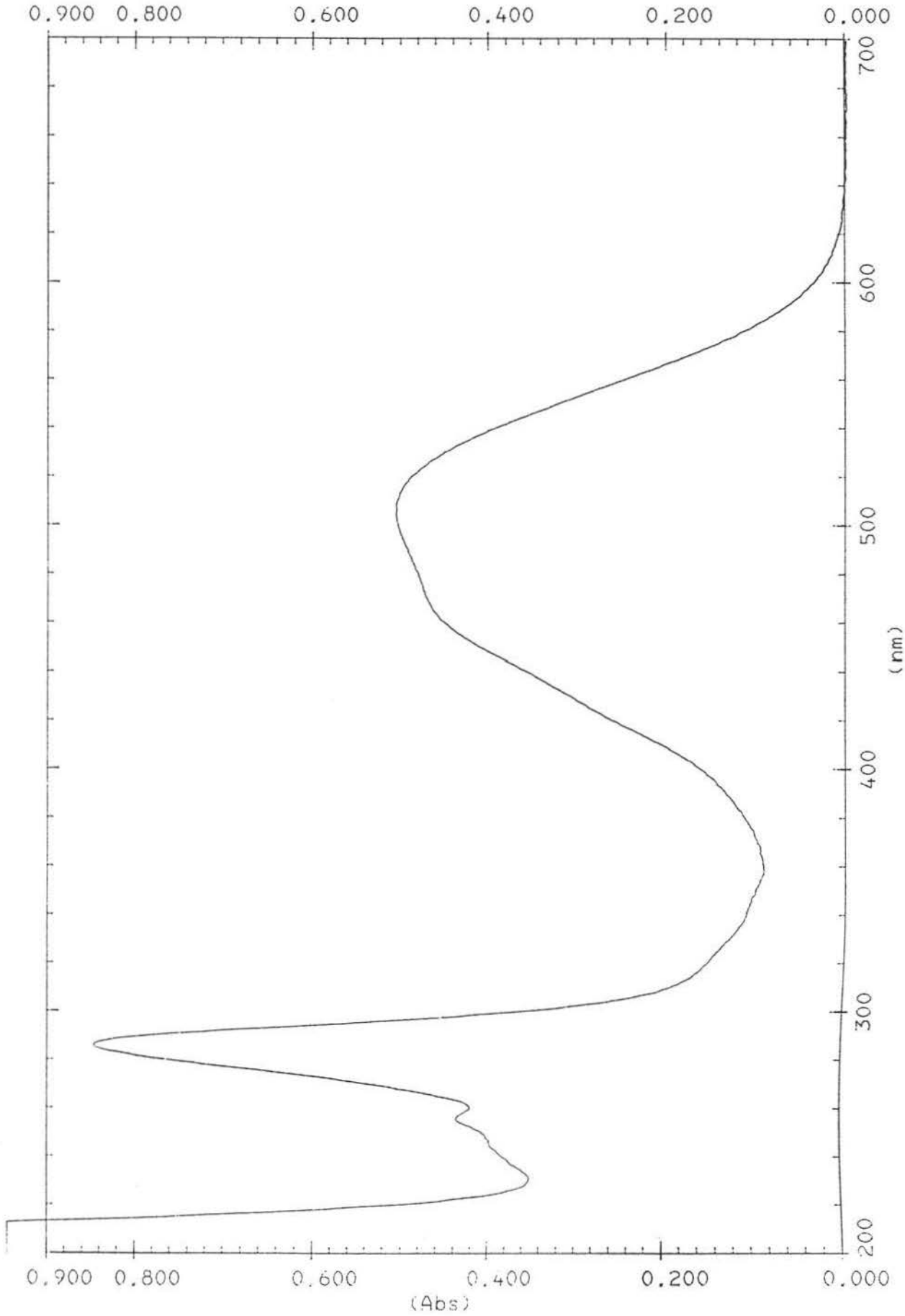

Figure 3.38 UV-Vis spectrum of $[Ru^{II}(bpy)_2(phen\text{-}azo\text{-}phenol)](PF_6)_2$ in methanol with 10% NaOH (aq) added

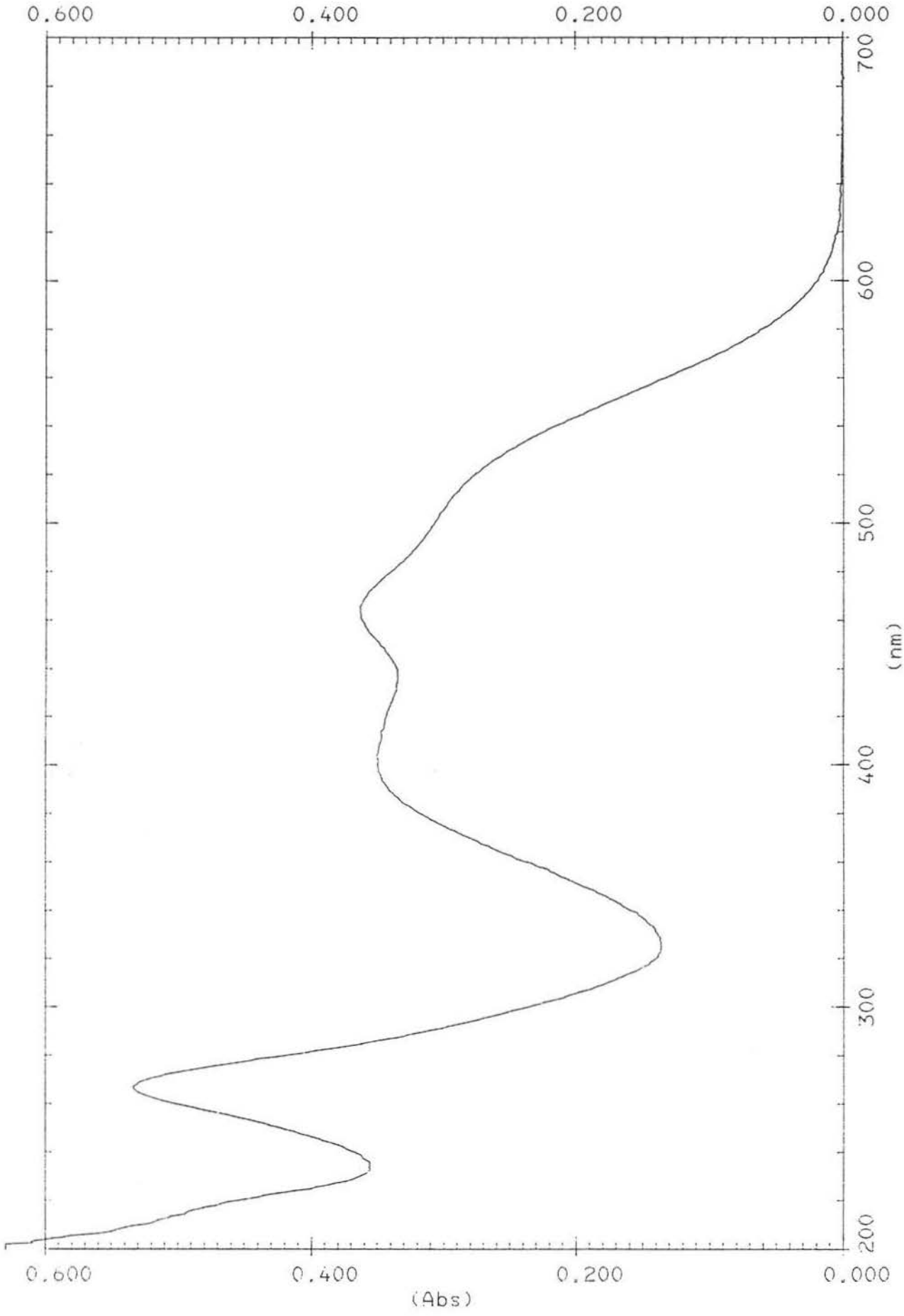

Figure 3.39 UV-Vis spectrum of $[Ru^{II}(phen\text{-}azo\text{-}phenol)_3](PF_6)_2$ in methanol

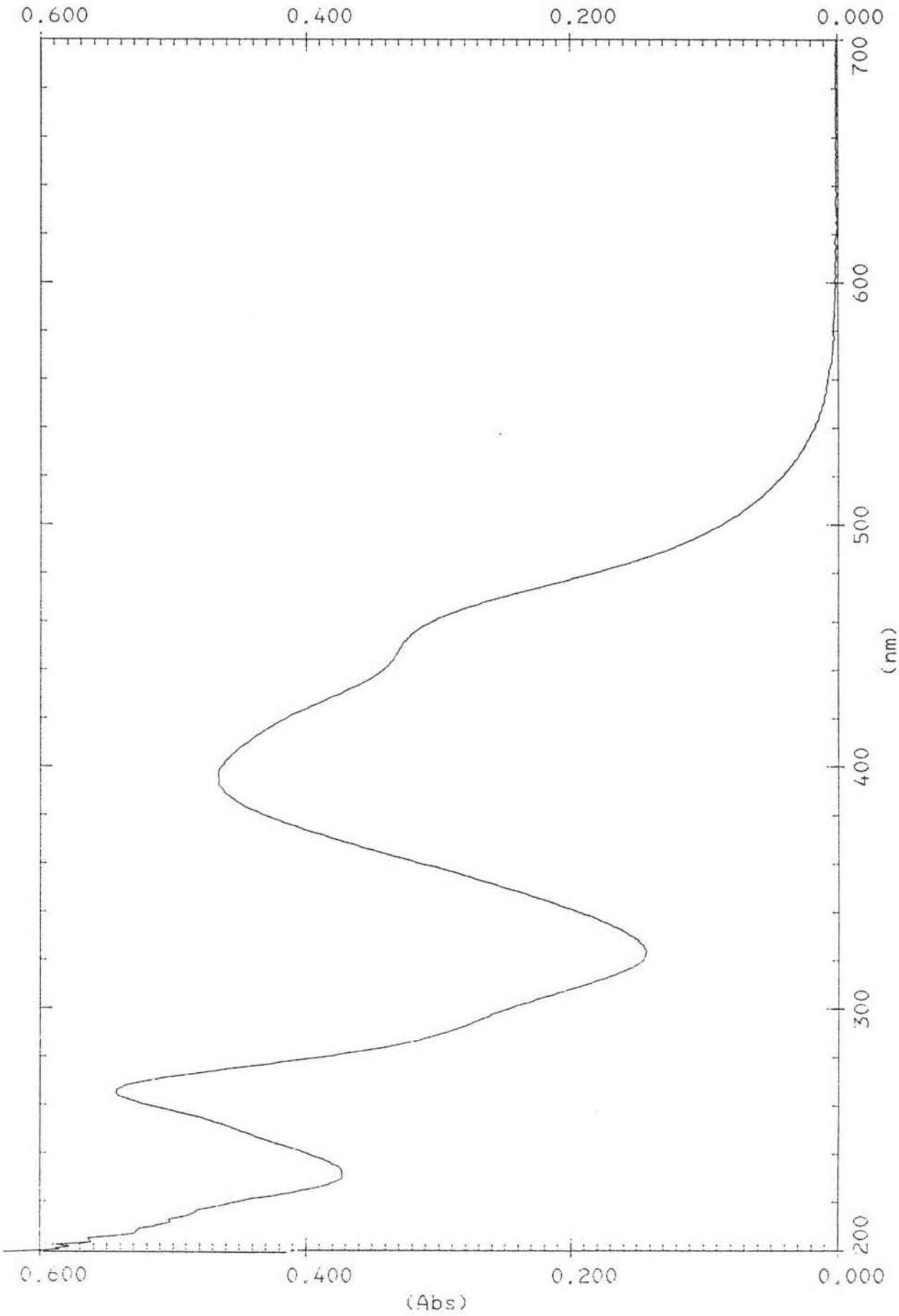

Figure 3.40 UV-Vis spectrum of $[Ru^{II}(phen\text{-}azo\text{-}phenol)_3](PF_6)_2$ in methanol with conc. H_2SO_4 added

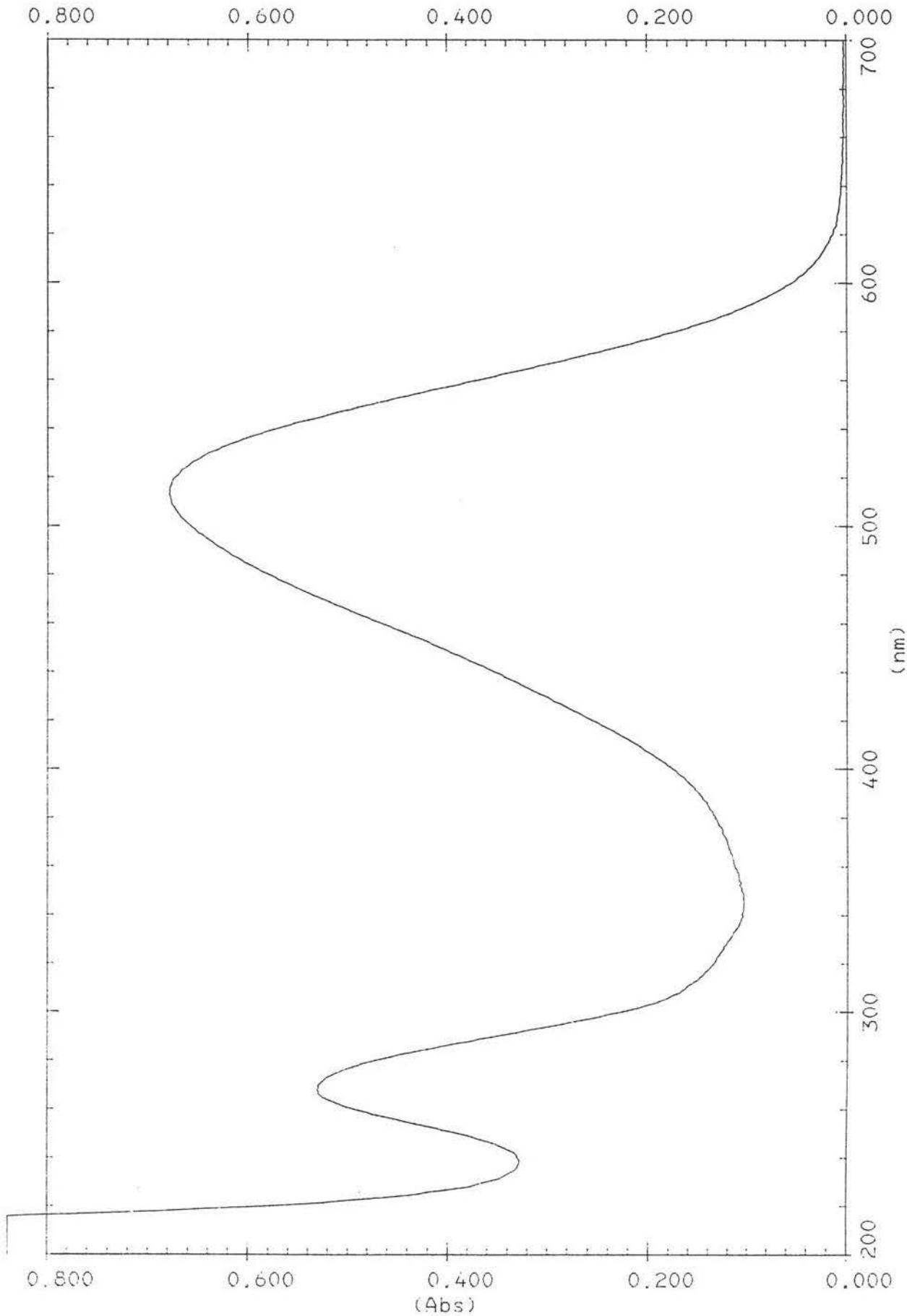

Figure 3.41 UV-Vis spectrum of $[Ru^{II}(phen\text{-}azo\text{-}phenol)_3](PF_6)_2$ in methanol with 10% NaOH (aq) added

References

1. Kalyanasundaram, K. *Coord. Chem. Rev.* **1982**, *39*, 159.
2. Juris, A.; Belser, P.; Zelewsky A. von; Barigelletti, P.; Balzani, V. *Coord. Chem. Rev.* **1988**, *84*, 85.
3. Kalyanasundaram, K. *Photochemistry of Polypyridine and Porphyrin Complexes*; Academic: San Diego, 1992; Chapters 2, 5, 6, 11.
4. Belser, P.; Von Zelewsky, A.; Juris, A.; Tucci, A.; Balzani, V. *Chem. Phys. Lett.* **1982**, *89*, 101.
5. Barigelletti, F.; Belser, P.; Von Zelewsky, A.; Balzani, V. *J. Phys. Chem.* **1985**, *89*, 3680.
6. Scandola, F.; Balzani, V. *J. Chem. Educ.* **1983**, *60*, 814.
7. Kavarnos, G.J.; Turro, N.J. *Chem. Rev.* **1986**, *86*, 401.
8. Kalyanasundaram, K.; Grätzel, M.; Pelizzetti, E. *Coord. Chem. Rev.* **1986**, *69*, 57.
9. Meyer, T.J. *Acc. Chem. Res.* **1989**, *22*, 163.
10. Ziessel, R. *Nouv. J. Chim.* **1983**, *7*, 613.
11. Lehn, J.M.; Ziessel, R. *Proc. Nat. Acad. Sci. USA*, **1982**, 79, 701.
12. Hawecker, J.; Lehn, J.M.; Ziessel, R. *J. Chem. Soc., Chem. Commun.* **1983**, 536.
13. Hawecker, J.; Lehn, J.M.; Ziessel, R. *J. Chem. Soc., Chem. Commun.* **1985**, 56.
14. Hawecker, J.; Lehn, J.M.; Ziessel, R. *Helv. Chim. Acta*, **1986**, *69*, 1990.
15. O'Regan, B.; Grätzel, M. *Nature* **1991**, *353*, 737.
16. Amadelli, R.; Argazzi, R.; Bignozzi. C.A.; Scandola, F. *J. Am. Chem. Soc.* **1990**, *112*, 709.
17. Mallouk, T. *Nature* **1991**, *353*, 698.

18. Balzani, V.; Scandola, F. *Supramolecular Photochemistry*; Horwood: Chichester, 1990.
19. Balzani, V.; Sabbatini, N; Scandola, F. *Chem. Rev.* **1986**, *86*, 319.
20. Ruminski, R.R.; Peterson, J.D. *Inorg. Chem.* **1982**, *21*, 3706.
21. Sahai, R.; Morgan, L.; Rillema, D.P. *Inorg. Chem.* **1988**, *27*, 3495.
22. Anderson, P.A.; Strouse, G.F.; Treadway, J.A.; Keene, F.R.; Meyer, T. *J. Inorg. Chem.* **1994**, *33*, 3863.
23. Zollinger, H. *Color Chemistry: Syntheses, Properties and Applications of Organic Dyes and Pigments*, 2nd rev. ed.; VCH: New York, 1991; Chapters 2, 7.
24. Mao, M. M.S. Thesis, Eastern Illinois University, 1997.
25. Amouyal, E.; Homsi, A.; Chambron, J.; Sauvage, J. *J. Chem. Soc., Dalton Trans.* **1990**, 1841.
26. Nasielski-Hinkens, R.; Benedek-Vamous, M.; Maetens, D.; Nasielski, J. *J. Organomet. Chem.* **1981**, *217*, 179.
27. Van Wallendael, S.; Shaver, R.J.; Rillema, D.P.; Yoblinski, B.J.; Stathis, M.; Guarr, T.F. *Inorg. Chem.* **1990**, *29*, 1761.
28. Yoblinski, B.J.; Stathis, M.; Guarr, T.F. *Inorg. Chem.* **1992,** *31*, 5.
29. Pavinato, R.A. M.S. Thesis, Eastern Illinois University, 1994.
30. Wang, Y.; Perez, W.J.; Zheng, G.Y.; Rillema, D.P.; Huber, C.L. *Inorg. Chem.* **1998**, *37*, 2227.
31. Huang, H. M.S. Thesis, Eastern Illinois University, 1993.
32. Marugyma, M.; Matsuzawa, H.; Kaizu, Y. *Inorg. Chim. Acta.* **1995**, *237*, 159.
33. Luong, J.C.; Nadjo, L; Wrighton, M.S. *J. Am. Chem. Soc.* **1978**, *100*, 5790.
34. Staniewicz, R.J.; Sympson, R.F.; Hendricker, D.G. *Inorg. Chem.* **1977**, *16*, 2166.
35. Caspar J.V.; Meyer, T.J. *Inorg. Chem.* **1983**, *22*, 2444.
36. Wrighton, M.; Morse, D.L. *J. Am. Chem. Soc.* **1974**, *96*, 998.
37. Crosby, G.A.; Perkins, W.G.; Klassen, D.M. *J. Chem. Phys.* **1965**, *43*, 1498.
38. Fabian, R.H.; Klassen, D.M.; Sonntag, R.W. *Inorg. Chem.* **1980**, *19*, 1977.

39. Dean, J. *Lange's Handbook of Chemistry*, 14th ed.; McGraw-Hill, inc. 1992.